A Process for Manufacturing Metal-Ceramic Cellular Materials with Designed Mesostructure

Dean Andrew Snelling Jr.

Dissertation submitted to the faculty of the Virginia Polytechnic Institute and State University in partial fulfillment of the requirements for the degree of

Doctor of Philosophy
In
Mechanical Engineering

Christopher B. Williams
Alan P. Druschitz
Brian Y. Lattimer
Carlos T. A. Suchicital
Pablo A. Tarazaga
Robert L. West

February 16, 2015
Blacksburg, VA

Keywords: Additive Manufacturing, 3D Printing, Binder Jetting, Sand Casting, Bonded Sand Molding

A Process for Manufacturing Metal-Ceramic Cellular Materials with Designed Mesostructure

Dean Andrew Snelling Jr.

ABSTRACT

The goal of this work is to develop and characterize a manufacturing process that is able to create metal matrix composites with complex cellular geometries. The novel manufacturing method uses two distinct additive manufacturing processes: i) fabrication of patternless molds for cellular metal castings and ii) printing an advanced cellular ceramic for embedding in a metal matrix. However, while the use of AM greatly improves the freedom in the design of MMCs, it is important to identify the constraints imposed by the process and its process relationships.

First, the author investigates potential differences in material properties (microstructure, porosity, mechanical strength) of A356 – T6 castings resulting from two different commercially available Binder Jetting media and traditional "no-bake" silica sand. It was determined that they yielded statistically equivalent results in four of the seven tests performed: dendrite arm spacing, porosity, surface roughness, and tensile strength. They differed in sand tensile strength, hardness, and density.

Additionally, two critical sources of process constraints on part geometry are examined: (i) depowdering unbound material from intricate casting channels and (ii) metal flow and solidification distances through complex mold geometries. A Taguchi Design of Experiments is used to determine the relationships of important independent variables of each constraint. For depowdering, a minimum cleaning diameter of 3 mm was determined along with an equation relating cleaning distance as a function of channel diameter. Furthermore, for metal flow, choke diameter was found to be significantly significant variable.

Finally, the author presents methods to process complex ceramic structure from precursor powders via Binder Jetting AM technology to incorporate into a bonded sand mold and the subsequently casted metal matrix. Through sintering experiments, a sintering temperature of 1375°C was established for the ceramic insert (78% cordierite). Upon printing and sintering the

ceramic, three point bend tests showed the MMCs had less strength than the matrix material likely due to the relatively high porosity developed in the body. Additionally, it was found that the ceramic metal interface had minimal mechanical interlocking and chemical bonding limiting the strength of the final MMCs.

DEDICATION

To My Wife Caylee and Daughter Jo

ACKNOWLEDGEMENTS

I would like to thank:

Dr. Christopher Williams for your support as an advisor and mentor. Thank you for giving me the chance to work in a revolutionary field with excellent people. You've imparted considerable knowledge not only by what you do, but the how you do it.

Dr. Alan Druschitz for your commitment to become my co-advisor part of the way through the PhD program. You've made learning enjoyable and have been an excellent example as an engineer and person. I've enjoyed the copious time spent in conversation learning from your experiences.

Dr. Suchicital for taking the time and resources to help and teach me analytical equipment to aid in my research.

Dr. Lattimer, Dr. Tarazaga, and Dr. West - for taking the time to serve on my committee. I've thoroughly enjoyed getting to know each one of you individually.

To all my friends and colleagues in the DREAMS Lab. I could not do it without the diverse group of people that give the DREAMS Lab character and make it successful.

TABLE OF CONTENTS

LIST OF FIGURES

LIST OF TABLES

1. INTRODUCTION

Cellular material structures are low density, porous structures that provide excellent characteristics including high strength, high stiffness, and energy absorption, while maintaining low mass [1–3]. Lightweight cellular materials are increasingly of interest due to the continual need for energy efficient systems in automotive, aerospace, military, and infrastructure industries and can be used in applications such as filters, heat exchangers, biomedical prostheses, and blast resistant panels [3,4]. Additionally, these structures contain less material as compared to solid structures with similar dimensions, therefore reducing cost of production (although there are other cost considerations such as the performance of the material and processing costs) [5]. The term "cellular materials" encompasses all materials which feature voids in metallic phase, and are classified on the order of the void phase: either stochastic or ordered (Figure 1.1). Stochastic materials include foams that feature structures with cells of random shape, morphology, and distribution, while ordered cellular materials contain selectively placed material for specific applications [6]. Ordered cellular materials contain a unit cell or repeating structure throughout the part [7]; their performance is therefore predictable when compared to stochastic materials. As a result of the complex internal geometry, manufacturing a component with ordered cellular mesostructure is impossible with traditional subtractive machining. As such, researchers have looked to advanced manufacturing technologies, specifically Additive Manufacturing (AM), to produce ordered cellular class of materials.

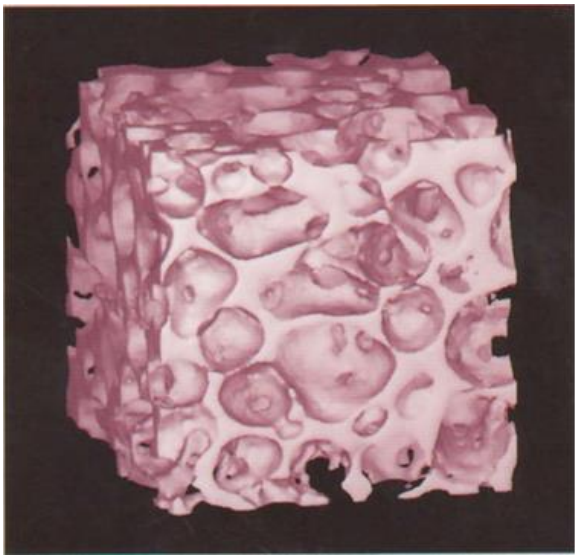

a)

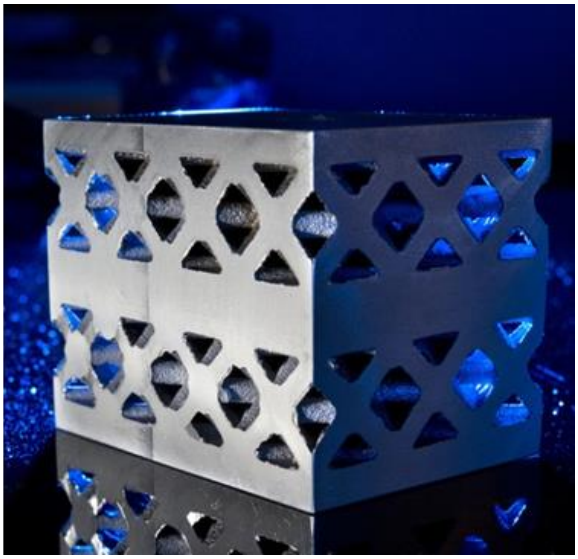

b)

Figure 1.1. a) Stochastic [3] and b) ordered cellular materials

1.1. Overall Research Goal

Additive Manufacturing has been successfully used to create cellular geometries, which enables freedom in complexity by its layer-wise manufacturing process [8]. For example, by combining AM and investment casting, metallic complex cellular structures can be developed with designed mesostructure, however limitations exists. One limitation is scale. Current AM systems are limited in their build volume and many of the recently proposed cellular structures are only able to create a single layer. Additionally, materials used in the AM process as a substitute for wax, for example photopolymer from the PolyJet material jetting AM process, have much higher thermal expansion, which can result in cracked investment molds [9]. Finally, ceramic slurry used for investment casting can be difficult to remove in intricate geometries. It can also require chemically leaching of residual material from the final part, which results in increased manufacturing cost.

Additionally, direct-metal AM processes, which selectively scan an energy source (a laser or electron beam) over a metal powder bed, are capable of fabricating fully-dense metal artifacts without the need for additional post-processing. Selective Laser Melting [10,11], Electron Beam Melting [12,13], and Direct-Metal Laser Sintering [14] have all been employed in research targeted towards fabricating cellular materials. For example, Yang and coauthors (2012) created

auxetic lattice structures with electron beam melting using Ti-6Al-4V [13]. Four designs were tested in compression to compare the effect of density and poisson's ratio on strength and modulus. These results were compared to analytical equations for these auxetic structures, which were primarily validated. While these processes have been successfully used to fabricate parts with cellular geometries, their ability to make parts of designed mesostructure is limited by inherent process constraints [7]. For example, direct-metal AM processes have a limited set of working materials, have high residual stresses requiring the use of support structures or anchors, have high cost and low throughput, and limited in part size with the largest commercial build box being approximately 402 x 402 x 402 mm [15].

The goal of this work is to address these limitations with an Additive Manufacturing process chain that combines Binder Jetting AM with metal casting to create multi-material parts with structured topology. Existing research on the use of Binder Jetting for metal casting has been primarily focused in casting case studies and studies of resultant material properties [16–20]. The technology has been shown to be effective in obtaining cast prototypes with dimensional tolerances that are consistent with metal casting processes [21]. AM technologies have been used in foundry practice to produce patterns and core boxes for sand casting [22]. Laser Sintering (LS) has been used to selectively melt a resin coated quartz sand in a layer-by-layer fashion in order to create printed sand molds [17,23]. An augmented stereolithography process (Optomec), which selectively cures viscous ceramic-resin slurry via exposure to UV energy, has also been used to directly fabricate sand molds [24]. However, there is not any literature pertaining to the use of Binder Jetting to fabricate complex geometries through Binder Jetting of patternless sand molds [25]. Studies in which part complexity was explored were limited to case studies in which existing products were cast with redesigned mold and core shapes [26,27].

Therefore, a manufacturing process is proposed wherein complex cellular ceramics can be printed with Binder Jetting AM and implemented into molds printed with a separate printing process. By integrating printed ceramics into the printed sand molds, metal can be cast into the molds in order to create metal matrix composites. This unique method of combining two AM processes advances the state-of-the-art by creating lightweight metal-ceramic cellular composites with designed mesostructure, which is not able to be done with existing manufacturing

technologies. The resultant cellular composite structures combine the mechanical characteristics of ceramic materials to enhance the final properties of the manufactured part providing higher strength, stiffness, wear resistance, lower thermal coefficient of thermal expansion [28]. The proposed process can be seen in Figure 1.2.

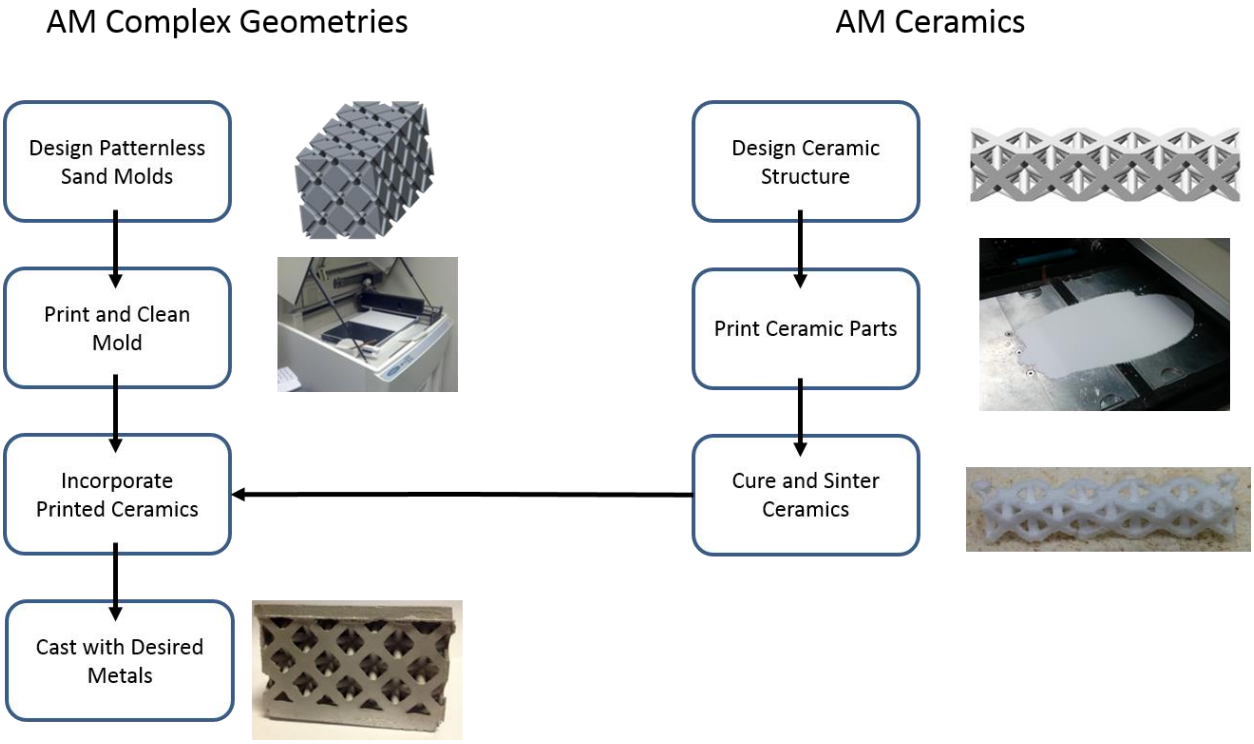

Figure 1.2. Proposed procedure for creating a novel process for manufacturing complex MMCs

The work to realize metal matrix composites by two separate AM processes is guided by a primary research goal:

Primary Research Goal
To develop and gain an understanding of a manufacturing process to cast complex metal-ceramic composite geometries via Binder Jetting technology.

Because this process has not been studied extensively, additional research must be explored to better comprehend the proposed manufacturing process. An understanding of the process will be gained by exploring the effect of the mold on the final part (Research Question 1), the manufacturing constraints (Research Question 2), and ceramic manufacturing for complex MMCs via AM (Research Question 3).

1.2. Research Question 1: The Effect of Printed Mold on Part Quality

Although AM of sand molds has enabled designers to commercialize and implement this technology in industry, little is known about the materials systems' effects on metal castings. Knowledge of how the process affects the resultant material properties is critical in the design of the cellular materials. By understanding these material properties, the author can predict the outcome of the final metal properties, for example, porosity and surface roughness. Unfortunately, the existing understanding of sand molds on metal casting cannot be directly applied to AM sand materials systems, as their working materials are dissimilar. Furthermore, prior research that explores the effects of 3D printable mold material on castings was limited. Instead, most of prior research was focused in studying the molds produced by ZCast® [18,20,21]. Due to the limited knowledge on the interactions of sand molds created by the Binder Jetting process on cast parts, Research Question 1(RQ1) was formulated.

Research Question 1
How do castings made from two different 3D Printed sand molding materials compare to those of traditional no-bake molding methods?

Because the ExOne material system incorporates a two part binder system into a silica sand molding material similar to traditional no-bake, it is hypothesized the ExOne printed parts will have similar properties with those made with the traditional approach. In contrast, ZCast® uses a single part binder system that requires significantly more binder in the creation of molds for castings [29]. From the existing understanding of traditional sand and the effects on cast metals, Hypothesis 1 is proposed.

Hypothesis 1
Castings from no-bake and ExOne molds will produce similar results, as compared to those produced via ZCast®.

1.3. Research Question 2: Manufacturing Constraints

In order to utilize these manufacturing methods to generate complex cellular structures, the designer must have an idea of the constraints imposed on the process. Although not as limiting as traditional manufacturing methods, the Binder Jetting process has inherent constraints in both build and post-processing steps. An understanding of these constraints will enable the designer

to model their part more confidently. One constraint to examine is the minimum part feature size that can be achieved with the process. There are two aspects of the process that might limit the achievable feature size: (i) metal casting and (ii) depowdering the printed mold. Although the printing process may be constrained by printed feature sizes, post-processing of molds contribute greater limitations on the overall manufacturing process.

When poured in a mold, molten metal eventually freezes based on the thermal gradient of the mold wall in contact with the metal and the thermal conductivity of the mold material. Freezing is accelerated when the metal flow encounters small channels due to a larger modulus (Volume to Surface Area) based on Chvorinov's rule [30]. Fortunately, freezing of cast metals have been studied extensively and can be modeled using casting melt flow analysis software.

The constraint on minimum feature size might also come from the post-processing phase of mold cleaning. Specifically, it might be possible that the constraint on feature size is dependent on the smallest area of a mold that can be successfully depowdered in complex geometries. Although it may be printable, it is possible that unpatterned sand cannot be removed. Depowdering small channels is material and machine dependent and can be tested experimentally to determine the smallest cleanable area. After determining this, modeling solidification of flow as it passes through multiple angles for complex geometries will be studied.

No previous research has been published on identifying the smallest cleanable area using ExOne technology and solidification of flow in complex AM molds. Research Question 2, and its associated sub-research questions, is presented to guide the development of a research plan to fill this gap in knowledge.

Research Question 2	
What are the resolution constraints of the Binder Jetting printing process and how is it limited by metal depowdering and solidification?	
Sub Question 2.1	**Sub Question 2.2**
How are the resolution constraints limited by depowdering complex geometries?	*How are the resolutions constraints limited by metal solidification through complex geometries?*

Vayre and coauthors (2013) conducted studies on depowdering of metallic round channels printed via Electron Beam Melting (EBM). From this study, an equation was determined to aid designers when considering the post processing of loose unsintered powders [31]. They determined that the effect of removal followed a linear trend in the experimental data which leads to Hypothesis 2.1.

Hypothesis 2.1
The cleaning length of circular channels printed via Binder Jetting is dependent on the smallest cleanable diameter, cleaning diameter, and connectivity.

There currently is limited literature that models flow of metal through channels of complex geometries due to the manufacturing constraints imposed by the molding process. There are however standard testing equipment for determining the fluidity of metals to determine the length metal can flow through a channel before freezing [30]. Utilizing basic knowledge of metal flow and solidification, Hypothesis 2.2 is developed.

Hypothesis 2.2
Complex geometry will promote freezing due to an increase in path length and change in direction.

1.4. Research Question 3: The Metal-Ceramic Interface

In order to produce MMCs using two separate AM processes, manufacturing process parameters need to be established for printing ceramics. Upon successful printing of ceramics, a proof of concept MMC will be fabricated by combining the printed ceramics and MMCs. Finally, the parts will be mechanically tested using standard three point bend tests.

1.4.1. Incorporation of Ceramics to Create Metal Matrix Composites

As discussed in Section 1.1, Binder Jetting enables the production of ceramic materials. Using this capability, one is able to create intricate geometries for application-specific designs. The author will explore utilizing AM for the manufacture of ceramics that will be embedded into sand molds for the creation of metal-ceramic composites. The manufacturing process parameters of the MMCs will be evaluated as well as their effects on flexural strength and flexural modulus. These effects are guided by Research Question 3.

Research Question 3
How are mechanical properties (flexural strength and modulus) of MMCs created via Binder Jetting and Metal Casting affected by the manufacturing process parameters (powder preparation, sintering temperatures, and casting process)?

Upon successful printing of a ceramic and embedded in a cast metal matrix, the manufacturing process can be applied further to embedding of ceramics with complex geometries in printed sand molds. This enables the user more control of the manufacturing process.

Hypothesis 3
MMCs produced from printed ceramics with higher density and good bonding (mechanical or chemical) at the metal-ceramic interface will have better mechanical properties (flexural modulus and strength) compared to the matrix material alone (zinc).

1.5. Dissertation Roadmap

The format of this dissertation includes publications and planned publications incorporated as chapters. Chapter 1 provided an introduction to cellular materials along with the primary research goal and research questions driving this work. Binder Jetting and sand casting were proposed as an alternative manufacturing method for realizing ceramic-metal composite cellular structures with a designed mesostructure.

Next, Chapter 2 details the proposed manufacturing process chain to produce a proof of concept metal-ceramic composite cellular structures. Analytical modeling was performed on the cellular structure to determine the blast effects of the resultant structure. In Chapters 3, the author compares traditional molding techniques to printed ZCast® to determine the effects of gas generation via binder on final castings. Because the printed ZCast® molds had a large effect on castings, and additional study (Chapter 4) was conducted to determine the effects of ZCast® and second printed material (ExOne Binder Jetting AM) on castings (Research Question 2). Final cast properties such as microstructure, porosity, hardness, density, surface roughness, and tensile strength as well as molded sand tensile strength were studied. In Chapter 5, the author studied the geometry constraints imposed by Binder Jetting patternless molds (Research Question 2). Two critical sources of process constraints on part geometry were determined and examined: (i) depowdering unbound material from intricate casting channels and (ii) metal flow and

solidification distances through complex mold geometries. Research Question 3 is examined in Chapter 6 with details of advanced ceramic manufacturing and characterization and by the creation of a proof of concept MMC. In Chapter 6, a new process idea was explored to print ceramics and combine with metal casting to create MMCs. The manufacturing process parameters were studied and the resultant proof of concept MMC was tested on the basis of flexural strength and flexural modulus (Research Question 3). Additionally, the metal-ceramic interface was examined. Finally, the conclusions and broader impacts are discussed in Chapter 7.

Table 1.1 lists the publication title, incorporated as chapters, with its respected publication plan.

Table 1.1. Chapter/Publication Plan

Publication Title/Chapter	Submission Status	Journal
Lightweight Metal Cellular Structures Fabricated via 3D Printing of Sand Cast Molds (Chapter 2)	*Accepted (2015)*	Advanced Engineering Materials
Mitigating Gas Defects in Castings Produced from 3D Printed Molds (Chapter 3)	*Accepted (2014)*	International Foundry Research
The Effects of 3D Printed Molds on Metal Castings (Chapter 4)	*Planned (2015)*	International Journal of Metalcasting
Effects of Complex Geometries on Depowdering and Solidification in Sand Molds Fabricated via Binder Jetting (Chapter 5)	*Planned (2015)*	Additive Manufacturing
Binder Jetting Advanced Ceramics for Metal-Ceramic Composite Structures (Chapter 6)	*Planned (2015)*	International Journal of Advanced Manufacturing Technology

1.6. Summary of Proposed Manufacturing Process Goal and Scientific Contributions

Successfully answering the presented research questions will result in a better understanding of the proposed manufacturing process capable of producing metallic-ceramic cellular structures with designed mesostructure. Leveraging previous research in ceramic-metal composites, additive manufacturing, and metal casting, the author evaluates key relationships for combining

two distinct additive manufacturing processes to integrate ceramics manufactured via Binder Jetting with printed molds for metal infiltration. Having control of these parameters enables the user to manufacture parts that can be tailored for specific applications that contain higher strength, stiffness, wear resistance and lower thermal coefficient of thermal expansion [28]. A summary of the overall goal is presented as well as the research questions, hypotheses, methods, and impact motivating this work in Table 1.2 - Table 1.5.

Table 1.2. Overall research goal for manufacturing MMCs with Binder Jetting AM

Overall Goal
To develop and gain an understanding of the manufacturing process of casting of complex metal-ceramic composite geometries via Binder Jetting technology by identifying manufacturing constraints and determining materials relationships.

Table 1.3. The Effects of 3D Printed Molds on Metal Castings (Research Question 1, Hypothesis 1, Methods, and Impact)

Research Question 1
How does printed sand, manufactured via Binder Jetting, affect the metal properties being cast?
Hypothesis 1
Castings from no-bake and ExOne molds will produce similar results, as compared to those produced via ZCast®.
Methods
Tests will be performed to determine the effects of sand manufactured via Binder Jetting on cast metal properties: • *Binder burnout tests to determine binder percentage – binder directly correlates to the amount of off-gassing* • *Sieve Analysis – Particle size* • *Surface Roughness* • *Micrographs - Porosity and dendrite arm spacing* • *Density* • *Hardness* • *Compression*
Impact
The characterizations will provide new understanding of how binder jetted sand affects cast metal properties.

Table 1.4. Effects of Complex Geometries on Depowdering and Solidification in Sand Molds Fabricated via Binder Jetting (Research Question 2, Hypotheses, Methods, and Impact)

Research Question 2	
What are the resolution constraints of the Binder Jetting printing process and how is it limited by metal solidification and depowdering?	
Sub Question 2.1	**Sub Question 2.2**
How are the resolution constraints limited by depowdering complex geometries?	*How are the resolutions constraints limited by metal solidification through complex geometries?*
Hypothesis 2.1	**Hypothesis 2.2**
The cleaning parameters of circular channels printed via Binder Jetting are dependent on the length to diameter ratio of the channel.	*A complex geometry will promote freezing due to an increase in path length and change in direction.*
Methods	**Methods**
Controlling the channel diameters through set length printed parts and cleaning with constant air pressure. Length will be changed as a second variable to verify length to diameter ratio.	*Using modeling (ProCast), different angles of flow will be used to determine fill of casting. These will then be experimentally tested.*
Impact	**Impact**
It is necessary to understand the smallest cleanable space when designing molds for castings. Although printable, the molds might not be cleanable.	*Freezing is currently accounted for in traditional casting methods, but has not been studied in complex molds produced by Additive Manufacturing. An understanding of freezing will be considered in structures that previously were not able to be manufactured.*

Table 1.5. Binder Jetting Ceramics for Metal-Ceramic Composite Structures (Research Question 3, Hypotheses 3, Methods, and Impact)

Research Question 3
How are mechanical properties (flexural strength and modulus) of MMCs created via Binder Jetting and Metal Casting affected by the manufacturing process parameters (powder preparation, sintering temperatures, and casting process)?
Hypothesis 3
MMCs produced from printed ceramics with higher density and good bonding (mechanical or chemical) at the metal-ceramic interface will have better mechanical properties (flexural modulus and strength) compared to the matrix material alone (zinc).
Methods
By evaluating printing parameters experimentally, flexural strength and modulus, and metal ceramic interface.
Impact
The evaluation of a new printed ceramic and manufacturing process to the AM community. Additionally, a new manufacturing process is used for fabrication of ordered cellular ceramics with a metal matrix MMCs.

2. LIGHTWEIGHT METAL CELLULAR STRUCTURES VIA 3D PRINTING OF SAND CAST MOLDS

2.1. Motivation

As military vehicles and infrastructure face ever increasing lethal threats, there is continued interest for lightweight ballistic armor that will improve vehicle performance and safety and decrease vehicle transportation costs. Cellular materials (metallic bodies with inter-dispersed voids) are a promising class of structures for addressing this need. Cellular materials offer high strength accompanied by low density [32] and can offer high stiffness, good impact-absorption, and thermal and acoustic insulation [2].

Recent cellular material research has focused on designing the mesoscopic topology (the geometric arrangement of the solid phases and voids within a material or product of the size range of 0.1 to 10 mm) in order to effectively support and improve multiple design objectives [33–35]. Example applications of designed cellular mesostructure include a jet engine combustor liner that has sufficient strength to withstand extreme pressures and stresses from thermal expansion while still maintaining open cells that allow for active cooling via forced convection [36] and a lightweight blast resistant panel that efficiently absorbs impact from large impulse forces [4].

Due to their complex internal geometry, manufacturing a component with cellular mesostructure is impossible with traditional subtractive machining. As such, researchers have looked to advanced manufacturing technologies to produce this unique class of materials.

2.1.1. Traditional Cellular Material Manufacturing Methods

Stochastic metal foaming processes feature generating gas in liquid metal (Alporas, Hydro/Alcan/Combal, Gasar/Lotus processes), or by mixing metal powders with a blowing agent which is then compacted and melted (Alulight/Foaminal techniques) [32]. While these processes result in structures with cells of random shape, morphology, and distribution [5], they “place material in locations where it contributes little to material properties (other than density)” [34]. The largest limitation of stochastic cellular structures is the complete lack of control that a designer has over the topology of the mesostructure; the techniques do not provide repeatable, or

even predictable, results [2]. Furthermore, these techniques limit a designer in the types of macrostructure that can be produced.

Ordered cellular structures are characterized by a periodic unit cell or by a repeating structure throughout the part and are therefore predictable as compared to stochastic materials. Compared to stochastic materials, ordered structures have superior mechanical properties, including energy absorption, strength, and stiffness [1]. Ordered cellular materials have been made by stamping or crimping thin sheets of metal into a corrugated shape and then joining them to create periodic structures [37]. Alternatively, they have been created by joining and bonding slotted metal sheets [38], extrusion and electro-discharge machining [39], and weaving and brazing metal filaments to form a periodic textile [40,41]. In the early 2000's Jamcorp Inc. explored the use of sand casting to process Lattice Block Materials (LBMs) [42]. The company used specially made preforms to create trussed structures. Due to the difficulty in fabricating complex patterns for creating the sand molds, the resulting parts had a planar macrostructure, and a fixed (pyramidal) mesostructure. To alleviate these geometric constraints, the company also investigated casting of LBMs. However, the resulting components suffered from porosity due to the inability of the fluid to access all parts of the truss structure [37,43]. Although these fabrication techniques for producing ordered cellular structures offer repeatable part quality, they limit the macrostructure of resulting parts to planar geometries [44], and constrain a designer to the use of a specific homogeneous mesostructure throughout a part.

2.1.2. Context: Producing Cellular Materials via 3D Printing and Sand Casting

While the aforementioned manufacturing techniques are capable of producing cellular materials, they in some way limit the designer's ability to selectively prescribe the location of material throughout the part in order to achieve optimal performance. An ideal cellular material manufacturing technique would enable the creation of any part macrostructure and mesostructure across the entire part volume. With this as an overall goal, the author introduces a cellular material manufacturing process chain that incorporates 3D Printing and sand casting. Specifically, the author's process entails use of Binder Jetting Additive Manufacturing (AM; also referred to as "3D Printing" or 3DP) technology to first print a cellular sand mold, which is then used in a sand casting operation, resulting in a cast metal cellular artifact.

Previous efforts in using AM to fabricate cellular materials are reviewed in Section 2. An overview of the author's hybrid 3DP/casting process chain is presented in Section 3. A sample part geometry – a sandwich panel featuring an octet truss unit cell – is presented as a case study to illustrate (i) geometric freedom chain and (ii) structural performance of designed and fabricated components that can be made by the process chain. Preliminary results for impact numerical simulation of the octet truss sandwich panel are described in Section 4. Experimental results of quasi-static tests on manufactured artifact, and results of numerical simulations of the impact response of cellular and solid structures are provided in Section 5. Finally, closure and future work is offered in Section 6.

2.2. Fabricating Cellular Materials via Additive Manufacturing

Given the existing limitations of cellular material manufacturing processes, and the design constraints that they impose on the resultant cellular parts, the goal of this work is to develop a manufacturing process capable of producing metallic cellular structures with a designed mesostructure. To achieve this goal, the author uses AM for providing the design freedom needed to overcome existing manufacturing processes' limitations.

2.2.1. Introduction to Additive Manufacturing (AM)

The AM provides freedom of design in creating complex parts by building them in a layer by layer fashion. In the AM process (Figure 2.1), a part is modeled in a computer aided design (CAD) program and exported as a .stl file. The file is then imported into slicing software and divided into layers. Additionally, the software determines the correct location of support material for overhanging structures. After the part is printed, the 3D object is removed for use.

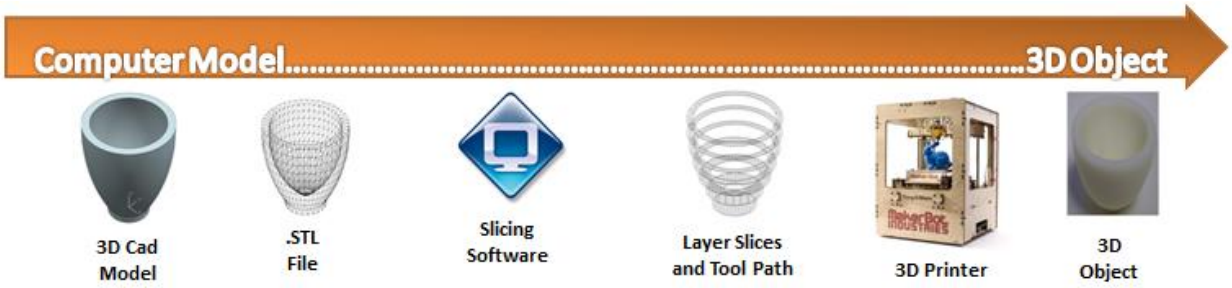

Figure 2.1. AM process from CAD model to 3D object

2.2.2. AM & Metal Casting Hybrid Processes

To address the geometric constraints imposed by traditional casting and pattern fabrication, a few hybrid manufacturing processes have been proposed. In these processes, AM techniques are used to fabricate polymer patterns, which are then used to create ceramic molds for metal casting. For example, Hattiangadi and Bandyopadhyay employed Fused Deposition of Ceramics (FDC) to produce geometrically complex ceramic molds for casting with metal [45]. Similarly, Chiras et al. used AM to create truss structure patterns for investment casting process with a high fluidity Be-Cu alloy [46]. In addition to extrusion, Material Jetting AM (3D Systems' Multi-Jet Modeling) has been used to fabricate wax patterns for a lost wax casting technique to fabricate complex heat exchanger designs [47]. By combining AM and investment casting, metallic complex cellular structures can be developed with designed mesostructure. However, such processes have following limitations:

- *Scale:* Current AM systems are limited in their build volume and many of the recently proposed cellular structures are only able to create a single build layer.
- *Burnout:* Materials used in the AM process are not suitable for the burnout process in investment casting. For example, photopolymer from the Multi-Jet Modeling and Stereo-lithography processes, have much higher thermal expansion than traditional wax, and typically result in cracked investment molds.
- *Cleaning and Cost:* The ceramic slurry used for investment casting can be difficult to remove from the cellular materials' intricate geometries, and in many cases requires chemically leaching the residual material from the final part, which increases the manufacturing cost.

2.2.3. Fabricating Metallic Cellular Materials with Direct-Metal Additive Manufacturing

Direct-metal AM processes, which selectively scan an energy source, such as a laser or an electron beam spot over a metal powder bed, are capable of fabricating fully-dense metal artifacts without the need for additional post-processing. Selective Laser Melting [10,11], Electron Beam Melting [12,13], and Direct-Metal Laser Sintering [14] have all been employed in research targeted towards fabricating cellular materials. For example, Yang et al. created auxetic lattice structures with electron beam melting using Ti-6Al-4V [13]. Four designs were tested in

compression to compare the effect of density and Poisson's ratio on strength and modulus. These results were found to compare well with predictions from analytical models for auxetic structures.

While these processes have been successfully used to fabricate parts with cellular geometries, their ability to make parts of designed mesostructure is limited by inherent process constraints [7]:

- *Limited Material Selection*: Direct-metal AM processes have a limited set of working materials; for example, aluminum alloys are challenging to process due to high thermal conductivity and high optical reflectivity.
- *Residual Stresses and Support Structures*: Fabricated parts also suffer from residual stresses [48,49] and/or require the use of support structures or anchors when fabricating large parts with significant overhanging geometries [50]. The required use of support scaffolds (which must be manually removed later) is especially limiting when trying to create large cellular geometries, as they would be difficult to remove from the interior cells.
- *Cost and Throughput:* These processes are relatively expensive and have a low throughput due to their use of a 1D energy patterning mechanism (i.e., a laser).
- *Part Size*: Due to the difficulty in effectively managing the thermal loads in a powder bed, direct-metal powder bed fusion AM techniques are not capable of fabricating cellular structures of a large scale. The largest build box on a commercially available machine is 40 x 40 x 40 cm. This prevents these technologies from fabricating large scale cellular materials that would be well suited for applications such as vehicle armor.

2.2.4. Fabricating Metallic Cellular Materials via Binder Jetting Patternless Sand Molds

Binder Jetting is an AM technology that creates artifacts through the deposition of binder into a powder bed of raw material. Once a layer has been printed, the powder feed piston rises, the build piston lowers, and a counter-rotating roller spreads a new layer of powder on top of the

previous layer. The subsequent layer is then printed and is stitched to the previous layer by the jetted binder. A schematic of the Binder Jetting AM process is given in Figure 2.2.

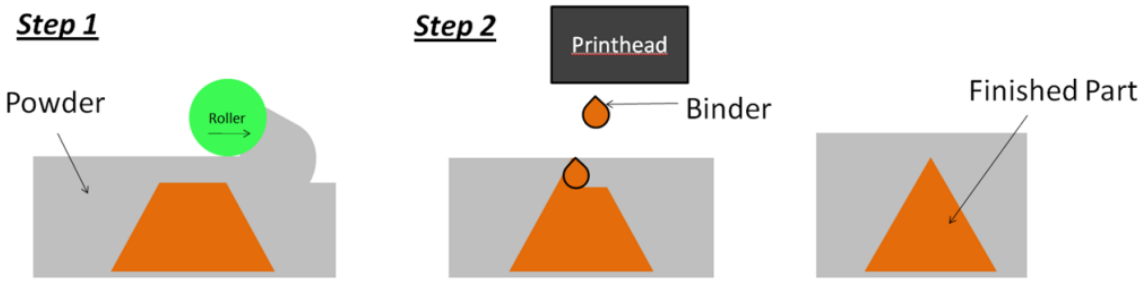

Figure 2.2. Schematic of Binder Jetting AM Process

By selectively printing binder into a bed of foundry sand layer-by-layer, Binder Jetting can be used to directly fabricate molds for metal casting. As with all AM processes, 3DP offers tremendous design freedom for altering mold geometry; with this technology, molds can be fabricated with integrated gating systems, embedded cores, and without the need for a pattern. The technology is commercially offered by ZCorp's ZCast material [51], ExOne's S-Max and M-Flex machines [52], and VoxelJet [53]. Direct digital fabrication of sand molds for casting eliminates the costs associated with pattern tooling and is thus ideal for low volume production [54,55].

Binder Jetting is a suitable AM process for the fabrication of complex cellular geometries when compared to other AM processes. These factors include:

- *Scalability:* the use of 2D material deposition (i.e., large inkjet print heads) provides relatively short build times when compared to other 1D deposition processes (e.g., powder-bed fusion direct-metal processes).
- *Modular Molds:* Molds created from the Binder Jetting process provide the ability to be modular, meaning they can be built and assembled to create a larger homogeneous metal part.
- *Wide Range of Materials*: Any castable metal compatible with molding materials may be used for the creation of parts. For example, silica sand and furan binder used in ExOne technology can withstand materials with temperatures up to cast steel.

Additionally, because this is an indirect process, other materials, such as refractories with much higher melting points, may be introduced into the mold during casting.

- *Microstructure Control*: Binder Jetting gives the user the potential to control microstructure of materials through better control of heat transfer by use of chills or varying wall thickness of outer molds.
- *Mold Package Optimization:* Producing molds via Binder Jetting combined with solidification modeling, permits the user to optimize metal flow for better quality castings – for example, by creating a hyperbola shaped down-sprue to decrease the chance of turbulent entrainment while pouring [56] and thus defects in castings. In contrast, the properties of Direct-metal suffer from residual stresses due to large thermal gradients during the manufacturing process which are difficult to predict.
- *Support Material Constraints:* There is no need for a separate support material that must be removed in post-processing [57]. Overhanging structures are supported by the unbound powder within the powder-bed during fabrication. Once printing is complete, the unbound powder is removed from the printed part using compressed air or vacuum.

Existing research on the use of Binder Jetting for metal casting has been primarily focused on case studies and determining properties of resultant materials [16–20]. The technology has been shown to be effective in obtaining cast prototypes with dimensional tolerances that are consistent with metal casting processes [21]. AM technologies have been used in foundry practice to produce patterns and core boxes for sand casting [22]. In addition, AM processes have enabled the direct production of sand molds without the need for fabricating a pattern. From previous work, proof-of-concept cellular structures were successfully produced using ZCorporation printer and ZCast sands [25]. From this initial exploration, it was discovered that the resultant castings suffered from large voids due to off-gassing of the large amount of printed binder. In this paper, the author report on the results from the use of a refined process chain, which features a sand system with significantly less binder (as analyzed in previous work [29]), and thus less off-gassing. In addition, the results of analytical impact and quasistatic modeling and experimental quasistatic tests on realized parts are reported. In addition to the work by the author, studies in which part complexity is explored are limited to case studies in which existing products are cast with redesigned mold and core shapes [26,27].

2.3. Binder Jetting of Sand Casting Molds for Cellular Material Fabrications

The proposed procedure for creating cast metal parts with a designed mesostructure via indirect 3D printing follows five distinct steps: (1) digital mold design, (2) 3D Print sand mold, (3) depowder and clean the printed mold, (4) cast metal into printed mold, and (5) clean the cast metal part. With this process, the author was able to create a wide variety of cellular geometries from a range of castable metals. In this section, the author further describes the process, and its ability to fabricate complex cellular structures, through the creation of example part geometry: a sandwich panel with octet truss cellular structure.

2.3.1. Digital Mold Design

The Binder Jetting process allows for simple creation of complex mold structures from a 3D solid model. The complex mold can be designed in CAD or using software that is specialized for modeling cellular materials (e.g., netfabb's Selective Space Structures (SSS) software [58]). To create the final mold, the designed truss structure is Boolean-subtracted from a prismatic solid. An example of this process is shown in Figure 2.3. Using CAD, a single unit cell is designed and patterned to create the desired structure. A repeating octet truss structure is designed using netfabb SSS software; the corresponding mold is created via a Boolean subtraction from a 10 x 5 x 5-mm solid cube.

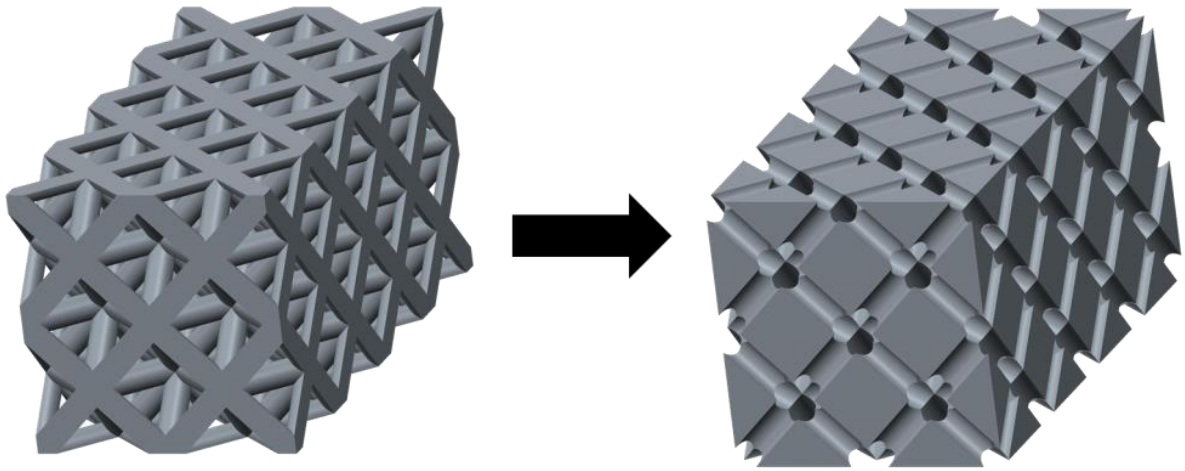

Figure 2.3. Desired final shape and necessary printed mold (after Boolean subtraction)

2.3.2. Mold Fabrication

With the digital creation of the mold completed, and exported to a .STL format, the file is imported into the 3D printer's accompanying software, where it is oriented, scaled, and positioned. As with other powder-bed processes (with direct-metal being the exception), Binder Jetting printing allows for the build volume to be completely filled with parts, thus further increasing the throughput of the process, and further improving the time-to-cast compared with traditional casting mold creation.

For this work, an ExOne S-Print machine is used for printing complex cellular molds. The ExOne technology utilizes a furan binder system which binds refined coated silica sand and has no thermal curing cycle. The silica sand is capable of casting ferrous metals, such as steel, allowing for greater variety in the final casting product. While printing, the part's atmosphere conditions including temperature and humidity are controlled in order to produce consistent molds. After printing, excess powder is vacuumed from the internal passageways of the complex mold. An example of the completed mold is given in Figure 2.4.

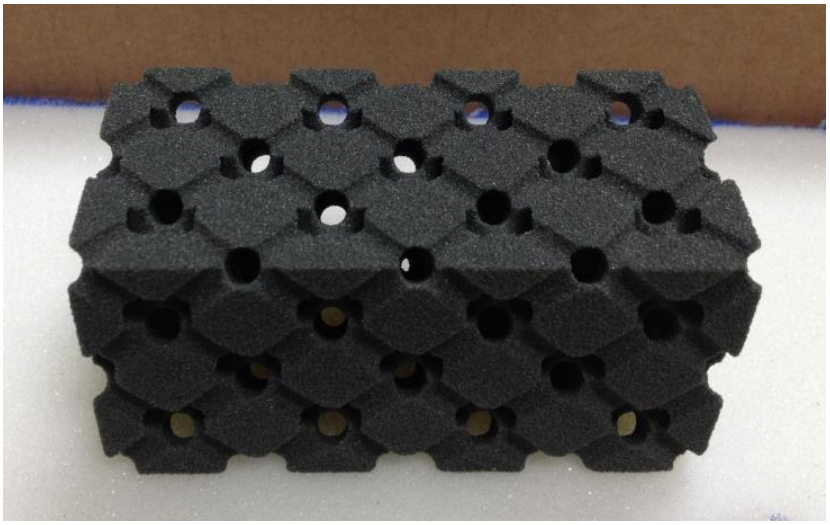

Figure 2.4. Complex cellular geometry printed by ExOne

Although Binder Jetting enables the direct production of entire molds, the printed molds for this example were used as sand cores, with chemically bonded sand as the casting cavity (as shown in Figure 2.5). An outer mold, consisting of a downsprue, gates, and runners, was formed to enable the filling of the printed mold. These mold elements direct the molten metal flow as

desired; i.e., filling the printed mold from the bottom to the top. The design of the outer mold also allows for additional characteristics to be added to the desired mesostructure; in these examples, a gap between the outer mold and the printed mold creates a solid plate both above and below the designed mesostructure.

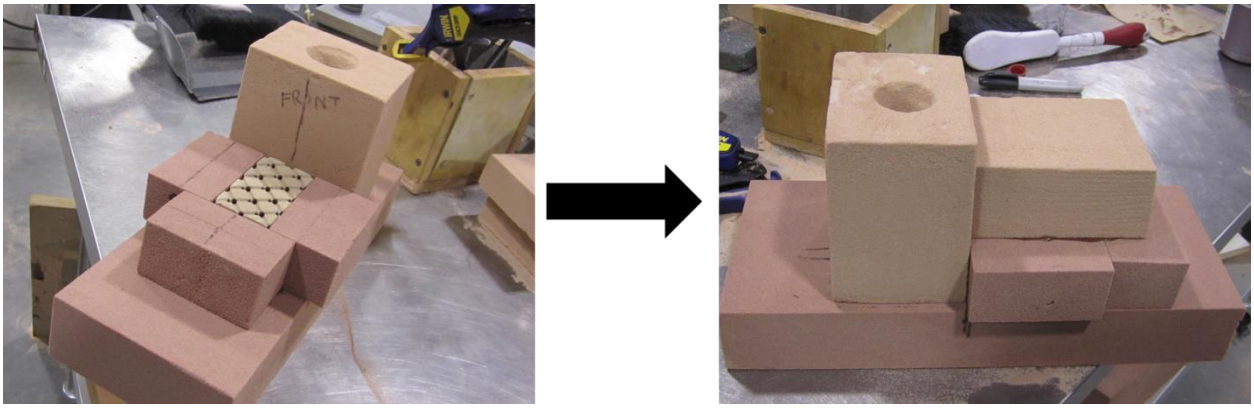

Figure 2.5. Printed mold encased by traditional no-bake sand

2.3.3. Part Creation via Metal Casting

Once the mold is formed, it can be filled with any traditional casting alloy. For this example, castings were poured in A356 alloy, a common aluminum alloy used in safety critical automotive applications due to its good combination of mechanical properties and castability. A356 ingot was melted in a SiC crucible using an electrical resistance furnace. The temperature of the metal in the furnace was limited to a maximum of about 760 °C (1400 °F); molten metal temperature was measured using an immersion thermocouple. Approximately 2 minutes before pouring, TiBor (Al-5wt%Ti-1wt%B) was added for grain refinement and Al-10wt%Sr was added for silicon modification. The castings were poured along with a chilled spectrometer sample for determining chemistry. The actual pouring temperature was not measured but is expected to be ~10-20 °C lower than the temperature in the furnace (actual pouring temperature: ~740-750 °C, ~1365-1380 °F).

The gating system for metal pouring was designed to fill the mold as quickly as possible and had sufficient head height to fill the complex core. A lower flow rate increases the chance of solidification before complete fill. The part was bottom-gated, and metal was fed through a one inch down sprue fabricated from the chemically bonded sand-outer mold. Castings were

relatively easy to clean. Sufficient heat was available to burn-out enough of the binder such that only light pressure from a pointed instrument was enough to break the mold apart. No sand burn-on or metal penetration into the mold was noted. Sand or shot blasting was not necessary to produce a clean casting.

The cleaned castings were given a standard T6 heat treatment (solution treatment followed by artificial aging) to produce a good combination of strength and ductility. The castings were heated to 540 °C (1005 °F) in an air circulating furnace and held for about 11-12 hours at constant temperature to spheroidize the silicon particles and put the strengthening elements into solid solution. At the end of the high temperature cycle, the castings were removed from the furnace and quenched in a bucket of room temperature water. Next, the castings were purposely aged at 154 °C (310 °F) for 5 hours. During heat treatment, the actual casting temperature was measured using a chromel-alumel thermocouple attached to the casting.

2.3.3.1. Metal Casting Results

Upon casting, fully homogeneous sandwiched cellular prototypes were created. Preliminary results had relied on ZCorp's Spectrum 510 for the creation of cellular structures and resulted in poor casting quality (Figure 2.6a) due to off-gassing associated with high binder content used for the ZCast material system [25,59]. Large voids were present, producing incomplete structures and therefore unusable parts [25,59]. When using the ExOne system (as described in Section 2.3.2), resultant castings were completely filled (Figure 2.6b).

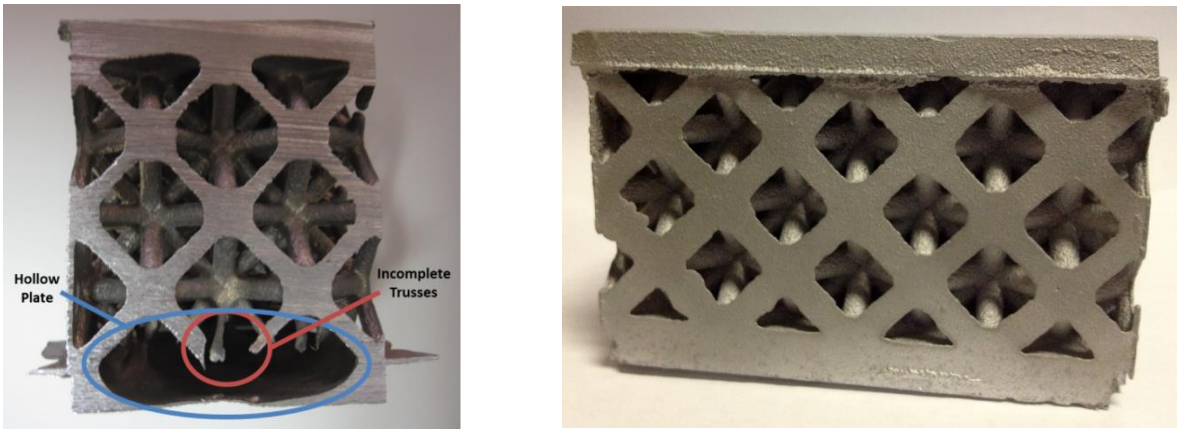

a) **b)**

Figure 2.6. a) Large voids produced from off gas in ZCast System [25] **and b) complete structures produced by ExOne Systems**

One of the distinct advantages of cellular materials is decreased weight. The final parts produced by this method clearly demonstrate this potential reduction. The cubic piece, for example, is nominally 4,297 cubic centimeters (262.19 cubic inches) in volume, if the cubic space were entirely filled and there were no plates on either side of the truss section. With the ordered mesostructure, the part volume is decreased to 99.31 cubic centimeters, only 23% of the initial volume. At a density of 2.67 g/cc for the A356 alloy, the truss part would only have a mass of approximately 265 g.

2.4. Quasi-static testing and numerical simulations of deformations

To characterize mechanical properties of the cellular structure, quasi-static compression tests were performed on both solid cylinders and cellular truss structures manufactured by the proposed Binder Jetting process. Also quasi-static and dynamic compressive deformations of the cellular structure were numerically simulated by using the commercial software ABAQUS [49] based on the finite element methodology. The computed results for quasi-static deformations are found to agree well with the corresponding experimental findings.

2.4.1. Quasi-static Tests on Solid Cylinders

Six 25.4 mm long x 12.7 mm diameter cylinders of the cast material were tested under quasi-static compression. Two cellular structures, 50.8 x 50.8 x 50.8 mm with 6.25 mm thick face sheets, were also tested in quasi-static compression. A screw driven testing machine (Instron)

with a special compression loading fixture was employed to compress the structures at the rate of 1.5 mm/min at room temperature, and the axial load versus the crosshead displacement was recorded. The true stress vs. true strain curves for the six cylinders found from the test data are exhibited in Figure 2.7. It is clear that the curves for five specimens are very close to each other. Young's modulus for the material was determined by fitting a straight line by the least squares method to the initial portion of the true axial stress-true axial strain curves. However, before doing so, the stress-strain curves were corrected for the initial toe regions which could be attributed to the initial slack in the loading frame, e.g., see the corrected curve in Figure 2.8. Young's modulus for specimen 6 is found to be 21 GPa and for the six specimens tested the mean value of Young's modulus is calculated to be 20 GPa with a standard deviation of 1.1 GPa.

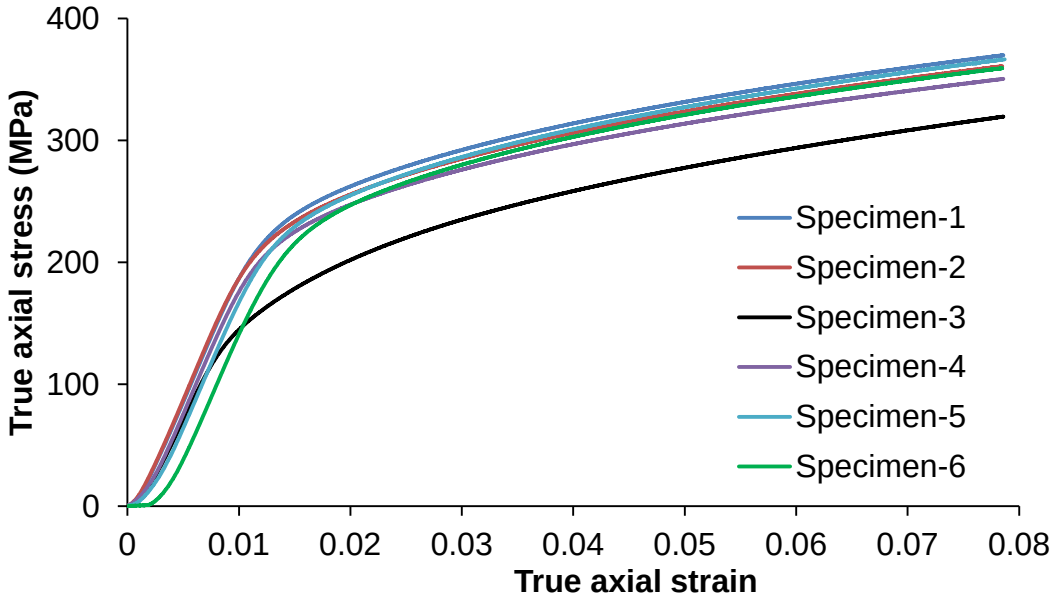

Figure 2.7. Experimental true axial stress vs. true axial strain curves for A356 alloy specimens

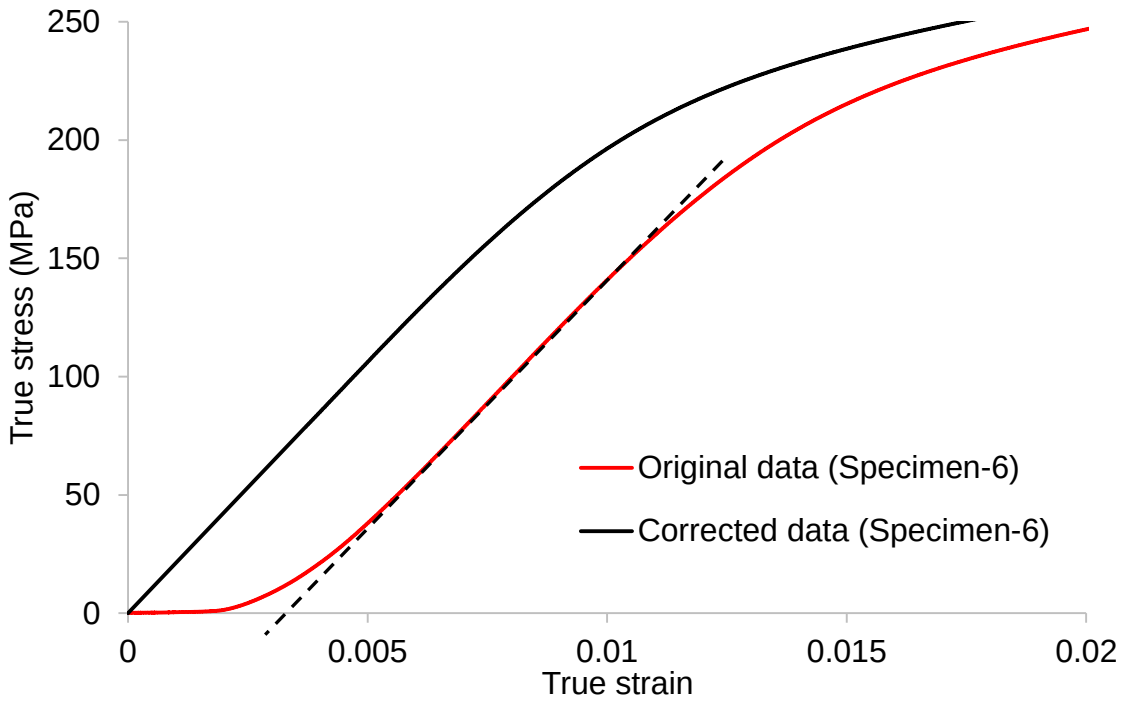

Figure 2.8. Correction for the initial toe region in the stress- strain data for specimen 6

For numerically simulating deformations till failure of the cellular structure, stress-strain relations beyond the elastic limit are needed. Here it is assumed the material to be isotropic, homogeneous and Hookean for elastic deformations and obeying the von Mises yield criterion with the yield stress depending only upon the effective plastic strain. The power law relationship given by Equation (2.1) is used to describe the strain hardening rule. In Equation (2.1) ε^{pl} is the equivalent

$$\boldsymbol{\sigma_y = A + B\left(\varepsilon^{pl}\right)^n} \qquad \textbf{(2.1)}$$

plastic strain, the parameter *A* equals the initial yield stress of the material, and parameters *B* and n described its strain hardening, measured at room temperature. Values of the material parameters *A*, *B*, and *n* obtained by curve fitting computed values for homogeneous uniaxial compressive deformations to the experimental axial stress-axial strain curve of Figure 2.7 are: *A* = 162 MPa, B = 355.7 MPa and *n* = 0.304. Poisson's ratio of the material is taken to be 0.3, and a material point is assumed to have failed when the effective plastic strain there equals 0.5. The

value of the failure strain was iteratively found till the computed axial stress – axial strain curve was found to be close to the experimental one.

2.4.2. Quasi-static Tests on Cellular Structures

A photograph of the virgin test specimen placed in the Instron machine is shown in Figure 2.9, and that of the failed specimen in Figure 2.10. The axial compressive load vs the axial displacement curve for the cellular structure is exhibited in Figure 2.11. The test results for the 1st specimen indicated that the structure can support a maximum load of 123.2 kN before trusses in the structure began to fail. The steps in the load-displacement curve were due to the incremental failure of the trusses. The force then begins to increase after the cellular voids collapse from the failed trusses. However, for the 2nd specimen, when the load reached 133.45 kN (Figure 2.11) the software in the Instron machine stopped the test before the specimen began to fail. Because of plastic deformations of the structure, it could not be re-tested.

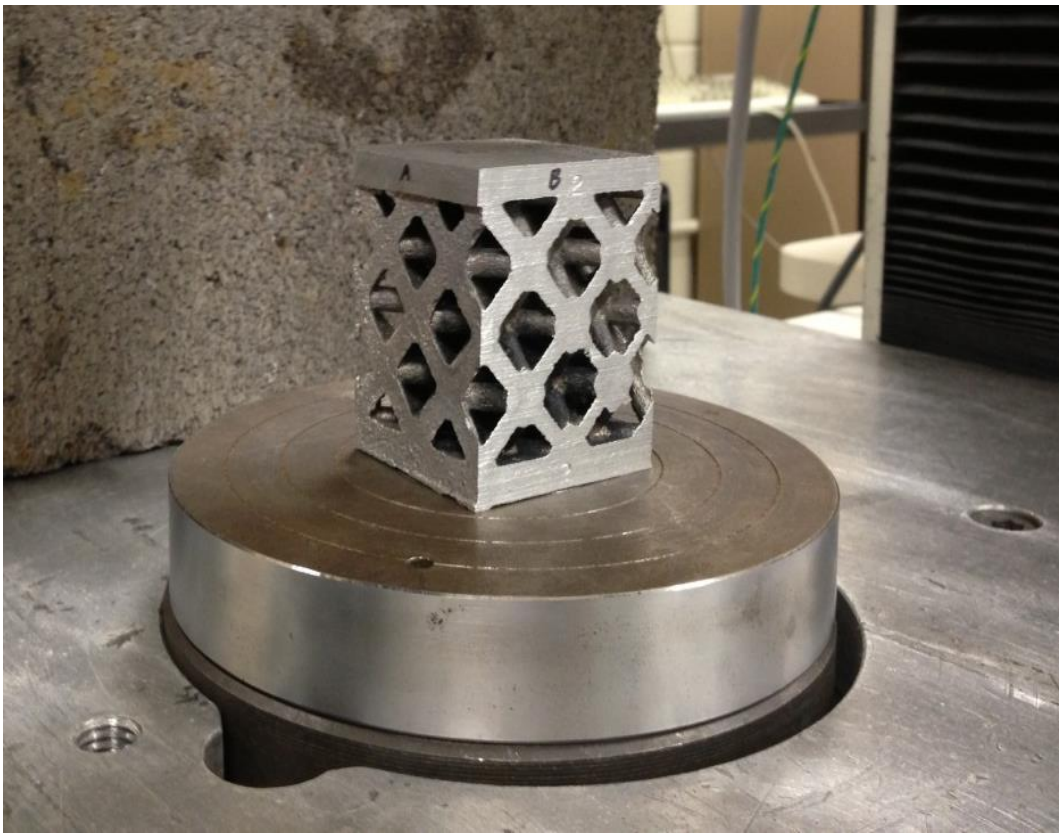

Figure 2.9. Sectioned cellular structure placed in compression fixture

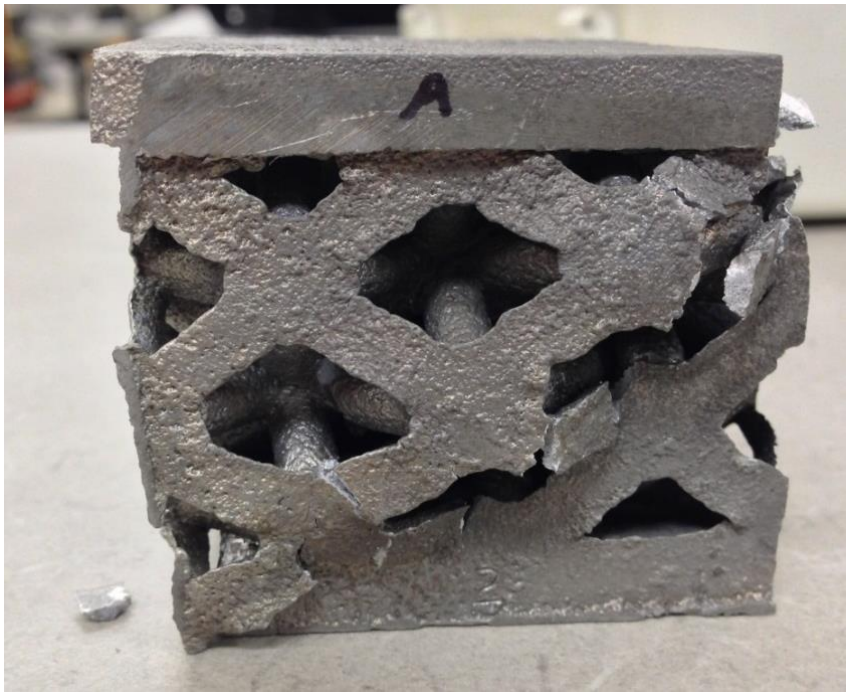

Figure 2.10. Cellular Structure after failure in compression

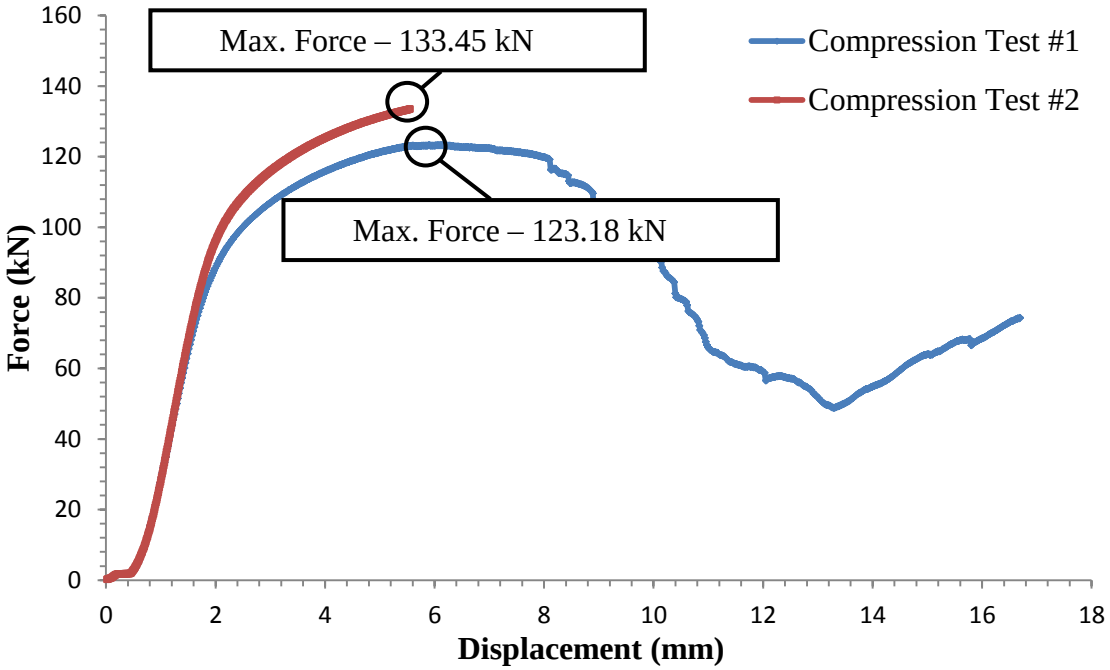

Figure 2.11. Axial force vs. axial displacement curve for cellular structure deformed in compression

2.4.3. Simulations of quasi-static deformations of the cellular structure

Due to the symmetry of the structure and the applied boundary conditions about the two centroidal vertical planes, quasi-static deformations of only one-quarter of the structure depicted in Figure 2.12 were analyzed with symmetry boundary conditions applied on the plane X = Y = Z = 0, and the lateral surfaces kept traction free. Two extreme cases are of infinite friction where in-plane motions of particles should be zero, and that of no friction in which case tangential tractions should be zero. In practice the situation is somewhere between these two cases. St. Venant's principle is not applicable to the problem being studied because of large inelastic deformations involved. However, it is assumed that deformations in the central portion of the structure, away from the top and the bottom surfaces, are not affected much by boundary conditions at the contact surfaces. Therefore, lateral surfaces were assumed to be smooth and estimated that it would affect the energy dissipated by less than 5% as compared to a perfect bonding (or infinite friction) condition. Points on the bottom surface are assumed to be restrained from motion in the Z – direction and those on the top surface are incrementally moved vertically downwards for a total displacement of 10 mm. The cellular structure was discretized using 10-node tetrahedral elements with 4 integration points (C3D10M). The total number of the elements in the FE mesh equaled 273,828. The discretized structure is shown in Figure 2.12.

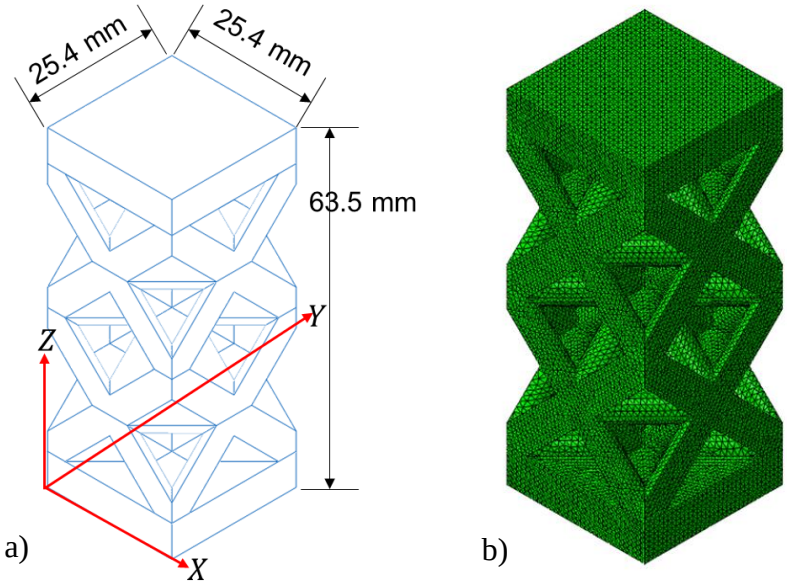

Figure 2.12. a) Geometry of one quarter of the entire structure, and b) its discretization into modified 10-node tetrahedral elements

This problem was analyzed with ABAQUS/Explicit [60] using the reduced order integration rule to numerically evaluate various element matrices, and mass scaling, i.e., artificially reducing the mass density to increase the wave speed. ABAQUS/Explicit is used to analyze dynamic problems. While checking the energy balance, the kinetic energy and the hourglass energies were found to be negligible and the total work done by external forces was found to equal the sum of the strain energy of the body and the energy dissipated due to plastically deforming the body. The general contact algorithm built in ABAQUS/Explicit was used to model contact at all interfaces including that between new surfaces formed due to element deletion. When an element had failed, both the hydrostatic pressure and the deviatoric stress components in it were set equal to zero and remained zero for the rest of the analysis. The computed and the experimental true axial stress vs. the true axial strain comparison curves plotted in Figure 2.13. differed at most by 16.4% which was taken to be within the acceptable range. Thus values of material parameters stated above can be used to simulate deformations of the cellular structure. It is important to note, that by increasing the dimensional accuracy of the resultant part, would eliminate error between the model and experimental results. This can be accomplished by printing the entire mold, including the outer walls otherwise made by forming traditional sand. Additionally, although compression specimens used as input data into the ABAQUS/Explicit model were cast using the same material and heat treatment, the casting modulus (Surface Area to Volume) difference between the compression specimen and proof of concept cellular structures could vary microstructure. This change in microstructure (dendrite arm spacing) will slightly affect the strength and contribute to the error.

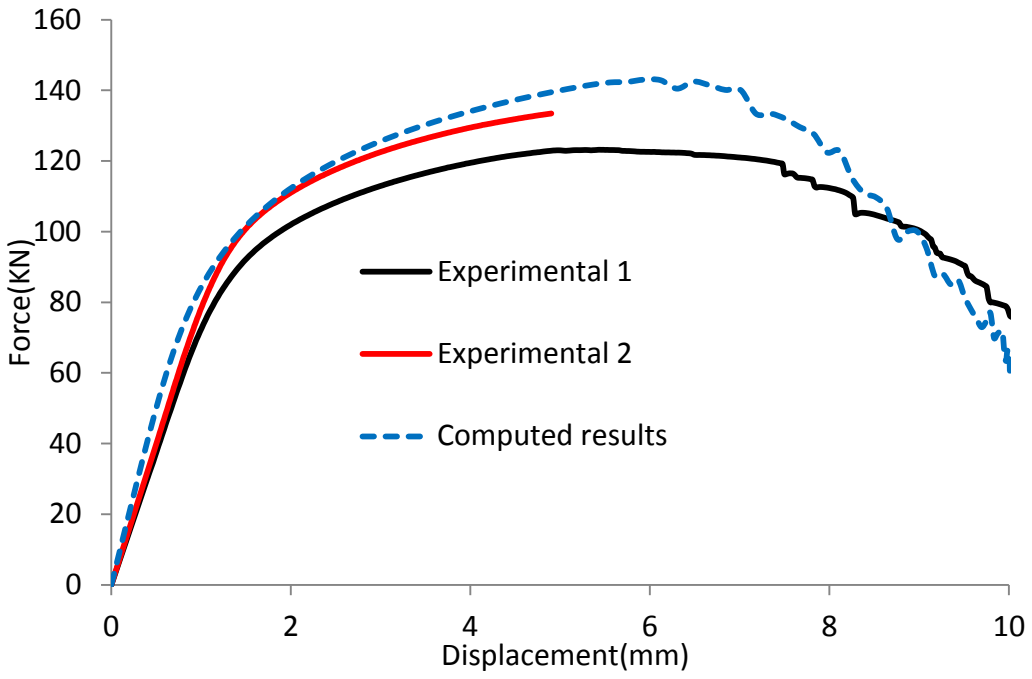

Figure 2.13. Comparison of the computed results and experimental results for the quasi-static compression tests for the cellular structure

2.5. Modeling impact loading of cellular structure

Transient deformations of the cellular structure due to impact loading were analyzed to delineate advantages, if any, of cellular structures over that of solid structures of the same area density. Although not optimized for blast loading, the octet-truss geometry was chosen because it exhibits excellent characteristics under compressive loading and has been thoroughly studied in the literature [61]. Cellular truss structures composed of repeated unit cells have been analytically studied by analyzing deformations of a unit cell [61], and experimentally by testing cellular materials under shear or compressive loads [37,38,41,44,46].

2.5.1. Impact Modeling of Truss Structure and Solid Block

As for the quasistatic deformations studied above, transient deformations of a quarter of the cellular structure and a 25.4 x 25.4 x 31.9 mm solid plate of the same areal density were analyzed with ABAQUS/Explicit with a uniformly distributed time-dependent pressure of peak magnitude 500 MPa applied on the top surface. The time dependence of the applied pressure is depicted in Figure 2.14. The 31.9 mm high solid plate was discretized into 250,000 8-node brick

elements (C3D8R) with 1-point integration rule. The same contact algorithm and the element deletion technique as that for the quasi-static deformations studied above were employed.

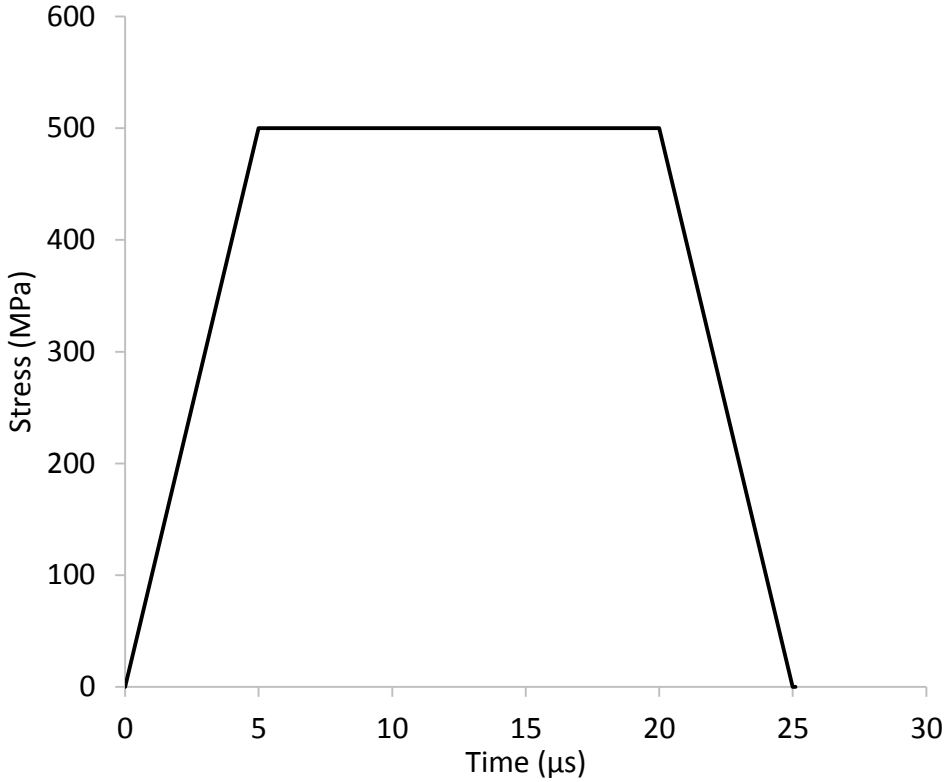

Figure 2.14. Impulse loading history

2.5.2. Results and discussion for the impact loading

The work done by the applied pressure loading during deformations of the cellular (solid) structure equaled 64.9 J (45.1) of which 25.7 J (41.9) was used to elastically and plastically deform the structure and 39.6 J (3.3) to increase the kinetic energy of the structure. It was thus clear that the cellular structure is more severely deformed than the solid plate that should also be evident from the deformed shapes exhibited in Figure 2.15. Whereas no element failed in the solid block, nearly half of the trusses in the cellular structure failed. However, the bottom plate of the cellular structure remained intact. Due to the reaction force exerted by the bottom rigid plate supporting the structures, the cellular and the solid structures bounced upwards at 300 and 50 μs, respectively, as indicated by the plot in Figure 2.16 of the time histories of the reaction force. The peak force (283 kN) exerted on the rigid supporting plate by the solid structure was considerably more than that (36 kN) exerted by the cellular structure thereby providing

significantly more protection to the structure to which they were bonded. Also, the impulse transferred to the substrate by the cellular structure was much less than that transmitted by the solid structure.

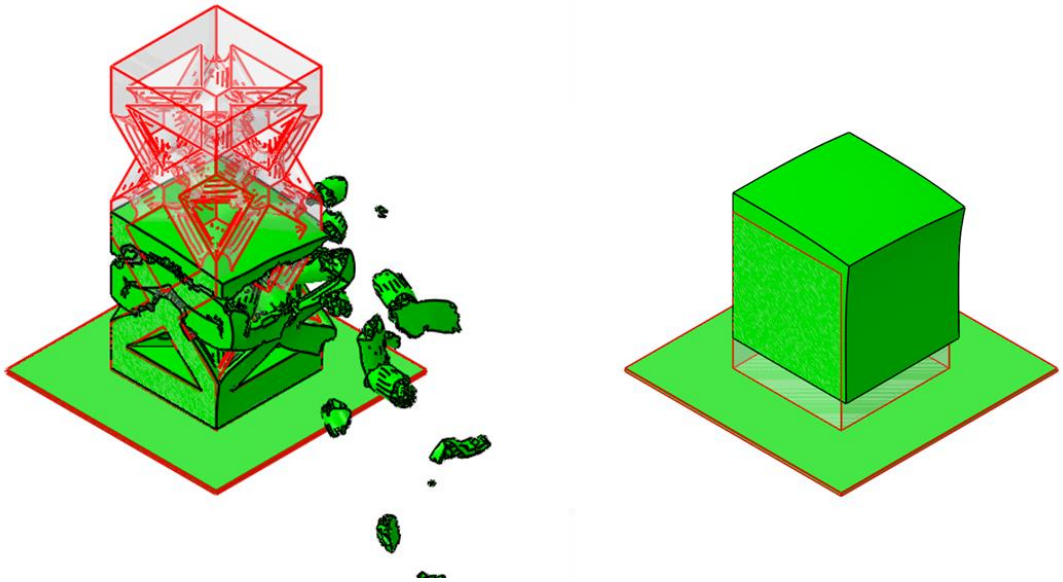

Figure 2.15. Undeformed (red lines) and deformed (black lines) shapes of the cellular structure and the solid block at time = 480 *μs*

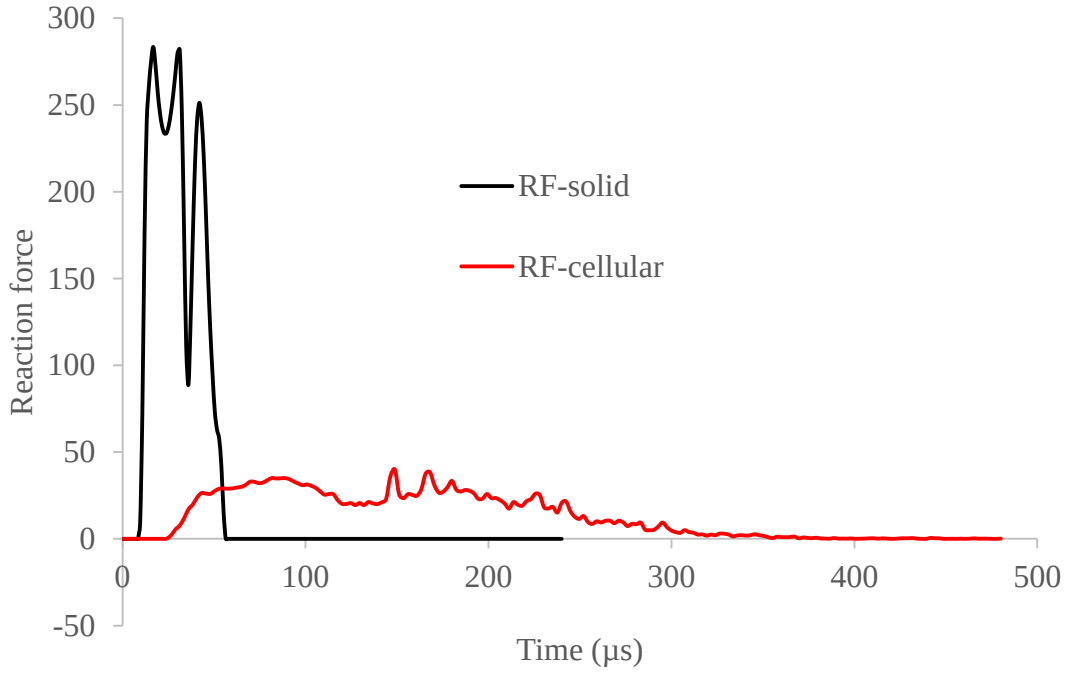

Figure 2.16. Reaction forces applied on structure by the rigid plate supporting the

2.6. Conclusions and Recommendations for Future Work

In this paper, a method for the creation of lightweight, metal cellular structures was presented utilizing the capabilities of Binder Jetting and traditional casting techniques. Binder Jetting is advantageous in that it is scalable and relatively inexpensive, and the printed powders used for casting allow processing of many different alloys. A proof of concept octet truss structure with fully homogeneous sandwich panels was manufactured using the proposed Binder Jetting process. The resulting part quality, while partially dependent on part geometry, demonstrated that this method is capable of producing lightweight cellular structures with designed mesostructure through metal casting.

Quasistatic and transient deformations of the cellular and solid structures were studied by using values of material parameters determined from the test data and the commercial software ABAQUS. For the same time-dependent pressure load applied on the top surfaces of the two structures with their bottom surfaces supported on smooth rigid plates, the total force exerted on the rigid plate by the cellular and the solid structures equaled 283 and 36 kN, respectively. Furthermore, the total impulse transferred by the cellular structure to the rigid plate is considerably less than that by the solid structure.

For future work, efforts will be focused on combining topology optimization with the proposed Binder Jetting process. Using topology optimization during the initial digital mold creation phase will allow for structures that are tailored to perform optimally under certain loading conditions. In addition, efforts will be undertaken to analytically model the flow of the molten metal through the mold, ensuring that the final parts are poured and completely filled, regardless of geometry. Modeling of deformations under quasi-static and impact loads will be used to optimize the design of cellular structures for minimizing the momentum and the peak pressure transferred to the substrate being protected by the cellular structure. Collaboration with outside sources will be sought for tests under blast loads. Additionally, by printing the entire mold including gating system, core, and outer mold assembly, will provide better geometrical tolerances. The resultant part will lead to less error between analytical and quasistatic results.

2.7. Acknowledgements

The author gratefully acknowledges the financial support received from the Institute for Critical Technology and Applied Science (ICTAS) at Virginia Tech.

3. MITIGATING GAS DEFECTS IN CASTINGS PRODUCED FROM 3D PRINTED MOLDS

3.1. Introduction

Metal casting is commonly used in manufacturing to create high-quality low-cost products. While capable of producing a wide range of geometries, the sand casting process inherently constrains the design of a part to geometries that can be produced by forming sand around pre-made patterns (and removal of the pattern from the sand). Several "design for manufacturing" guidelines must be followed for successful part design for sand casting: e.g. including draft angles for pattern release, and pattern geometries that are able to be removed from sand, etc. Recently, engineers have looked to using Additive Manufacturing (AM) to overcome these geometric restrictions. The integration of AM technologies to the foundry industry has increased the efficiency of design and casting production including reducing time and cost associated with the traditional methods of development while still maintaining high accuracy [8,17].

In addition to using AM for the production of expendable patterns for investment casting, AM technologies have been used in foundry practice to produce patterns and core boxes for sand casting [22]. In addition, AM processes have enabled the direct production of sand molds without the need for fabricating a pattern. This pattern-less sand molding approach enables the sand casting of complex mold geometries that could not be made by traditional means thanks to the ability to directly print entire molds (including vents, downsprues, runners, etc.) from a single CAD file. For example, Laser Sintering (LS) has been used to selectively melt a resin coated quartz sand mixture in a layer-by-layer fashion in order to create printed sand molds [17,23]. An augmented stereolithography process (Optomec), which selectively cures viscous ceramic-resin slurry via exposure to UV energy, has also been used to directly fabricate sand molds [24].

The most common AM process for the direct fabrication of sand molds is the indirect 3D Printing process (3DP) (Figure 3.1). In this process, Direct Metal casting, commercialized by Z Corporation and ExOne corporations, layers of proprietary plaster-sand mixtures are bonded together, via the selective inkjetting of a binder solution into a powder bed. A layer of "sand" is spread from the feed tray to the build tray. Binder is jetted over the sand, the build tray lowers,

and a new layer is spread. The process is continued layer-by-layer until the part is completed. Figure 3.2 shows a Z Corporation Spectrum Z510 printer with ZCast 501 sand. Recent research with printed ZCast 501 sand, has characterized compressive strength, permeability, dimensional accuracy, and other mechanical properties in order to provide more effective design of molds [17,21].

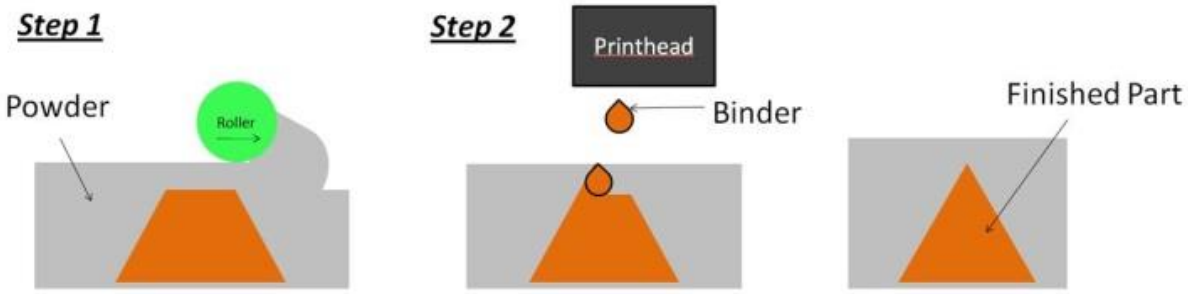

Figure 3.1. Binder Jetting 3D Printing Process

Figure 3.2. Z Corporation Spectrum Z510 at Virginia Tech

The purpose of this paper is to address one of the limitations of using 3DP to directly produce sand molds: the formation of gases during pouring due to excessive binder content in the printed mold. This limitation was identified by Meisel, Williams, and Druschitz, wherein their initial attempts in casting complex cellular structures using 3D printed molds were unsuccessful due to incomplete filling of the mold at the bottom of the structure (Figure 3.3) [25]. Like foundry sand, binder in the printed mold produces gases that must be allowed to escape; otherwise gas defects may occur.

In this work, the author explored techniques for minimizing the formation of gas defects in parts fabricated via sand casting in 3D printed molds. Specifically, the author investigated mold curing processes (after printing) that reduced the amount of binder present in the printed mold, and thus reduced the amount of gas produced while pouring. However, by burning out binder with a higher temperature post-process curing cycle, the strength of the overall mold could be jeopardized.

To characterize the proposed curing cycles, and to explore its effects on the mold and gas defects in resultant parts, the author conducted tensile strength measurements for 3D printed sand that had been post-processed at a variety of temperatures. In addition, the tensile strength values of 3D printed sand were compared to traditional no-bake foundry sand. Similar tests have been performed by McKenna et al. (2008) to produce a more efficient mold and study the effects of curing time and temperature on permeability and compressive strength. In this work, however, casting data, binder burnout percentages, and total binder content were characterized to determine the relationship between mold curing cycles with gas defects in 3D printed molds.

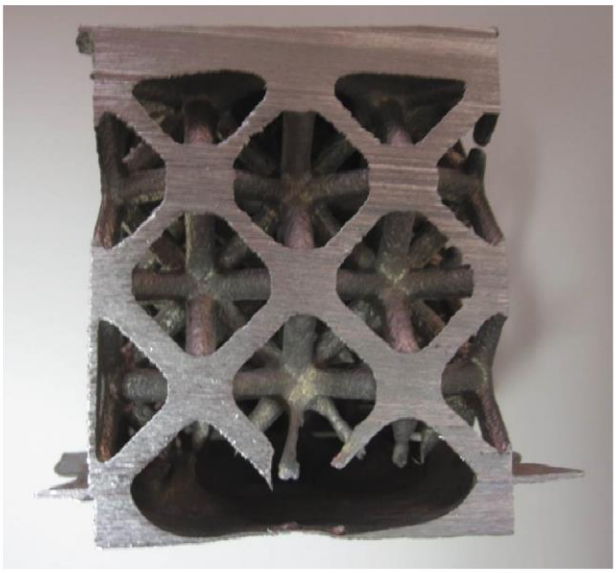

Figure 3.3. Gas defect in complex cellular structure casting produced using 3D printed mold (Meisel et. al., 2012)

3.2. Experimental Methods

Sand Characterization

As there are no formal standards for materials characterization of this new technology, 3D Printed sand characteristics were compared to an existing material in which properties are known. Printed sand and traditional foundry sand are bonded by two different methods creating different responses to metal casting. For this test, round silica sand mixed with binder, also known as no-bake sand was used for comparison. Binder makeup for the no-bake sand was a ratio of 4:1 of ester cured phenolic resin to hardener/catalyst, which accounted for approximately 1.6% of the sand mixture. Foundry sand and binder were mixed using a Palmer M50XLD continuous sand mixer.

First, standard sand tests were used to compare both 3DP sand and no-bake sand. Specifically, these two sands underwent a standard sieve test according to AFS 1105-00-S to determine particle size distribution and AFS 1106-00-S for grain fineness number [62]. This is an important test as particle size distribution heavily influences mechanical characteristics (e.g., strength and permeability [22] of the mold), which are important to this study. In addition, particle size data provided a better understanding of the proprietary 3DP sand because the only

data available was through a MSDS [63] provided by the manufacturer, which revealed only vague chemistry makeup.

Binder Burnout

In ordinary no-bake sand, strength is a function of binder content, which is proportional to the amount of gas produced. For example, the more binder present in a mold, the higher its strength, but the more gas will be generated during pouring. This will increase the likelihood of incomplete fill or gas defects. This is especially troublesome in complex structures (e.g., Figure 3.3) where access to internal structures is not possible. To examine if the same interdependences hold for 3DP sand, several burnout cycles were performed to characterize binder content (weight loss) and strength vs. curing cycle.

McKenna et al. (2008) determined that the strength of printed sand increased with temperature to approximately 173°C. After this prescribed temperature strength began to decrease. During the printing process, correct amounts of binder are added to produce sufficient mold strength while minimizing gas generation during pouring [22]. To determine binder burnout percentage, small cubes of both no-bake sand and 3DP sand with dimensions of 0.5in x 0.5in x 0.5in were given curing cycles at different elevated temperatures. Ten no-bake cubes were formed and 12 3DP cubes were printed for testing and can be seen in Figure 3.4. Specimens for both sands were weighed together before undergoing any curing cycle in order to get a base weight reading. One-hour curing cycles were performed for both sets of cubes starting at 105°C to 150°C and in 50°C increments to 900°C. After each cycle, the cubes were weighed and the weight recorded.

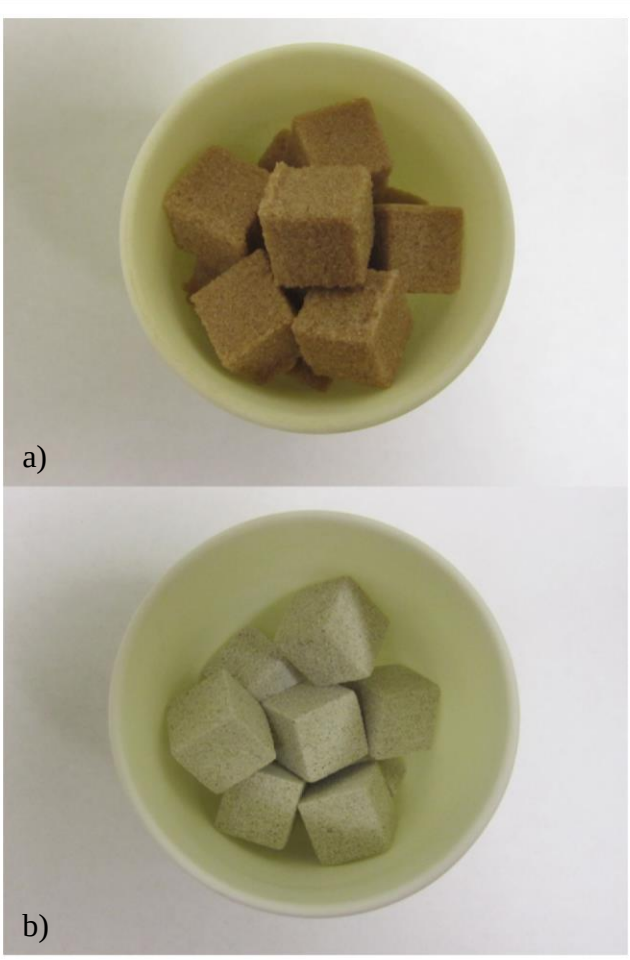

Figure 3.4. Binder burnout specimens (a) No-bake sand cubes and (b) printed sand cubes

Mechanical Strength

After determining the binder burnout percentages, these values were utilized to determine curing cycle temperatures to test mold strength. Strength tests were performed according to AFS 3342-00-S for both no-bake and 3DP sands [62]. No-bake sand specimens were produced using multi-cavity core-boxes. Equivalent 3DP specimens were created in CAD using dimensions given by the AFS standard. Three sets of three specimens for the printed sand were cycled to temperatures of 204°C for 8 hours, 121°C for 1.75 hours followed by 232°C for 1.75 hours, and 316°C for 1 hour. All sets underwent a drying cycle at 104°C before entering the curing cycle due to the high moisture content of the material [17]. In addition, one set underwent only a drying cycle at 104°C. After curing, all specimens were tensile tested to compare the strength of the printed sand to the no-bake sand.

Casting Trials

In addition to testing strength in the printed sand, molds were created and poured for each curing cycle. Casting data provided an overall performance of the mold to determine if the curing was satisfactory to create a quality casting. Continuing the work of Meisel et. al., molds for producing cellular parts were created using Netfabb Studio Professional 4.6 [25]. Primitives were formed with a repeating voxel unit cell, and a boolean subtraction was performed to create a negative of the structure. The negative was a CAD model of the mold (core) and can be seen in Figure 3.5. A .stl file was exported and printed using ZCorporation's ZPrint software. After the mold are printed, various elevated temperature curing cycles were performed.

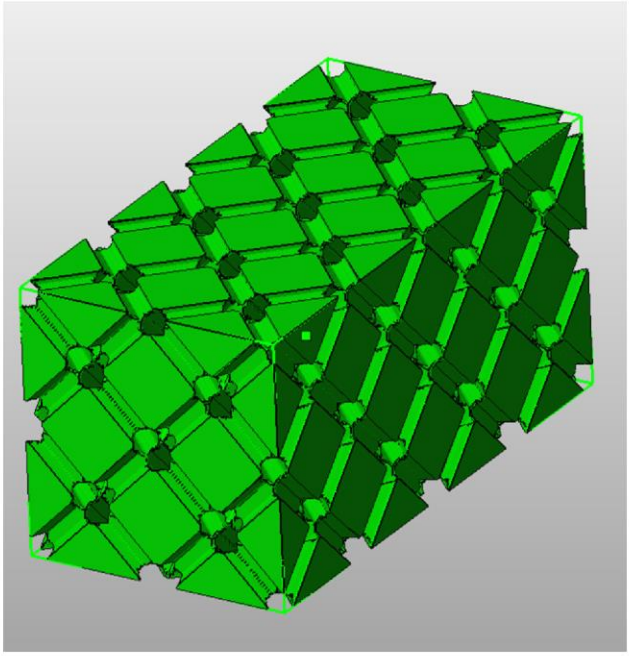

Figure 3.5. CAD Model of the Printed Core

The mold was a bottom fill design with a no-bake drag mold with well and runner, no-bake downsprue, no-bake sides and a no-bake top [25]. By sandwiching the printed core between blocks of conventional no-bake sand, the amount of costly printed sand was minimized and venting was maximized since small gaps between the individual pieces were unavoidable. The construction of the complete mold with the printed core can be seen in Figure 3.6.

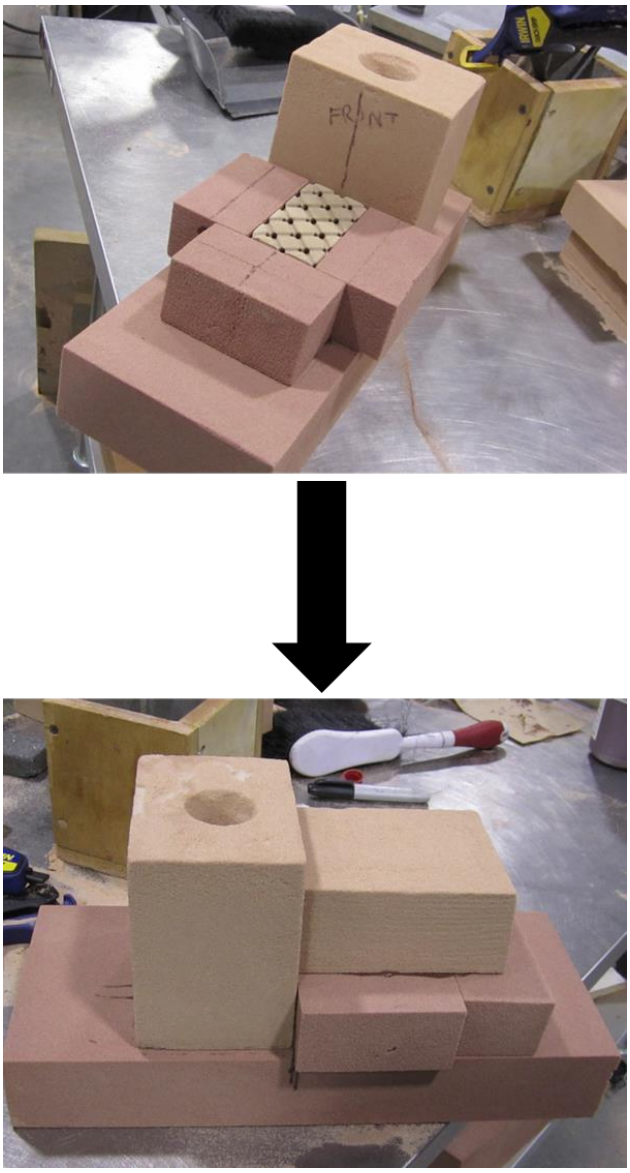

Figure 3.6. Printed Core and No-Bake Mold

3.3. Results and Discussion

Sand Characterization

The sieve tests were performed for both sand types using a Ro Tap Model E sieve analysis machine. Particle size distribution for the silica sand and 3DP sand is shown in Table 3.1.

Table 3.1. Sieve Analysis and AFS Grain Fineness Number for both Sands

	Silica Sand	3DP Sand
Seive Size	Percent Retained	Percent Retained
12	0.00	0.00
20	0.00	0.00
30	0.00	0.00
40	1.34	0.00
50	34.54	0.17
70	32.79	4.29
100	19.94	21.03
140	8.81	25.52
200	2.23	19.59
270	0.33	15.50
pan	0.01	13.90
Total	100.00	100.00
AFS GFN	57	143

Unfortunately, the particle distribution data was not accurate because of clumping of the 3DP sand particles. Despite these difficulties, the 3DP sand proved to be much smaller in size and to have a much larger surface area per gram; approximately four times larger than silica sand. The small particle size of the printed sand requires more binder therefore generating more gas at elevated temperatures. The result could lead to a defective casting and voids caused by excessive gas generation. Photographs of both sands can be seen in Figure 3.7.

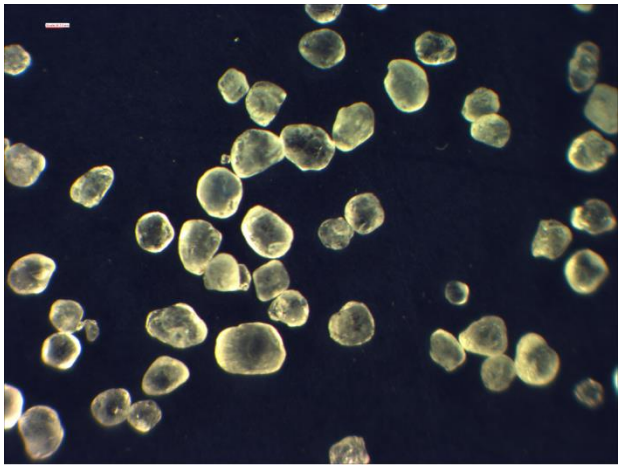

a)

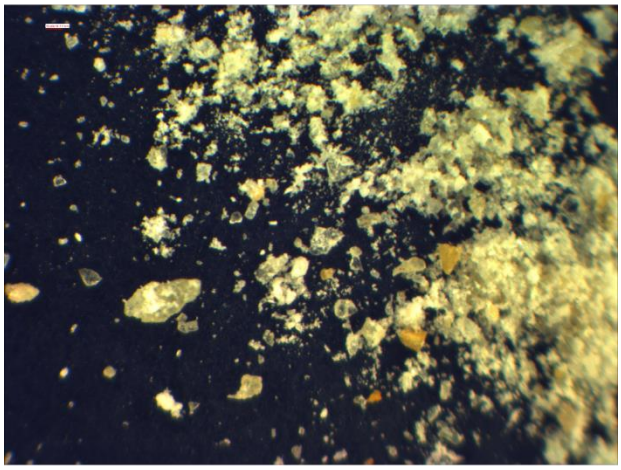

b)

Figure 3.7. a) Rounded Silica Sand and b) 3DP Sand

Binder Burnout

The greatest amount of binder in a 3DP sand mold is before any curing cycle is performed – before any binder burnout has occurred [17]. Printed molds require more binder to adhere finer particles due the larger surface area per gram. These results further explain the gasses trapped while pouring the molten metal.

In determining the amount of binder in both sands and their effect to temperature, binder burnout data was taken at prescribed temperatures. "Green" cubes were made and weighed for both sands. Figure 3.8 shows temperature vs. binder burnout percentage.

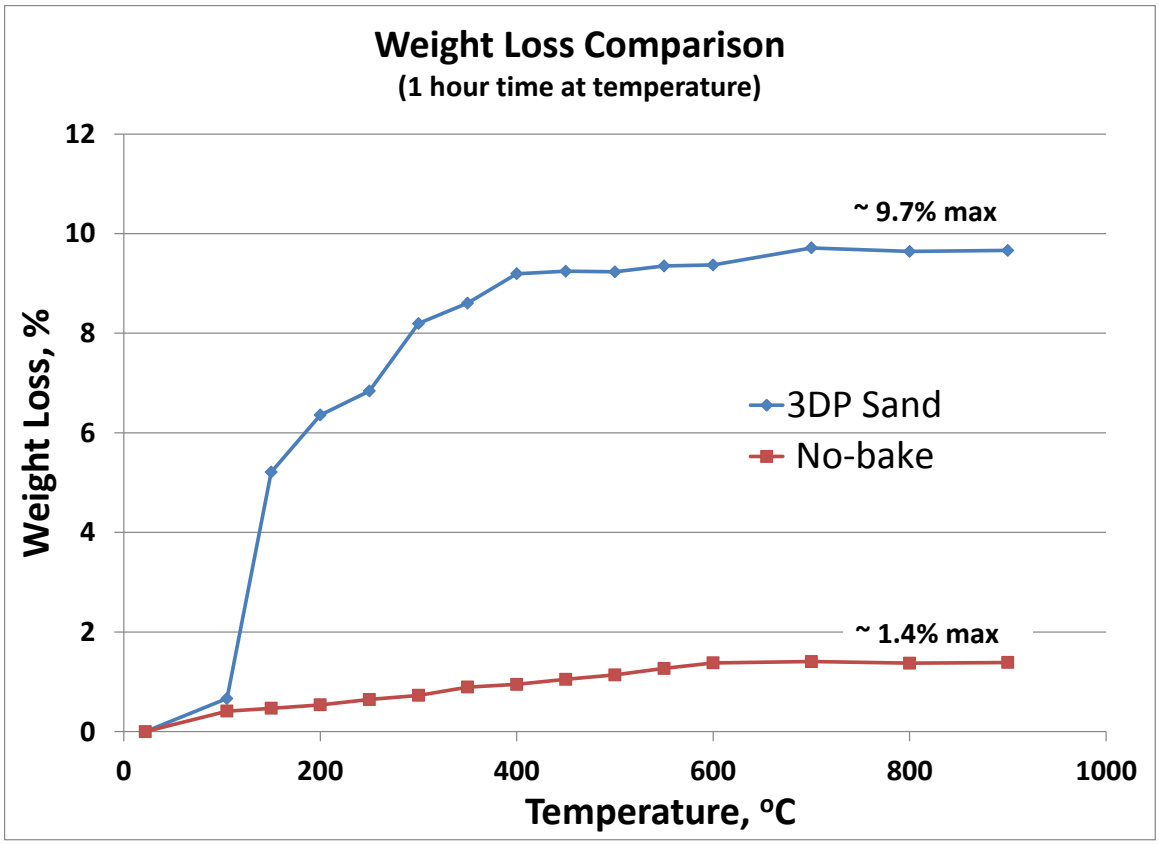

Figure 3.8. Weight Loss Comparison of No-bake and 3DP Sand Cubes

The no-bake sand gradually lost mass whereas the printed molds showed a large percent loss after exposure to 100°C for 1 hour. The large increase between 100°C and 200°C was due to the combination of water loss and binder burnout in the printed cubes. The printed cubes lost more than 9% in weight over the entire test compared to about 1.4% for the no-bake sand cubes. Because of the greater amount of binder in printed molds (as shown by weight loss), much more gas will be produced while pouring possibly inhibiting a complete fill or pushing the liquid metal out of the casting cavity before solidification is complete.

Mechanical Strength

Binder in both traditional no-bake molds and printed molds give strength, therefore the amount of binder is crucial to the integrity of the mold. During binder burnout tests, it was necessary to determine a trend in behavior of the mold strength. Following the AFS 3342-00-S testing standard for foundry sand, both sand types were formed or printed into "dog bone" specimens (Figure 3.9) [62]. Three specimens each were tested at room temperature on a Com-

Ten 95 Series tensile machine to determine their strength. Average strength data for both sand types are listed in Table 3.2. As the temperature of the curing cycle increased, strength decreased due to binder burnout.

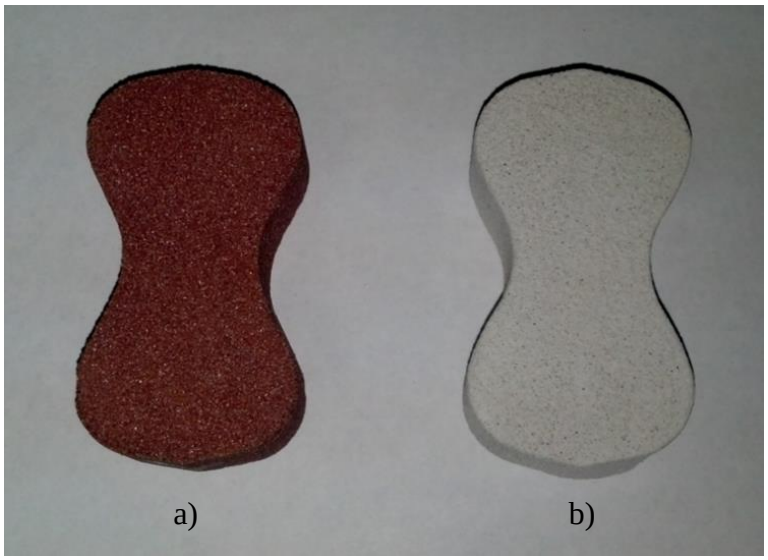

Figure 3.9. Dog Bone Tensile Specimens of (a) No-bake and (b) 3DP Sands

Table 3.2. Strength Data of Both Sands

	Average Strength MPa (psi)	
Curing Cycle	No-bake	ZCast®501
as-made	0.56 (81.44)	X
104°C/2 hrs (dried)	X	0.39 (57.08)
204°C/8 hrs	X	0.19 (28.04)
121°C/1.75 hrs & 232°C/1.75 hrs	X	0.16 (23.30)
316°C/1 hr	X	0.06 (9.11)

Casting Trials

The curing cycles were chosen from the manufacturer's recommendations and results from the printed sand binder weight loss data. The manufacturer's recommended settings were from 177°C to 204°C from 4 to 8 hours. The curing cycle was run at 204°C for 8 hours to ensure that the maximum binder was burned out. A second curing cycle was chosen from to the weight loss data in Figure 3.7, at 316°C >8% binder was burned out while still maintaining a small amount

for strength. The third curing cycle was chosen at 121°C for 2.5 hours followed by 232°C for 1.75 hours because it had temperatures between 204°C and 316°C with percent weight loss between 4% and 8%.

Castings were not made in uncured or dried only (104°C/2hours) condition due to their large amount of binder present. For each of the other three curing cycles, molds were poured to determine casting quality. All molds were poured using aluminum alloy A356. Using the manufacturer recommended curing cycle; the casting (Figure 3.10) had similar defects as in Figure 3.3 except with less void space at the bottom of the casting.

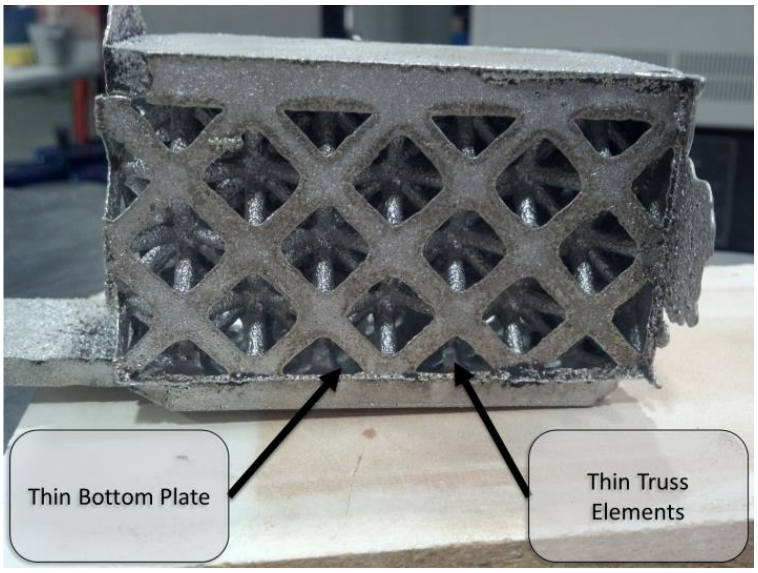

Figure 3.10. Defective Casting Produced Using Manufacturer Recommended Curing Cycle (204°C for 8 hours)

With the curing cycle of 121°C for 2.5 hours followed by 232°C for 1.75 hours, the quality was also poor (Figure 3.11). The defects in these castings were similar to the initial problem resulting in a conclusion that binder content had a strong influence on gas defects and casting quality.

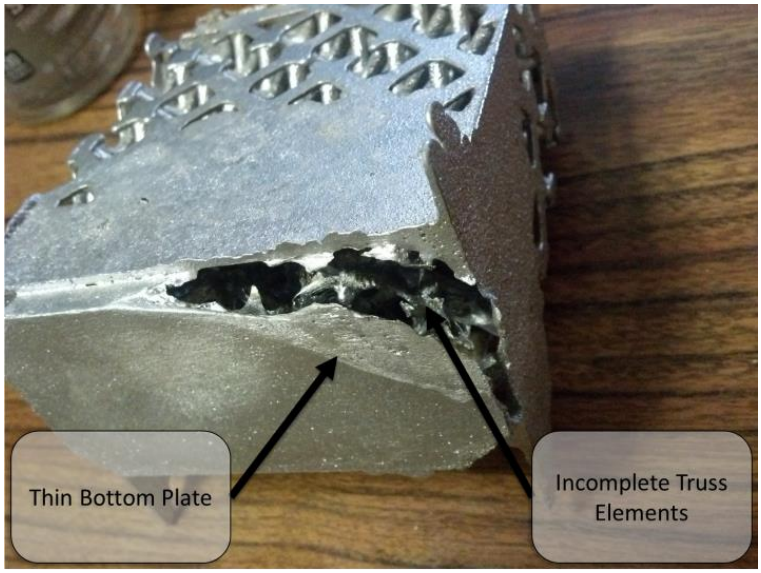

Figure 3.11. Defective Casting Produced Using Second Curing Cycle (121°C for 2.5 Hours followed by 232°C for 1.75 hours)

The final curing cycle at 316°C for 1 hour produced a high quality casting with no visible defects or cavities and can be seen in Figure 3.12. This curing cycle consisted of a shorter time at a higher temperature, which is feasible for volume production. Using this curing cycle, the printed mold had sufficient strength and sufficiently low binder content.

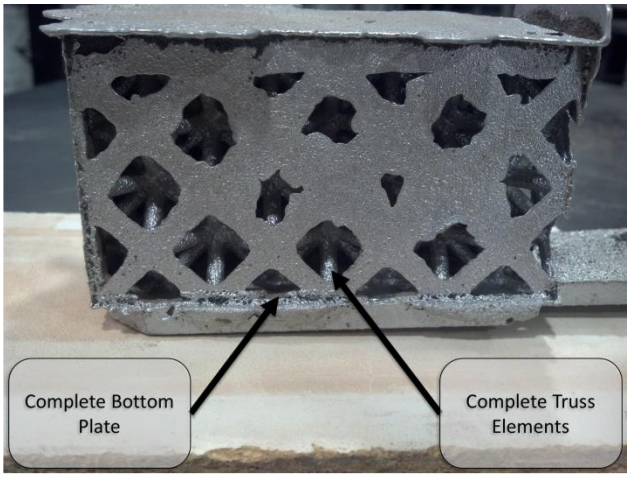

Figure 3.12. Good Casting Produced Using High Temperature Curing Cycle (316°C for 1 hour)

3.4. Conclusions

Improvements in 3DP have enhanced the metal casting process by cutting cost and time while providing the ability to create complex structures unable to be produced by traditional

processes. For example, the author has shown that this technology can be used to cast light-weight complex cellular structures. However, due to significant binder content in printed sand molds, there are challenges in producing a quality casting due to gas defects caused by binder burnout during pouring. In this paper, the author explored the effects of printed mold curing cycle on casting quality. Specifically, the author explored how increased curing temperatures affected residual mold binder content, mold strength, and gas defects in poured parts.

The amount of residual binder in the printed molds after curing was the primary cause of gas defects during casting. Several tests to characterize the proprietary printed sand were performed including a sieve test, binder burnout tests, and tensile tests. All tests compared traditional "no-bake" foundry sand to printed 3DP sand used in 3D printing. From the burnout data, the total amount of binder in printed sand was determined to be a much higher percentage compared to the no-bake (8-9% compared to 1.4%, respectively). The larger percentage of binder equates to a larger amount of generated gas and the observed casting defects. Tensile tests per AFS standards were performed on specimens to determine the effect of binder burnout on strength. A higher curing temperature of 316°C for 1 hour was determined to eliminate enough of the binder while still maintaining sufficient strength for handling and pouring. This improvement over the manufacturer's recommended curing process enabled the successful casting of complex cellular geometries.

4. THE EFFECTS OF 3D PRINTED SAND MOLDS ON METAL CASTINGS

4.1. Effects of Molding Materials on Castings

4.1.1. Additive Manufacturing of Sand Molds for Metal Casting

Additive Manufacturing (AM) enables the direct production of molds without the need for a pattern. Specifically, the Binder Jetting process can be used to directly fabricate sand molds and core boxes by selectively jetting binder into a powder bed of foundry sand [22].

A schematic of the Binder Jetting process is provided in Figure 4.1. During Binder Jetting, a polymer binder is printed onto a bed of powder using a traditional inkjet print head to bind together sand particles in the image of one cross-sectional layer of the part. After a layer of binder is printed, the powder bed lowers, and fresh powder is spread over the powder bed using a roller or doctor blade. Then, the next layer of the part is patterned onto the powder bed atop the previous layer. In this manner, the object is constructed layer by layer.

After the mold is printed, the excess powder is removed using compressed air or vacuum. Often, the printed molds are then cured in an oven to eliminate a portion of the binder (as with single-part binder systems). The printed sand part can be used as a core (

Figure 4.2a) or as a complete mold (

Figure 4.2b), which includes runners, gates, and a down-sprue [25]. Molten metal is then cast into the mold to create the casting (

Figure 4.2c). Binder Jetting of molds for metal casting has been commercialized by a variety of companies, including 3D Systems (formerly ZCorp) [51], ExOne [64], Viridis3D [65], and Voxeljet [66].

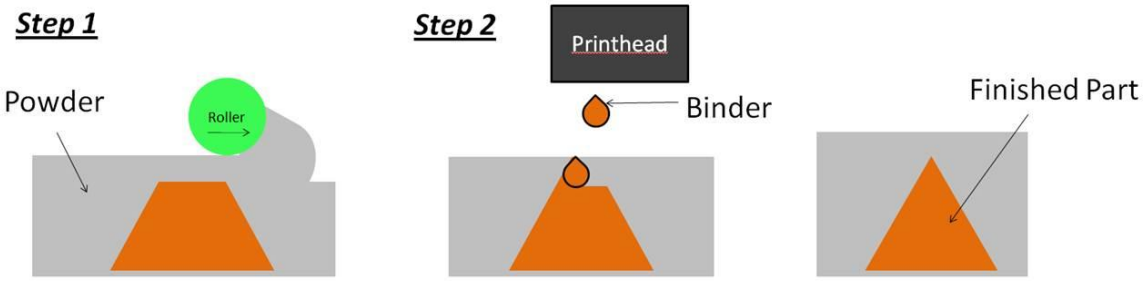

Figure 4.1. Schematic of the Binder Jetting process

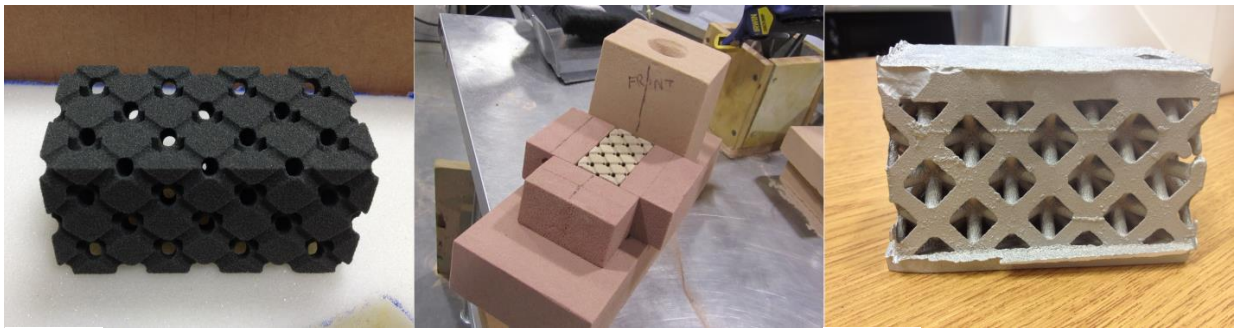

a) b) c)

Figure 4.2. a) Complex printed mold created using Binder Jetting, b) no-bake outer mold, and c) cast complex structure

Many of the applications for additively manufactured sand molds are in providing a means to offer flexible tooling for traditionally designed castings. However, an important asset of the process is that the geometric freedoms offered by AM can be leveraged to provide a means for metal casting of complex geometries that are not possible to fabricate via traditional casting means [8,25]. In addition, the layer-by-layer process of fabricating sand molds enables a designer to uniquely integrate vents, sprues, runners directly into the mold design. Finally, as the final metal part is created outside of the AM systems' build chamber, the Binder Jetting and casting process chain enables the creation of large metal geometries. Specifically, multiple molds may be printed and fitted together with core paste to enable the pouring of large metal castings.

4.1.2. Traditional Molding Material Effects on Castings

Although AM of sand molds has enabled designers to overcome manufacturing restrictions, little is known about the materials systems' effects on metal castings (Section 4.1.3). This gap in knowledge is contradictory to the existing knowledge base in traditional sand casting. Many of the common aggregates used for the formation of molds in traditional sand casting are comprised of silica sand, natural minerals, synthetics, and other particulate materials [67]; each component has differing characteristics such as composition, grain size, and binder or compaction requirement. As a result, the properties of subsequent metal castings vary due to their reaction to the mold. For example, the quality of a casting can change due to water vapor stored in the mold, free hydrogen, and organics as the metal flows and solidifies [67]. These reactions inherently

affect the final cast product and can produce defects such as porosity, oxidation, carbon formation, and surface roughness [67].

4.1.3. Prior Research in Binder Jetting of Sand Molds

This existing understanding of sand molds on metal casting cannot be directly applied to AM sand materials systems, as the working materials are dissimilar. There is limited literature that explores the effects of 3D printable sand mold material on castings. Instead, most of prior research was focused in studying the molds produced by ZCast® [18,20,21]. For example, McKenna et al. performed tests on ZCast®, to determine the effects of temperature and curing time on permeability and compressive strength of the mold. A mathematical model was used to determine an optimal curing time and temperature for both permeability and compressive strength [17]. In previous work, the author investigated the binder content of ZCast® material system and found it had a significantly higher binder content (up to 8% binder) than traditional no-bake foundry sand [29]. The higher binder content of the ZCast® printed molds causes molds to generate more gas during casting, which can cause defects in the final parts. A new curing cycle with higher temperatures for a shorter duration produced more consistent cast structures with fewer gas defects. In addition, Gill & Kaplas compared castings printed with ZCast® and investment casting using starch and plaster, including dimensional tolerances, hardness values, surface roughness, production cost, and shrinkage [19]. Experiments were also run at different shell thicknesses. It was determined that starch-based investment casting produced higher hardness values and slightly better surface roughness, where ZCast® produced better dimensional tolerances all from a recommended shell thickness range of 2-12 mm. It was also concluded there is optimal settings in terms of time and shell thickness to minimize cost based on individual builds. Drokina and coauthors performed study on fluidity, shrinkage, and mechanical properties of AK8L alloy cast in printed ZCast® [68]. It was found that the fluidity was 6 % higher in ZCast than in traditional sand-clay molds and while shrinkage remained the same for both. Finally, the printed molds were synthetically filled with iron shot and quartz sand for mechanical testing. The printed mold with iron shot filler had a larger ultimate and yield strength than those with quartz filler both exceeding the standard strength required for sand-clay molds by 7.5%.

4.1.4. Overview of Work

In order to ensure quality cast parts, the effects of different molding materials on final cast material properties needs to be studied. The primary goal of this work is to compare two commercially available Binder Jetting sands (ZCast®, produced by 3D Systems, and ExOne silica sand, produced by The ExOne Company) with traditional no-bake foundry sand. Additionally, this work compares the two Binder Jetting sands on the basis of the handleability of the resultant printed molds (measured by tensile strength) and the properties of the cast metal parts they produce. The comparison to traditional no-bake foundry sand enables an analysis of whether 3D printed molds can produce metal parts of comparable quality to traditional casting approaches. These goals define a fundamental research question:

Research Question
How do castings made from two different 3D Printed sand molding materials compare to those of traditional no-bake molding methods?

Because the ExOne material system incorporates a two part binder system into a silica sand molding material similar to traditional no-bake, it is hypothesized the ExOne printed parts will have similar properties with those made with the traditional approach. In contrast, ZCast® uses a single part binder system that requires significantly more binder in the creation of molds for castings [29]. The large amounts of binder can cause gas defects in the final cast part, thus decreasing overall cast properties (Section 4.1.3). Table 4.1 lists the expected comparisons between the two 3DP molds and traditional no-bake and discussed further in Section 4.2.1 & 4.2.2.

Hypothesis
Castings from no-bake and ExOne molds will produce similar results, as compared to those produced via ZCast®.

Table 4.1. Hypothesized comparison of 3DP molding materials to traditional "no-bake"

Metric	ZCast	ExOne
Sand Tensile Strength	Lower	Higher
Dendrite Arm Spacing	Higher	Equal
Porosity	Higher	Equal
Hardness	Equal	Equal
Density	Equal	Equal
Surface Roughness	Higher	Equal
Tensile Strength	Lower	Equal

To evaluate the research hypothesis, castings from all three material systems are characterized and compared. A description of the experimental procedure, which included tensile testing of sand molds and analysis of the surface roughness, density, hardness, porosity, microstructure, and tensile strength of their resultant castings, is presented in Section 4.2. The results of these tests are presented and statistically analyzed in Section 4.3. Closure and a discussion of areas of future work are given in Section 4.4.

4.2. Experimental Procedure

The primary goal of this research is to compare the properties of sand strength in terms of handleability and metal cast in (i) ZCast® molds, (ii) ExOne sand molds, and (iii) no-bake foundry sand molds. The two 3D printed sands prepared by Binder Jetting are treated as the experimental group; chemically bonded silica sand, also known as no-bake sand, is treated as the control group (as there exists published information about its casting properties [69]). The binder ratio in the no-bake sand was 4:1 of Phenoset RB to APR-015 hardener/catalyst, which accounted for approximately 1.6% of the sand mixture [59]. A Palmer M50XLD continuous sand mixer was used to mix the silica sand and binder to create the no-bake sand [59]. Seven tests were performed to characterize the differences of each mold type (Section 4.2.1 & 4.2.2) and are listed in Table 4.2. In Section 4.3, the values are statistically compared to determine if each mold type is statistically equivalent.

Table 4.2. Tests performed to characterize and compare two 3DP sand molds against no-bake molds

Characterization Metric	Methodology
Binder Jetted Sand Characterization	
• *Sand Tensile Strength*	• *AFS 3342-00-S*
Cast Metal Characterization	
• *Dendrite Arm Spacing*	• *Zeiss AxioImage A2m™*
• *Porosity*	• *ImageJ*
• *Hardness*	• *LECO Vickers Hardness Tester LV700AT*
• *Density*	• *Archimedes Principle*
• *Surface Roughness*	• *Phase II SRG Surface Roughness Tester*
• *Tensile Strength*	• *ASTM E8*

4.2.1. Characterization of Binder Jetting sand systems

Both ExOne and ZCast® sands are processed via a Binder Jetting AM process, and are designed for receiving molten metal for sand casting applications. However, ExOne sands are processed differently, requiring a two part furan resin system for chemically bonding sand particles similar to the no-bake system. ZCast® is a plaster based material, bound with a one-part binder system requiring sufficiently more binder and a curing cycle before pouring. Furthermore, ExOne, like no-bake, can be used to cast ferrous and non-ferrous alloys, while ZCast® has a maximum cast temperature at 2000°F (1093.3 °C) and can only be used for casting non-ferrous alloys. Additional differences between the three molding materials are identified by tensile testing of the various sand samples to compare the two Binder Jetting sands on the basis of the handleability of the resultant printed molds (measured by tensile strength).

Sand Tensile Testing

In order to compare the handleability of the molds, tensile test data from previous work was used to statistically compare the strengths of each molding type [29,70]. The mechanical strength of the molds was characterized via tensile testing. Tensile testing was performed on ZCast® powder and no-bake foundry sand according to AFS 3342-00-S [59] and six equivalent tensile specimens were printed using ExOne sand. Tensile testing was performed using a tensile testing machine to determine the mold fracture strength. Collected data and modes of fracture for ExOne tensile specimens were compared with ZCast®, as well as specimens made from the no-bake sand system.

4.2.2. Characterization of Cast A356 Cylinders

To prepare cast metal specimens for analysis and comparison, printed molds were first designed digitally in CAD for fabrication via Binder Jetting. The mold designs featured hollow cylinders with an inner diameter one inch, wall thickness of 0.5 inches, and length of 4 inches. The larger one inch diameter specimen design provides sufficient material to be machined to typical specimen sizes for ASTM tensile tests given in ASTM E8-13a [71]. Six cylindrical molds where then printed in both ZCast® and ExOne powders. ExOne printed cylinders using controlled process parameters (controlled humidity, binder content, and sand distribution) while ZCast® cylinders were printed on a ZCorporation Spectrum Z510 with recommended settings listed in Table 4.3. The resultant ZCast® molds were then cured at 475 °F (246 °C) for five hours according to the manufacturer's recommended specifications. An image of both ExOne and ZCast® molds can be seen in

Figure 4.3. No-bake foundry sand was used to create the down-sprue, runners and gates for the printed cylinders. Four cylinders in no-bake molds were created by packing sand around one inch diameter dowels.

Table 4.3. 3D Printed mold material manufacturer process parameter specifications

3D Printed Material	Saturation Level	Binder/Volume Ratio
ZCast®	*94% (Shell); 49% (Core)*	*0.2045 (Shell); 0.0531 (Core)*
ExOne	*Proprietary Information – Printed by ExOne*	

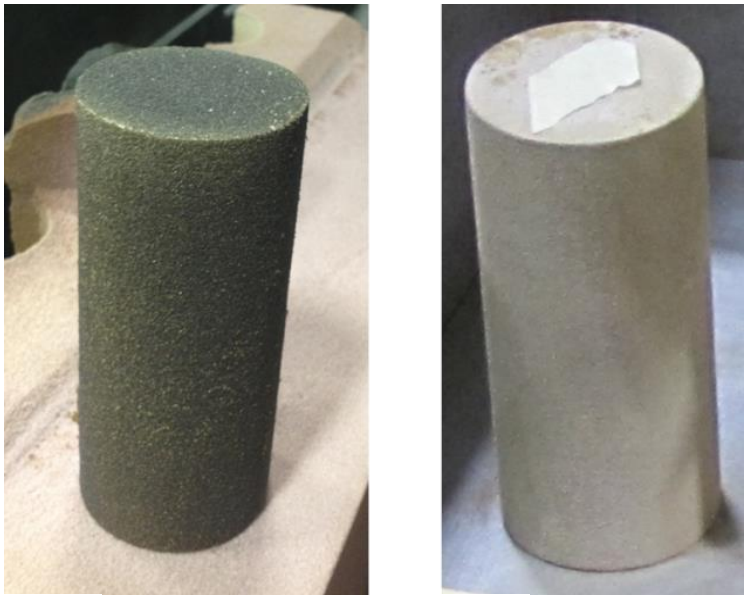

a) b)

Figure 4.3. a) ExOne and b) ZCast® printed molds

Following mold fabrication, A356-T6 alloy was cast into the two Binder Jetted mold materials and the traditional no-bake sand mold. All cylinder molds (no-bake, ExOne, and ZCast®) were poured with the same batch of aluminum. Before pouring, the aluminum was degassed using a rotary inert (nitrogen) degassing unit removing trapped hydrogen to reduce the effect of porosity. A standard T6 heat treatment of 1005°F (540.6 °C) for six hours and artificial aging at 315°F (157.2 °C) for five hours was applied to the cylinders. Compositional analysis was performed using a Bruker Q4 Tasman Advanced CCD-Based Optical Emission Spectrometer and verified that the material was in the range of standard A356 alloy chemistry values.

To aid in comparison of the castings, the resultant cast cylinders were then cut into top and bottom sections for material analysis, as shown in Figure 4.4. The primary top section was cut at the top and bottom to obtain the top and a middle specimen and the primary bottom was sectioned at the bottom for a bottom specimen.

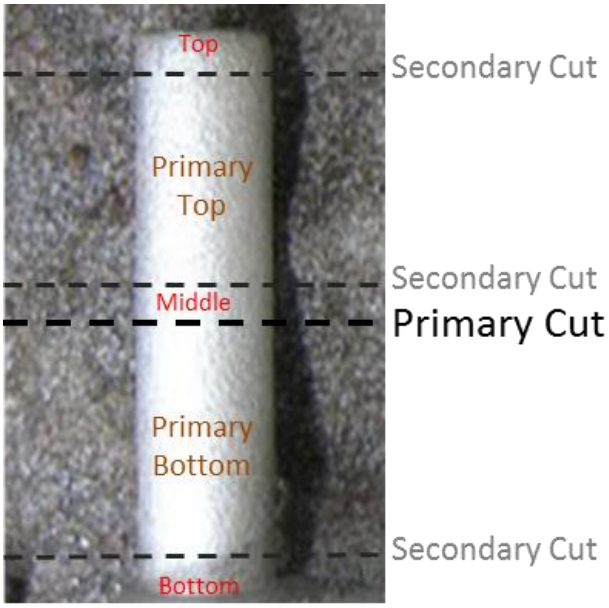

Figure 4.4. Sectioned cast cylinder for characterization of aluminum

Out of the six cylinders used for each material, three cylinders were cast in each of the three mold materials. A top section, middle section, and bottom section were obtained from each of the cast cylinders. These sections were mounted in epoxy to be analyzed for microstructure, porosity, and hardness. The three sections of each casting were compared to account for non-uniformity of properties along their lengths. The primary sections that were not used for microstructure, porosity, and hardness were used to evaluate density and surface roughness. The remaining three cylinders from both printed molding types were machined for tensile testing. The mean and standard deviation of material properties taken across all cylinders for each mold type are presented in Section 4.3.

Microstructure

The dendrite arm spacing was analyzed to determine if the different molds types provide a difference in micrsostructure which relates to mechanical properties for the aluminum cylinders. Finer dendrite arm spacing is desirable for better mechanical property performance and is a direct result of cooling rate. A faster cooling rate in Aluminum results in smaller dendrite arms, which in turn yields better mechanical properties. Samples were ground using 320 and 600 grit polishing paper on a MetPrep 3 grinder/polisher. The sample surfaces were polished using standard metallographic techniques with final polishing with 0.05 μm colloidal silica and a final

finishing cloth. No etching was required to examine the dendritic microstructure of aluminum. Optical microscopy was performed to characterize the microstructure and determine the dendrite arm spacing in each sample. Ten measurements were taken across the surface of each polished sample.

Dendrite arm spacing is a result of cooling rate which is dependent on thermal conductivity of molding materials. Because both ExOne and no-bake are molded using rounded silica, and therefore the same thermal conductivity it is expected that the microstructure of ExOne and no-bake will yield statistically equivalent dendrite arm spacing results. Furthermore, it is expected ZCast® will result in statistically different values, because it is made from plaster-based materials, which have different cooling rates. However, it is unknown if the thermal conductivity of ZCast® is larger or smaller compared to ExOne and no-bake sands.

Porosity

Porosity in cast specimens are defects and can significantly affect the strength and fatigue of the cast parts [67]. Five optical micrographs were taken of each sample for porosity measurements. ImageJ software was used to find the percent porosity by calculating the percentage of the total area covered by pores in each micrograph at 50x magnification [72]. These measurements were used to compare the quantitative relationship of porosity between molding materials. To accomplish this, the software was used to adjust the threshold of the image, highlight the pores, and measure the percent area of the pores. The threshold color brightness was adjusted until the pores were fully highlighted, and the size settings for analyzing particles were adjusted until the software recognized the pores. The ImageJ settings depended on the original saturation and contrast of the images. For example, micrographs with less contrast between black pores and surrounding material require higher threshold color brightness settings in ImageJ to fully highlight pores. The threshold color brightness values were adjusted to completely fill each pore before analyzing the porosity.

The overall porosity from ZCast® castings is expected to be larger due to the off-gassing discovered in the author's previous study [29]. It is also expected that the ExOne and no-bake will be similar as both use similar amounts of binder, which produce similar off-gassing

(although minimal) [70]. Additionally, throughout all molds, trapped hydrogen gas effects should not make any mold significantly more porous since the same batch of metal was used for all molds.

Hardness

Hardness testing was performed to further characterize the mechanical properties of the castings from each mold type. Testing was performed using a LECO Vickers Hardness Tester LV700AT. The cross-section hardness was measured in five locations of each polished cylinder cross section (15 per sample, shown in Figure 4.4). Upon testing hardness, it is expected that the hardness should remain the same throughout all specimens. Dendrite arm spacing affects mechanical properties, like fatigue strength, since it determines the size of the particles/phases [67]. Since hardness is a "macro" measurement, dendrite arm spacing has little effect. However, porosity could have minor effects on hardness from sub-surface pores beneath the load cell.

Density

Density was measured to compare the effect of porosity on the density of the part. Density of the cast A356 aluminum cylinders created by each of the mold types was measured via Archimedes' Principle using an A&D GX-2000 scale and Archimedes kit with distilled water. Three trials were conducted for each cylinder section. It is expected that the density of castings made from ZCast® will be lower than the other specimens due to the expected larger porosity. Similarly, ExOne and no-bake castings should have similar values for density since similar values were expected for porosity.

Surface Roughness

Surface Roughness can also have a large effect on mechanical properties including fatigue as well as geometrical resolution of the final parts being cast. Surface roughness was measured using a Phase II SRG Surface Roughness Tester. Roughness average (R_a) of the cylinders cast using different molds was measured. Surface roughness was taken of the outer edge of the casting in contact with the molding material. It is expected that castings made from ExOne and no-bake molds will have similar values for surface roughness. Because of the different size

distributions of both rounded silica sands (ExOne having a better controlled distribution), it is possible there will be slightly different values. ZCast® sand has a finer particle size, which could potentially increase surface roughness of the resultant casting. However, off-gassing effects could cause surface defects in the metal that is in contact with the mold, and thus have potential major effects on surface roughness.

Tensile Testing

To further evaluate the mechanical properties of the cast specimens, tensile specimens were machined from the cast cylinders to a gage diameter 0.35 in. and length of 4 in. according to ASTM standard E8-13a [71]. Tensile tests were conducted using an Instron 5984 Electro-Mechanical 150 kN Tensile Testing System. The strain rate was fixed at 5.0 mm/min. Ultimate tensile strength was recorded for comparison between cast cylinders produced by both printed mold types. Tensile tests were not performed on the cylinders cast using no-bake foundry sand since the tensile behavior of cast T6-A356 aluminum is published information [69]. As discussed in the previous section (Microstructure & Hardness), it is expected the tensile strength of the ZCast® will be statistically lower. These results are anticipated due to the expected change in microstructure and increased porosity. Additionally, it is expected that castings made via the ExOne material system will have similar properties as no-bake A356-T6.

4.3. Results and Discussion

Characterization data was collected for each of the three material types as indicated in Section 2. Statistical software (JMP 10.0.2) was then used to investigate potential significant differences in the data set. Characterization data for each mold type was tested for normality by plotting as a normal distribution and testing the goodness of fit. If the data failed the test for normality, a non-parametric Wilcoxon paired test was performed on the data; if data for all sand types are normal, a Tukey paired comparison was conducted. All data was analyzed using a level of significance (α) of 0.05. If the probability is less than the level of significance (<0.05), the values are considered statistically significant.

4.3.1. Properties of 3D Printing Powder

Sand Tensile Testing

Sand tensile specimens were produced from the mold materials and tested following the experimental plan outlined in Section 4.2.1. The results of tensile testing and subsequent statistical comparisons are reported in Table 4.4.

Table 4.4. Statistical comparison of sand tensile strength of the different mold materials

Mold Material	Mean (MPa)	SD (MPa)		Statistical Comparison	Wilcoxon *p*-Value
No-Bake	0.56	0.09		No-Bake < ExOne	0.0081
ExOne	1.34	0.07		No-Bake > ZCast®	0.0269
ZCast®	0.06	0.02		ExOne > ZCast®	0.0282

Upon investigating the potential statistical differences in the tensile strengths of the two printed mold materials and no-bake sands, it was found that the data set was not normally distributed. Thus the results of the non-parametric Wilcoxon tests were used to determine the *p*-values from the comparisons, as reported in Table 4.4. For sand tensile strengths, all molding types were significantly different: printed ExOne molds had the highest tensile strength followed by no-bake, and ZCast® sands.

The sand distribution of the ExOne Binder Jetting process must be well controlled for accurate placement of binders to increase geometrical accuracy and therefore contains a smaller mean particle size. The combination of ExOne (i) molds' two part furan binder and binder catalyst and (ii) refined sand distribution provide enhanced strength over the traditional no-bake sand molds. As with traditional binder systems, the two part binders used in the ExOne system rely on a chemical reaction to bond the sand particles together, which results in the significantly higher strength reported in Table 4.4. In contrast, the one part binders used for printing ZCast® do not provide the same level of strength as the two part binders in the ExOne product. Furthermore, the curing cycle required for minimizing binder off-gassing further decreases the molds strength.

4.3.2. Properties of Cast A356 Cylinders

Microstructure

After polishing the aluminum samples, optical microscopy was used to measure the dendrite arm spacing of the top, middle, and bottom sectioned surfaces (Figure 4.4). After determining the recorded data was normal, statistical analysis was performed using a Tukey HSD test. The statistical comparisons of the microscopy measurements are shown in Table 4.5 and micrographs displaying A356 microstructure from each mold type are shown in Table 4.5.

Table 4.5. Statistical Comparisons of Dendrite Arm Spacing

Mold Material	Mean (µm)	SD (µm)		Statistical Comparison	Tukey HSD *p*-Value
No-Bake	45.07	8.74		No-Bake = ExOne	0.9832
ExOne	45.28	7.22		No-Bake < ZCast®	<0.0001
ZCast®	51.88	7.68		ExOne < ZCast®	<0.0001

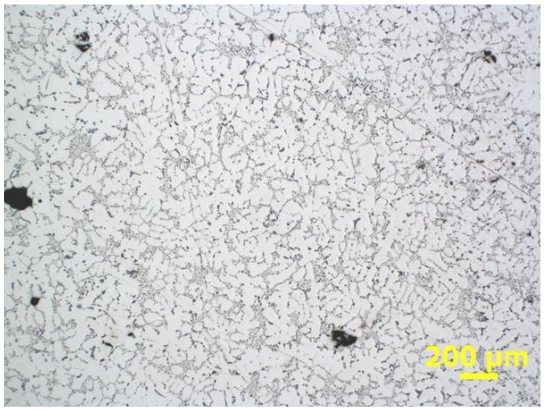

a)

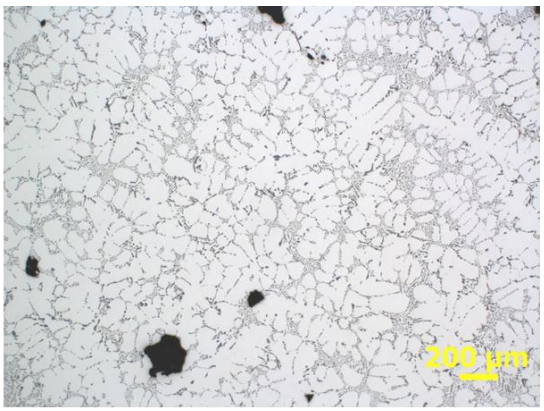

b)

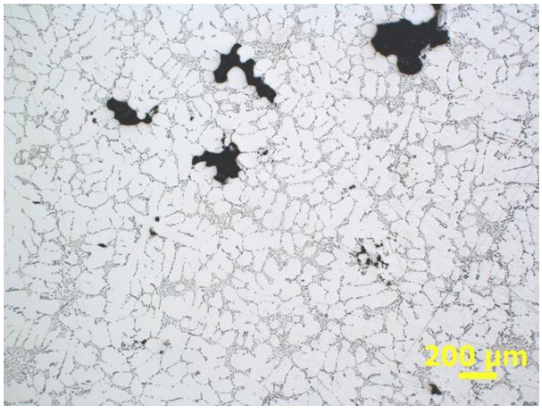

c)

Figure 4.5. Microstructure of A356-T6 alloy cast in a) no-bake, b) ExOne, and c) ZCast®

The dendrite arm spacing in the samples cast in no-bake (Table 4.5a) and ExOne (Table 4.5b) molds were not significantly different (45.28 & 45.07 μm respectively), thus verifying the initial hypothesis (Section 4.1.4). Both were significantly different from the castings resulting from ZCast® molds. Castings from ZCast® are better insulated, cool slower, and therefore have larger dendrite arm spacing due to the difference in thermal conductivity [67,73] in ZCast® materials (lower thermal conductivity value than silica in ExOne & no-bake molds). Therefore it was anticipated that the mechanical property values of ZCast® would be statistically significant from no-bake and ExOne.

Porosity

The amount of porosity present in the specimens was determined by using ImageJ software to analyze micrographs of the top, middle, and bottom polished aluminum sections of the three types of castings (Figure 4.4). Micrographs demonstrating the porosity of cast metal using the three different mold materials can be seen in Table 4.5. The statistical comparisons of the average porosity values for the entire samples are reported in Table 4.6. After determining the data was not normal, a non-parametric Wilcoxon test was used to determine if differences in the data were significantly different.

Table 4.6. Statistical Comparisons of Porosity

Mold Material	Mean (%)	SD (%)		Statistical Comparison	Wilcoxon *p*-Value
No-Bake	2.15	1.81		No-Bake = ExOne	0.5887
ExOne	2.02	1.91		No-Bake = ZCast®	0.1065
ZCast®	2.91	2.60		ExOne < ZCast®	0.0287

The porosity observed in samples cast using no-bake sand was statistically equivalent to both ExOne molds and ZCast® molds. However, ExOne and ZCast® molds were not statistically equivalent. ExOne had significantly less porosity as compared to ZCast®. As previously stated in Section 4.1.3, off-gassing of the binder in ZCast® molds during pouring caused entrapped gasses that lead to significant porosity in the final cast parts [29]. The resulting defects produce larger porosity measurements compared to both no-bake and ExOne molds, which was consistent with the initial hypothesis. ZCast® was statistically equivalent to no-bake due to the large

standard deviation in ZCast® and no-bake measurements. However, there were large differences between mean values of ZCast® and ExOne molds.

Hardness

The Vickers Hardness values of the metal cylindrical castings from the different mold materials were analyzed. After determining the data was not normal, a non-parametric Wilcoxon test was used to determine the statistical relationship of the castings. The statistical comparisons are reported in Table 4.7.

Table 4.7. Statistical Comparisons of Hardness Values

Mold Material	Mean (kgf/mm^2)	SD (kgf/mm^2)		Statistical Comparison	Wilcoxon *p*-Value
No-Bake	85.86	7.03		No-Bake < ExOne	0.04
ExOne	88.59	7.97		No-Bake < ZCast®	0.0341
ZCast®	89.10	6.91		ExOne = ZCast®	0.7993

The Vickers hardness values for specimens produced using ZCast® molds did not vary significantly from castings produced in ExOne molds. The test values for all specimens produced using printed molds fell within the normal hardness value range of 87.38 – 96.65 (kgf/mm^2) for the A356-T6 alloy [74]. However, both ExOne and ZCast® were significantly harder than castings produced by no-bake, which fell slightly below the published values.

It was expected (Section 4.2.2) that values for all cast specimens would be statistically equivalent. The low value of hardness for specimens cast from no-bake sand was surprising. Such a phenomenon could be caused by pores located in the polished surface. Although all samples had pores, two very low hardness values recorded for no-bake (66.4 & 72.6 kgf/mm^2) resulted in statistically lower values compared to ExOne and ZCast®. Without these values, all castings would be statistically equivalent. Furthermore, although gassing effects from ZCast® were significant enough to affect porosity measurements, they were not significant enough to produce large amounts of voids affecting hardness values.

Density

The overall density data for the specimens were normally distributed; as a result, a Tukey HSD test was used for statistical comparison. The statistical comparisons of the average densities of cylindrical specimens of A356-T6 aluminum cast from different mold materials are reported in Table 4.8.

Table 4.8. Statistical Comparisons of Densities

Mold Material	Mean (g/cm^3)	SD (g/cm^3)		Statistical Comparison	Tukey HSD *p*-Value
No-Bake	2.60	0.02		No-Bake < ExOne	0.0006
ExOne	2.62	0.01		No-Bake = ZCast®	0.8058
ZCast®	2.60	0.01		ExOne > ZCast®	<0.0001

The densities of the specimens cast from printed and no-bake molds were less than the standard reported density for the A356-T6 alloy (2.66-2.71 g/cm^3) [74]. Although density and porosity cannot be assumed proportional, porosity observed throughout the cast pieces (Table 4.6) did result in a lower overall density. The average density of no-bake castings did not vary significantly from ZCast®, whereas ExOne varied significantly from both no-bake and ZCast®. Porosity voids in the material caused a decrease in material per volume thereby decreasing the density of the specimen. It was expected that no-bake and ExOne castings would have statistically equivalent values. However, density of A356 alloy was mainly a function of silicon content [75]; because all of the samples were poured from one batch, regardless of what the actual theoretical value; the density was the same for all samples. The differences in density values can also be attributed to the error in measuring weight and a difference of 0.01 or 0.02 g/cc is within the measurement error. Furthermore, the differences in means for all specimens were small relative to the typical range of densities for aluminum.

Surface Roughness

The statistical comparisons of the surface roughness testing are reported in Table 4.9. After determining the data was normal, a Tukey HSD comparison was used to determine if the surface roughness of the cylindrical specimens cast using different mold materials were significantly different.

Table 4.9. Statistical Comparisons of Surface Roughness

Mold Material	Mean (μm)	SD (μm)		Statistical Comparison	Tukey HSD *p*-Value
No-Bake	13.15	4.17		No-Bake = ExOne	0.8055
ExOne	12.27	2.63		No-Bake < ZCast®	0.0008
ZCast®	18.60	5.37		ExOne < ZCast®	0.0001

Specimens prepared using ZCast® molds had the roughest mean surface finish. The samples produced using no-bake and ExOne were statistically equivalent. Samples made via ZCast molds had a significantly higher surface roughness than those made via ExOne and no-bake molds. From the author's previous work, it was discovered that ZCast® contains both a smaller particle size and higher binder content. Together, these features increase gas generation during pouring and provided limited permeability for off-gassing, which caused surface defects [29]. However, from a practical viewpoint, the surface roughnesses of castings from all sands were all acceptable for commercial sand castings, as industrial sand casting processes typically produce cast parts with surface roughness values between 12.5 and 25 μm [76].

Tensile Testing

Metal cylinders produced from the printed molds were machined to match tensile specimen requirements [71]. Following tensile testing, yield strength data were compared against published values to determine if the printed molds produced cast samples with mechanical properties comparable to traditional foundry techniques. A Tukey HSD test was used to determine if there were any significant yield strength differences between castings from no-bake, ExOne, and ZCast® molds. The statistical comparisons of the tensile testing are shown in Table 4.10.

Table 4.10. Statistical Comparisons of Ultimate Tensile Strengths

Mold Material	Mean (μm)	SD (μm)		Statistical Comparison	Tukey HSD *p*-Value
No-Bake	234 [77–79]	----		----	----
ExOne	236.36	6.54		----	----
ZCast®	180.90	10.32		ExOne > ZCast®	0.0809

The ultimate tensile strengths of the specimens cast using ExOne and ZCast® molds were significantly different. ExOne data was within the range of published experimental data for cast

A356-T6, while castings from ZCast® molds were considerably weaker. As expected, the decreased strength was due to the increased porosity (Table 4.6) and larger dendrite arm spacing (Table 4.5) of ZCast® castings (Section 4.2.2).

4.3.3. Visual Inspection

A comparison was made by visual inspection on mold filling of the two printed molds. Since both ExOne and ZCast® molds were cast together, the differences in filling were apparent upon shakeout (Figure 4.6). These slight differences in castings produced from ZCast® molds were attributed to the off-gassing occurring from the single part binder used in the molds.

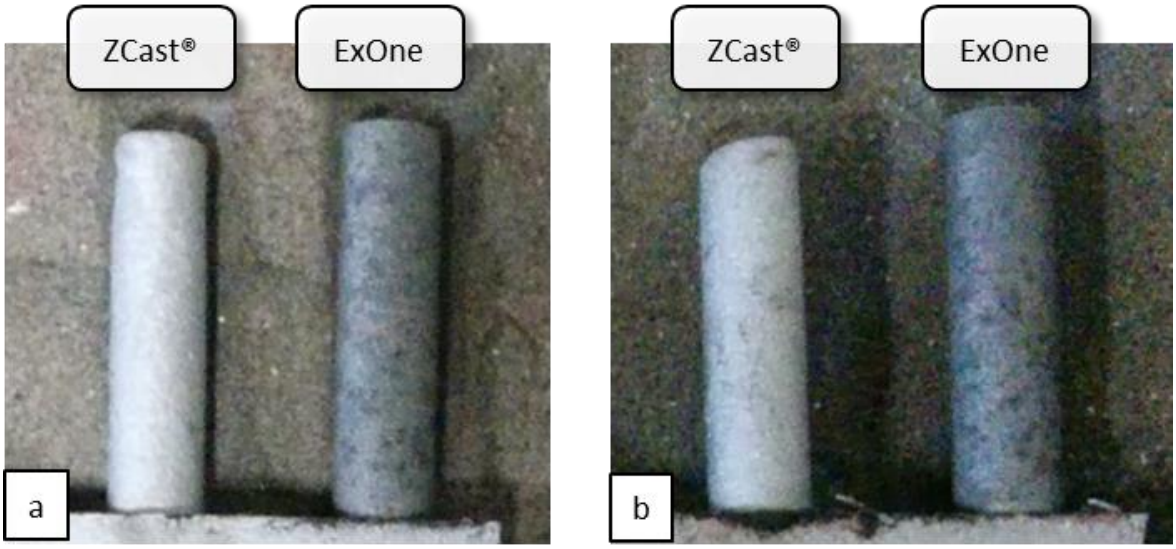

Figure 4.6. Visual comparison of two 3D Printed castings

4.4. Conclusions and Future Work

In this work, two Binder Jetting materials, ExOne and ZCast® sands, were compared against traditional no-bake sand to evaluate their ability to produce castings with equivalent properties. Specifically, the sands were compared on the basis of their handleability of the printed molds (sand tensile test) and quality of the cast metal they produced (microstructure, porosity, hardness, density, surface roughness, and tensile strength). It was hypothesized that the no-bake and ExOne molds would create similar quality parts because ExOne material system incorporated a two part binder system into a silica sand molding material similar to traditional no-bake. After characterization, it was determined that they yielded statistically equivalent results in four of the seven tests performed: dendrite arm spacing, porosity, surface roughness, and tensile strength.

They differed in sand tensile strength, hardness, and density. These differences were attributed to better control of sand distribution in ExOne sand molds, sub-surface pores affecting low hardness values in no-bake castings, and error associated in small relative mean differences for density. Castings produced in ExOne molds outperformed the other materials as they had better quantitative mean values in all seven tests. Furthermore, ZCast® molds produced poorer quality castings in comparison with no-bake and ExOne molds because of the gas defects associated with a high percentage of single part binder required for printing.

Comparing the two 3D printed materials, the manufacturing process (ZCorp's one part binder vs. ExOne's two part binder) and build materials (ZCorp's plaster vs. ExOne's silica) had a significant impact on the final part quality. Single part binders used for ZCast® relied on a larger quantity of binder and a thermal curing cycle to bind powders. Furthermore, the plaster-based ZCast® material had a smaller grain size, which required more binder to bond the larger surface area of the particles and lower mold permeability. All of this combined, produced off-gassing when in contact with molten metal during pouring. The resultant gas became entrapped in the mold, which caused porosity during solidification. Two part binders, however, bonded sands through chemical reactions of the hardener and resin to create molds, and thus had minimal off-gassing.

Although the three materials tested were statistically different in the selected tests run, the materials in general had a low difference of mean values on all tests conducted. In addition, the mean values from all seven tests were acceptable values for industrial cast parts. Furthermore, 3D printed molds delivered comparable parts to traditional no-bake molding system on the basis of handleability and casting quality.

Many of the difficulties faced with Binder Jetting sand in this work were due to off-gassing of large quantities of single part binder used in ZCast® material. Ultimately, it would be ideal to use a single part, environmentally friendly binder that requires no thermal curing cycle to produce molds comparable to traditional molding methods. This would eliminate the effects of off-gassing in single part binder systems and the need for a system to handle a two part resin and hardener. Additionally, utilizing flow modeling and casting rules would help to improve the

quality of castings. Additive manufacturing gives the designer the freedom to design complex gating systems (including sprue, gating, runners, risers, etc.) that cannot be manufactured by traditional molding techniques. Using these benefits of AM, flow may be optimized to decrease effects of oxide effects, microstructure can be altered or predicted by varying wall thickness controlling cooling rates and direction, and risers can be implemented to decrease shrinkage porosity. Controlling these values will affect the final quality of parts improving properties tested in this work (microstructure, porosity, hardness, density, surface roughness, and tensile strength).

5. EVALUATING PROCESS CONSTRAINTS IMPOSED ON SAND MOLDS FABRICATED VIA BINDER JETTING

5.1. Introduction

Metal casting is commonly used in manufacturing to create high-quality, low-cost products. While capable of producing a wide range of geometries, the sand casting process inherently constrains the design of a part to geometries that can be produced by (i) forming sand around pre-made patterns and (ii) careful removal of said pattern from the sand. As such, several "design for manufacturing" guidelines must be followed for successful part design for sand casting, for example: including draft angles for pattern release, avoiding sharp changes in cross-section, choosing only pattern geometries that are able to be removed from sand (e.g., undercuts), etc. [30,80]. The majority of casting constraints evolve from molds physically constraining the final casting promoting defects and/or metal solidification. These defects include porosity, solidification shrinkage, hot tears and distortion from linear thermal shrinkage, and stress concentrations from thermal gradients during cooling [67].

Recently, engineers have looked to using Additive Manufacturing (AM) to overcome these geometric restrictions. AM can be used to directly print the sand mold (i.e., patternless sand casting), thus removing some of the geometric constraints imposed by the need for draft angles and therefore avoid pattern geometries that would destroy the sand mold when removed [25,81]. The integration of AM technologies to the foundry industry has increased the efficiency of design and casting production including reducing time and cost associated with the traditional methods of development [17] while still maintaining high accuracy [8].

5.1.1. Binder Jetting Process and Capabilities

The most common AM process for the direct fabrication of sand molds is Binder Jetting. Binder Jetting is an Additive Manufacturing (AM) technology that creates artifacts through selectively inkjetting binder into a powder bed of raw material (Figure 5.1). Binder Jetting is a versatile method of printing powdered materials. Any powder material that can be synthesized, deposited, and bound with jettable binder may be used [81]. After printing each layer, the feed piston raises, the build piston lowers, and a counter-rotating roller spreads a new layer of powder

over the previous layer. Unbound powder fixes the part as it is being printed and also provides support/scaffolding for overhanging geometries. Each new layer is joined to the previous layer by the jetted binder. After the printing process is complete, the mold is removed from the build bed, and unbound powder must be removed from the casting cavities. This is done typically by either vacuum or compressed air. The mold is assembled and metal is cast into the mold as with traditional metal casting techniques. The technology is commercially offered by ZCorp's ZCast® material [51], ExOne's S-Max and M-Flex machines [52], and VoxelJet [53]. Direct digital fabrication of sand molds for casting eliminates the costs associated with pattern tooling and is thus ideal for low volume production [54,55].

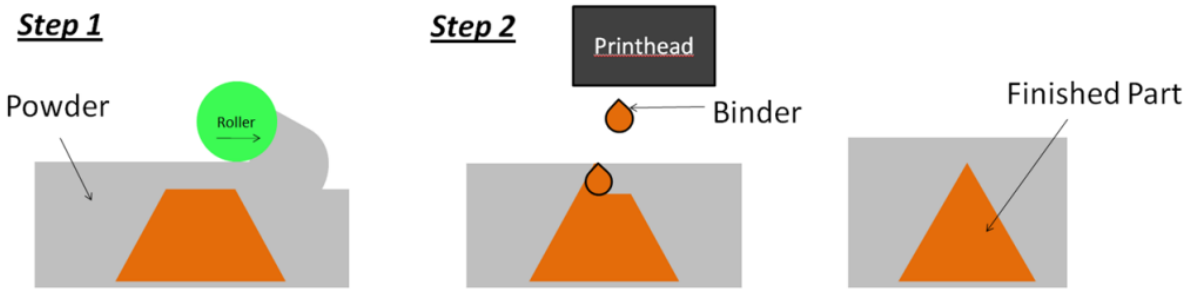

Figure 5.1. Binder Jetting AM Schematic

As with all AM processes, Binder Jetting offers tremendous design freedom for altering mold geometry; with this technology, molds can be fabricated with integrated gating systems, embedded cores, and without the need for a pattern. It also enables the creation of complex castings that could not be made by traditional means due to the layer-wise printing process and the support offered by unbound power. For example, printed molds (

Figure 5.2a) have been used to create complex cellular castings (

Figure 5.2b). The author's previous work have shown the potential of cellular materials to mitigate blast by dynamic modeling [82].

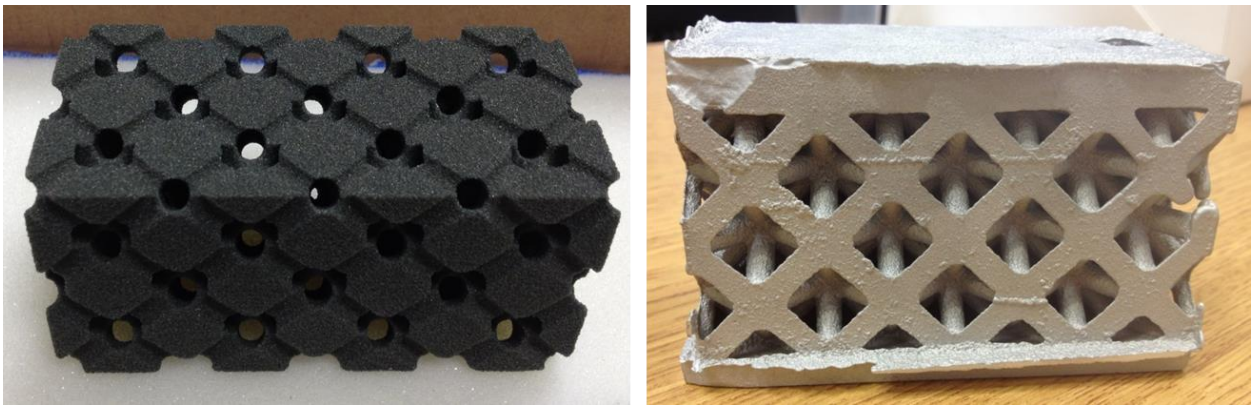

a) b)

Figure 5.2. Example a) printed cellular molds via Binder Jetting and b) resultant cellular castings

In order to utilize these manufacturing methods to generate complex cellular structures (

Figure 5.2), the designer must have an idea of the constraints imposed by the process. Although not as limiting as traditional manufacturing methods, the Binder Jetting process has inherent constraints in both build and post-processing steps. For example, feature size is limited by the resolution of the printer. Additionally, if the printer is able to print small features, removing unbound powder may not be possible from the printed features making the part unusable. Furthermore, if small features are able to be cleaned, feature size may be limited by the premature solidification of metals resulting in incomplete filling. Solidification may also limit geometries in complex parts (i.e. cellular geometries) due to abrupt change in flow path. Therefore, it is hypothesized that depowdering and solidification of molds made by Binder Jetting contribute greater limitations on the overall manufacturing process and thus will be the focus of this work. An understanding of these constraints will enable a designer to model a part with confidence that it will be able to successfully be printed and cast.

There has been limited literature on analyzing constraints by Binder Jetting AM technology on sand molds. Instead, past research in combining AM with metal casting has been focused in discovering new ways to implement the technology for metal casting either directly or indirectly. Some of these include Stereolithography (SLA) [83], Laser Sintering (LS) [17,23,84], Fused Filament Fabrication, and Binder Jetting technologies [25,27,85]. While there is not work identifying constrainst imposed by printed sand molds, there has been work in identifying

constraints on additively manufactured patterns for sand molds and investment castings. Frank and coauthors introduce a hybrid process for fabricating patterns for sand casting by adding "slab" layers and machining the layer to the desired shape [80]. The manufacturing process was constrained by the layer thickness (from the cutting tool length) and thin layers being sheared from the cut being made limiting feature size. Hague and coauthors studied the draining of uncured stereolithography resin from thin walls in sacrificial photopolymer parts for investment castings [86]. The "additional skins" setting on the sterelithography system was determined to have an effect on vertical ribs test articles, but only at an incline between 20-40° due to overcuring. Full drainage could be achieved at all variations of angles and "additional skins" at a minimum rib thickness of 3.0 mm. While process constraints have been identified in the area of printed patterns for sand castings and investment casting, they have not yet been defined for printed sand molds.

5.1.2. Overview of Work

The goal of the work in this section was to evaluate the limiting resolution constraints of the Binder Jetting process on sand molds. The critical constraints limiting the user's ability to cast small features was dependent the ability to (i) efficiently clean unbound powder from the printed mold and (ii) effectively cast metal through small intricate geometries. It was important to understand the proposed constraints to accurately take advantage of the design freedom in designing molds for metal casting with AM. This work was guided by an overarching research question that was divided into two sub-research questions:

Research Question	
What are the resolution constraints of the Binder Jetting printing process and how is it limited by metal solidification and depowdering?	
Sub Question 1	**Sub Question 2**
How are the resolution constraints limited by depowdering complex geometries?	*How are the resolutions constraints limited by metal solidification through complex geometries?*

Hypotheses and supporting literature are offered in Section 5.2. Section 5.3 will cover the experimental methods implemented to determine the constraints imposed by depowdering and metal flow and solidification. The results of the design of experiments of depowdering and

metal solidification are presented in Section 5.4. Finally, the conclusions and future work will be presented in Section 5.5.

5.2. Background

In order to determine the constraints imposed on complex geometries by the Binder Jetting AM processes, initial hypotheses were forumulated. Hypotheses for both sub-questions were derived from resulting literature and fundamental knowledge of metallurgy.

5.2.1. Depowdering Complex Cavities

Binder Jetting has the capability to manufacture small features. However, from experience, the constraint on feature size is imposed by the depowdering process as very small printed features are often accidently removed due to forces used in depowdering. Additionally, feature size is dependent on the smallest area of a mold that can be successfully depowdered in complex geometries. Based on material type used in Binder Jetting technology, there are multiple post processing methods of depowdering build material from the primitive part. These include dry processes such as compressed air [87], vacuuming [88], and vibration [87], as well as wet processes including ultrasonication [89], microwave-induced boiling [88], and CO_2 bubble generation in soda water [81,87]. For this work, the author will be using ExOne sand digital part materialization system and compressed air. ExOne is a common commercial Binder Jetting printer that uses a two-part furan binder system that is similar to that used in traditional chemically bonded sand molds. This system has been successfully used to create complex cellular geometries [82]. Compressed air is used to depowder parts due to the efficiency of powder removal and ability to accurately control pressure.

Across all AM systems, there has been limited research conducted on understanding the variables of the depowdering post-process. Vayre and coauthors (2013) conducted studies on depowdering of metallic round channels printed via Electron Beam Melting (EBM) to determine the geometric constraints imposed by powder removal (e.g., powder that could not be removed from small, long channels). The authors depowdered unsintered powder from EBM technology utilizing a Powder Recovery System (PRS) [31]. Several tests were conducted on cleaning the unbound to determine characteristics of cleaning printed parts. The PRS uses loose build material

powder (Ti6Al4v) under pressure to remove unsintered powder from channels (as opposed to compressed air used in Binder Jetting). Each part was cleaned for approximately 10 minutes. There were repeatability issues regarding cleaning depth and were attributed to the measuring device. The measuring device marginally compacted the powders depending on the amount of pressure applied while measuring. Additionally, the authors assumed changes in the PRS could contribute to variations in depth measurements. From this study, an equation was determined to aid designers when considering the post processing of loose unsintered powders [31]. They determined the effect of removal followed a linear trend in the experimental data where the height of the channel is directly proportional to the diameter. Utilizing this information, an initial hypothesis is proposed.

Hypothesis 2.1
The cleaning length of circular channels printed via Binder Jetting is dependent on the smallest cleanable diameter, cleaning diameter, and connectivity.

In this work, a series of experiments similar to that employed by Vayre and coauthors were employed to determine the smallest functional part feature that can be fabricated via Binder Jetting. In addition, a regression equation for using compressed air to clean powder from parts made with the ExOne Binder Jetting process was determined (Section 5.3.1).

5.2.2. Metal Solidification in Complex Channels

In addition to the constraints imposed by depowdering, additional constraints are imposed by metal flow and solidification through intricate channels. When poured in a mold, molten metal freezes based on the thermal gradient of the mold wall and the thermal conductivity of the mold material. Freezing is accelerated when the metal flow encounters small channels due to a larger casting modulus (Volume to Surface Area) based on Chvorinov's rule [30].

There currently is limited literature on solidification constraints imposed by the manufacturing process on complex geometries. There is, however, standard testing equipment for determining the fluidity of metals. Metal fluidity is typically performed using a spiral mold to decrease flow restrictions. The fluidity of the metal is determined by the length of the flow before freezing [30]. Similar tests will be performed in this work to determine the effects of the metal flow through complex geometries in printed molds.

When casting complex structures in binder jetted sand molds, metal must flow through a series of channel geometries that are not typical in traditionally fabricated castings. These long circular channels provide relevant data to determine the maximum length of metal flow due to a larger casting modulus [30]. A larger casting modulus has a less contact surface area to transfer heat from the metal, therefore solidification is slower [30] and thus maximizing the fluidity of the alloy being cast. Utilizing this existing knowledge, Hypothesis 2.2 was formulated.

Hypothesis 2.2
Complex geometry will promote freezing due to an increase in path length and change in direction.

5.3. Experimental Methods

The experimental approach consisted of two separate foci: determining the constraints imposed by depowdering (Section 5.3.1) and determining the constraints imposed by metal solidification (Section 5.3.2.) Depowdering constraints were evaluated to determine the maximum cleaning distance that can be achieved with respect to i) channel diameter and ii) connectivity (opened/closed). Metal flow constraints were examined for maximum flow before freezing while varying i) choke diameter, ii) flow direction angle, and iii) channel diameter. For both depowdering and solidification, a Taguchi design of experiments (DOE) was used to evaluate the independent variables, each with two factors.

5.3.1. Cleaning Printed Mold Channels

The goal of the depowdering experiments was to discover the smallest cleanable diameter and the effect of two constraining parameters (molds with varying diameters and connectivity) on cleaning distance. The cleaning characteristics and their relationships were determined through a design of experiments (DOE) and by the development of a regression equation. The cleaning of round channels was investigated as the cellular structures of interest (

Figure 5.2) were comprised of a series of circular channels that stretched throughout the length of the mold in straight paths to form the trusses of the final cast part. Therefore the constraints tested were limited to these types of cleaning paths.

It was hypothesized that the cleaning distance was dependent on the smallest cleanable diameter, channel diameter, and connectivity. To identify the smallest cleanable channel and the variables that affect cleaning length, depowdering experiments were conducted on mold channels of various diameters and connectivity conditions. Specifically, eight total individual diameters (1/2, 1, 2, 3, 4, 5, 6, 7 mm) (Figure 5.3) were designed and printed using ExOne's rounded silica sand material. Rounded silica provides the best flowability of unbound material, thus making it easier to remove. An open and closed variant of each diameter was printed and tested. The smallest channel diameter (0.5 mm), approximately the size of the largest particle in the printed material, was printed to ensure tests were performed on diameters that could not be cleaned. This provided the starting point for determining the smallest cleanable diameter.

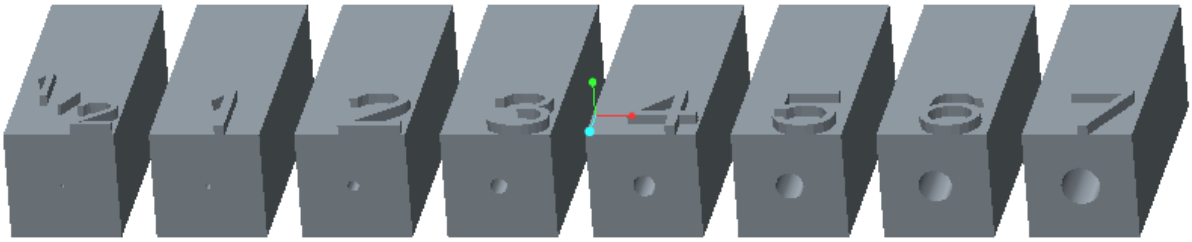

Figure 5.3. Test arrangement for cleaning channels in ExOne printed molds

Once printed, all molds were cleaned from one side only by using compressed air at a constant pressure (344.7 kPa) for approximately 10 minutes. Upon successful depowdering, the amount of removed powder was determined by measuring the length of the cleaned channel. Specifically, the author measured the length of a metal rod that was inserted into the channel until it came in contact with remaining powder. This ensured excess powder was no longer being removed. A fixture for the compressed air was designed and printed to ensure that the nozzle kept a constant distance of 5 mm from the opening of the channel. The fixture for cleaning is illustrated in Figure 5.4. Two tests for each mold were conducted for sufficient data for determining the smallest cleanable channel, the DOE, and regression equation.

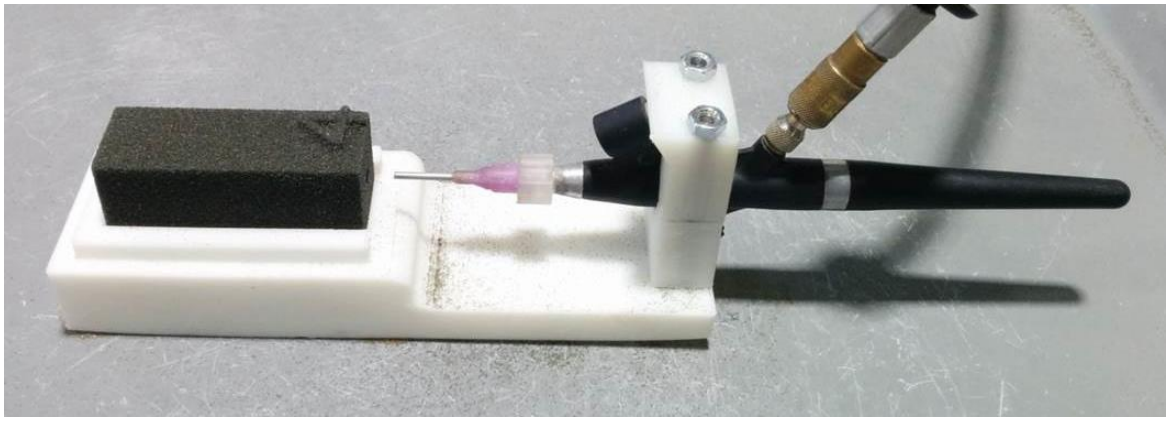

Figure 5.4. Fixture for cleaning channels in printed parts by ExOne technology

A Taguchi design of experiments (DOE) was used to determine the effects of independent variables on cleaning. Critical variables were evaluated with two factors each – a high and a low factor. The critical variables tested were diameter and connectivity (opened/closed). Although eight total diameters were used for cleaning tests, only two diameters were required by the DOE. These variables were chosen because they represent actual instances in cleaning complex molds. Small channels may not be cleaned or have a large effect on cleaning distance (diameter variable). Additionally, channels may suddenly end or change angle and therefore is uncleanable or has a channel that is open on both ends. Having open connectivity is ideal because it enables the designer to clean from each end and thus maximize the cumulative volume of powder able to be removed. For each variable, the DOE only requires two factors for analysis to determine if a variable affects cleaning distance. Two factors, a low (3 mm – smallest cleanable diameter) and a high (6 mm – larger diameter) were chosen. It was expected that the larger diameter will have a larger effect on the cleaning distance by increasing the ratio of channel volume to particle size allowing particles to move more freely. Although, connectivity could significantly increase channel cleaning if both ends are accessible, it was not expected to have a significant effect on cleaning from one end only. The variables (diameter/connectivity) and factors (low/high) are listed in Table 5.1. After inputting all elements into statistical software, JMP, eight total experiments were identified in a L4 orthogonal array. The final measurement was a "Larger is Better" input of depowdering distance through the channels. The "Larger is Better" was used, because the largest cleaning distance was desired for the DOE.

Furthermore, utilizing the results from the tests, a regression equation for cleaning distance as a function of diameter was found by plotting and fitting a curve to the data from the eight diameters.

Table 5.1. Design of Experiments Setup for Cleaning Circular Mold Channels

Independent Variables	Channel Diameter (mm)	Connectivity
Factors	*3.0*	*Opened*
	6.0	*Closed*

5.3.2. Evaluation of Solidification and Flow through Complex Printed Molds

After determining the smallest cleanable area for circular printed channels, multiple experiments were conducted to determine how complex part geometry can be constrained by metal flow and solidification within the mold. A knowledge of how flow is affected by complex geometries is important for the designer to confidently include features that may be printed and cast successfully. It was hypothesized that complex geometry will promote freezing due to an increase in path length and change in direction. Utilizing a design of experiments, the author determined the relationship of the parameters (angle change, channel diameter, and choke diameter) and how to utilize these variables to maximize flow distances before solidifying.

Specifically the goal of this work was to determine how mold geometry variables (angle change of molten metal, mold channel diameter, and mold choke diameter) affected flow distance through complex geometries (Figure 5.5). From prior research in metal flow in castings, molten metal does not change direction easily due to the momentum through channels [30]. It is expected that smaller angles to the horizontal flow direction will have shorter flow distances than those with larger angles. Additionally, it was expected that modifying the channel diameter would increase the distance of flow. An increased diameter decreases the amount of head loss and thus increases the flow distance, according to the Darcy-Weisbach equation [90]. Finally, a smaller choke would promote solidification, because it decreases the travel of liquid metal before freezing. This would decrease flow rate (continuity equation [90]) enabling more heat to be removed from the metal per distanced of flow. It was expected that the choke size would significantly impact solidification as small changes in its diameter has a large impact on flow rate (e.g., based on area calculations a 50% diameter increase will increase the flow rate by

225%). Channel diameter would have less effect on the flow rate because the diameter change between factors was of lower magnitude (33% vs. 50%).

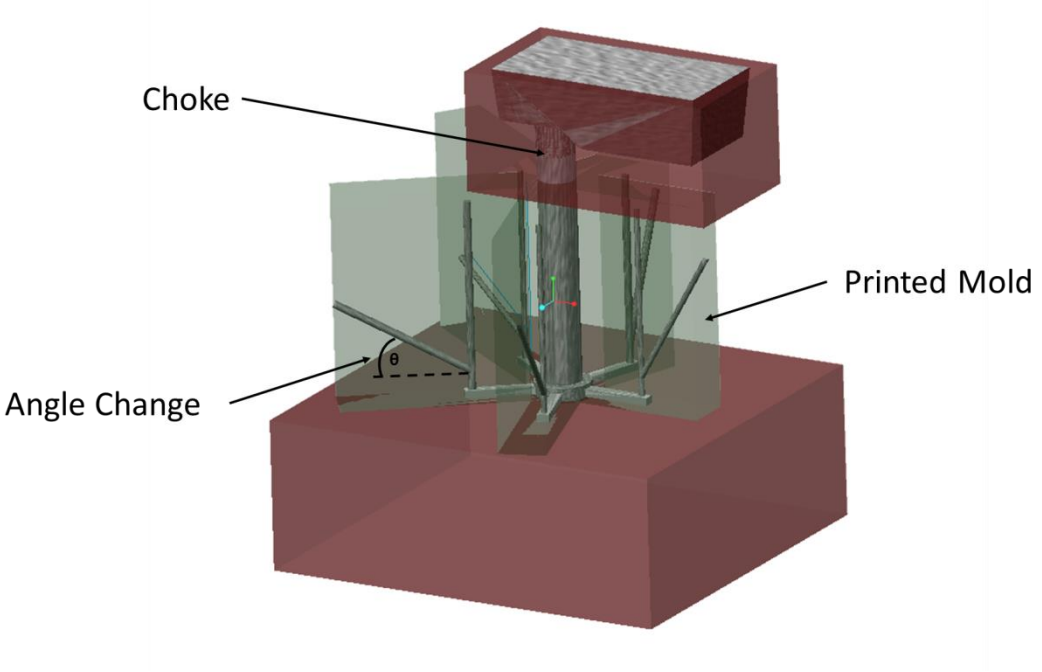

Figure 5.5. Experimental Setup for Testing Flow through Complex Channels

5.3.2.1. Molding Experimental Design

A design of experiments using Taguchi's Methods was used to evaluate the essential independent parameters (angle change, channel diameter, and choke diameter) of the flow experiment (Section 5.2.2). Taguchi DOE is used to eliminate the need for a full factorial experiment. For each independent variable, two factors were considered: a high and low factor. A large and a small angle (15 & 75 degrees) to the horizontal were chosen to determine the effects of the two extreme values on solidification through complex geometries. Two slightly different channel diameters (3.81 & 5.08 mm) and choke diameters (6.35 & 9.53 mm) were chosen to determine if their values had a significant effect on metal solidification. The final measurement was a "Larger is Better" input of metal flow distance before solidification. The "Larger is Better" criteria was used, because the maximum length of flow was desired. The critical independent variables for the DOE were inputted into statistical software (JMP). The software identified the combination of variables needed for each test to be performed.

Molds were designed in CAD to incorporate the limiting parameters in printed molds (angle change, channel diameter, and choke diameter) and fulfill the experiments identified by the DOE. The first parameter (angle change) was altered by designing all molds with vertical channels and channels branching from 5 different angles (15, 30, 45, 60, and 75 degrees) (Figure 5.5). The channel diameter (second parameter) was changed by creating two variations of molds with differing branch diameters. Finally, choke diameter (third parameter) was set by choking the pour basin of metal flow into the downsprue. The designed molds (experimental tests) with included independent variables identified by the DOE are listed in Table 5.3 and Table 5.2. Although only two channels out of five required by the DOE were used for analysis, the remaining three were designed as a fail-safe in case of any defects occurred from initial low and high factors that were chosen.

Like the depowdering tests, the molds were printed using the ExOne Binder Jetting AM process with rounded silica sand. Traditional no-bake sand was used for the base, pour basin, and to create a shell for the designed printed molds to minimize the amount of printed material.

Table 5.2. Mold combinations determined by Taguchi DOE

	Mold 1 – Choke 6.35 mm				
Angle (deg.)	*15*	*30*	*45*	*60*	*75*
Diameter (mm)	*3.81*	*5.08*	*3.81*	*3.81*	*5.08*

	Mold 2 – Choke 9.53 mm				
Angle (deg.)	*15*	*30*	*45*	*60*	*75*
Diameter (mm)	*5.08*	*3.81*	*5.08*	*5.08*	*3.81*

	Mold 3 – Choke 6.35 mm				
Angle (deg.)	*15*	*30*	*45*	*60*	*75*
Diameter (mm)	*5.08*	*3.81*	*5.08*	*5.08*	*3.81*

	Mold 4 – Choke 9.53 mm				
Angle (deg.)	*15*	*30*	*45*	*60*	*75*
Diameter (mm)	*3.81*	*5.08*	*3.81*	*3.81*	*5.08*

Table 5.3. Design of experiment independent variables and factors for solidifications

Independent Variables	Choke (mm)	Angle (deg.)	Diameter (mm)
Factors	*6.35*	*15*	*3.81*
	9.53	*75*	*5.08*

From each mold combination determined by the DOE, two castings were created – resulting in 8 total tests. Using this type of combination eliminated a full factorial experiment. The castings were poured at a controlled temperature range of 720 – 735 °C. An aluminum alloy, A356, was used as the base alloy for pouring the castings. The metal was heated using a 125 kW lift swing Inductotherm induction furnace to melt and pour. Four tests were initially poured using the same batch of metal and four more tests were repeated using the sprues, gates, and runners from the initial batch. After all eight castings were poured and left overnight to cool, the mold was removed and the length of each cast feature was measured. These values were inputted into the software JMP and evaluated to analyze the effects of the independent variables.

5.4. Results

5.4.1. Depowdering

The results from the depowdering experiments defined by the Taguchi DOE can be seen in Table 5.4. The parameter estimates are shown in Table 5.5.

Table 5.4. Results of the Taguchi Design of Experiments for Depowdering

Diameter (mm)	Angle (deg.)	Distance of Cleaning (mm) Trial 1	Distance of Cleaning (mm) Trial 2
3.0	Open	24.37	20.69
3.0	Closed	22.73	29.58
6.0	Open	44.66	41.49
6.0	Closed	43.94	44.73

Table 5.5. Parameter Estimates of Taguchi Design of Experiments for Depowdering

Parameter Estimates		
Term	**Estimate (mm)**	**Probability > |t|**
Intercept	*34.024*	*0.0111*
Diameter [3 mm]	*-9.681*	*0.0388*
Connectivity [Closed]	*1.221*	*0.2870*

As expected (Section 5.3.1), the cleaning diameter was found to be statistically significant. Furthermore, connectivity was not statistically significant. This is expected because the air pressure was only able to effectively move small volumes of sand from uncleaned areas and it was not dependent on open or closed channels. The statistically significant values can be seen using the prediction profiler (Figure 5.6) by observing differences in the slope of the line between low and high factors. A larger slope, representing a larger difference, has a greater effect on the variable.

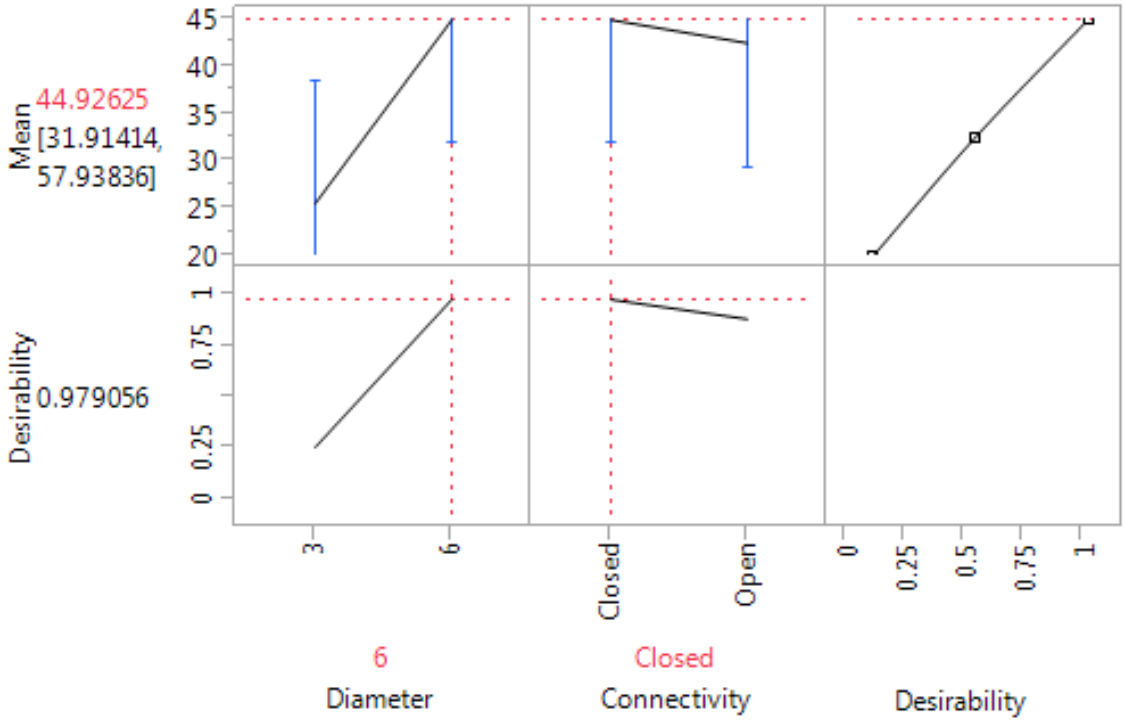

Figure 5.6. Prediction Profiler with Desirability Functions of Depowdering

Data for all eight diameters were plotted to determine both the minimum cleaning diameter and an equation that related cleaning distance to channel diameter (Figure 5.7). As determined by samples in Figure 5.3, the minimum cleanable diameter was 3 mm. A small distance was recorded for a cleaning diameter of 2 mm due to small amounts of loose sand being removed at the mouth of the channel. However these values were insignificant and could not be related to sufficient cleaning compared to diameters of 3 mm or greater.

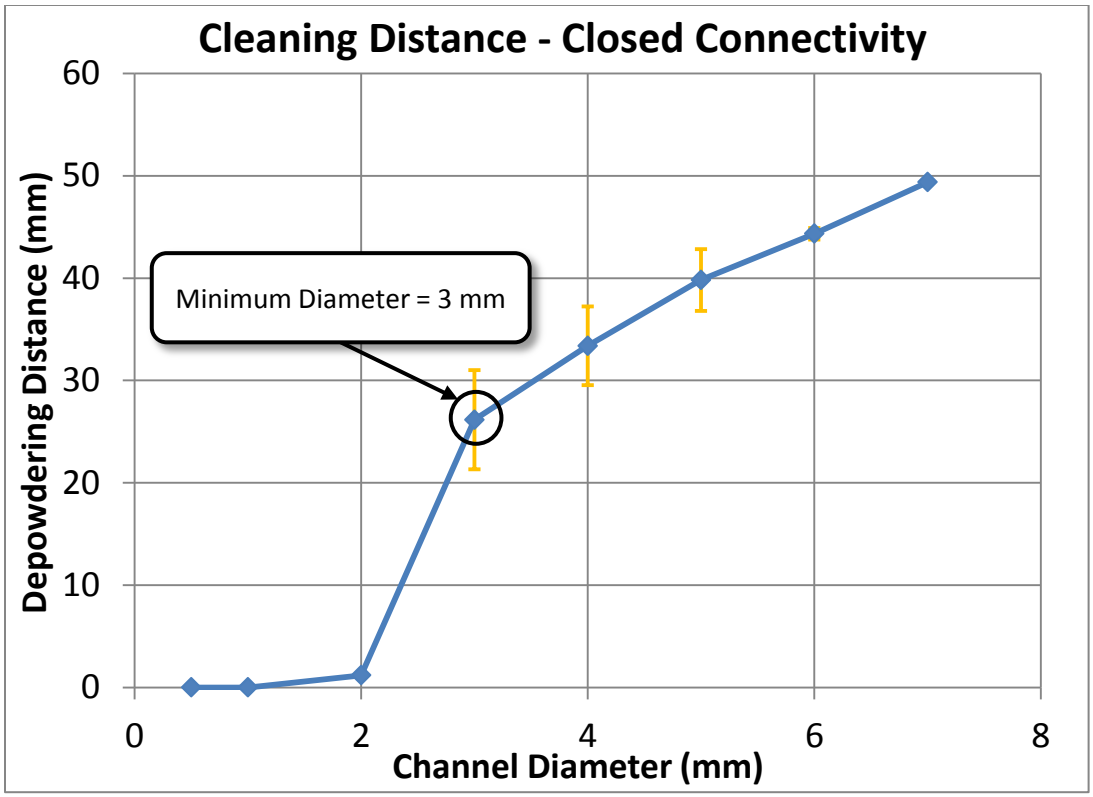

Figure 5.7. Depowdering Cleaning Distance vs. Channel Diameter

An relationship was determined correlating for all values greater than the minimum cleaning diameter and the depowdering distance (Equation 5.1). Furthermore, the results confirmed that depowdering was a dominant constraint as one is able to print smaller features than that which could be successfully cleaned. Utilizing this equation, designers can interpolate cleaning distance at diameters greater than 3 mm.

$$Depowdering\ Distance = 6.4 * Diameter + 7.6 \quad \textbf{(5.1)}$$

It is important to note that the values recorded for cleaning were based on ExOne OEM sand. These values were for "best case" cleaning, maximizing depowdering because of the spherical shaped silica sand in the manufacturing process. Using non-spherical or angular build material will decrease the depowdering distance due to reduced powder flowability. Additionally, the values attained using Equation 5.1 were for a pressure of >344.7 kPa. Larger distances may be accomplished by an increased pressure, but it could significantly erode internal channels, which could decrease the accuracy of the final casting.

5.4.2. Solidification

Upon determining the smallest printable feature, the relationships of critical parameters, and a regression equation that relates cleaning distance to channel diameter, the author sought to establish the effects of casting parameters and their relationship to metal solidification in complex channels. Following the experimental technique outlined in Section 5.3.2, the length of the resultant cast features was measured to determine total flow distances before solidification. These measurements were then input into statistical software JMP for analysis. The results from the Taguchi design of experiments are given in Table 5.6 and the parameter estimates in Table 5.7.

Table 5.6. Results of the Taguchi Design of Experiments for Depowdering

Choke (mm)	Angle (deg.)	Diameter (mm)	Distance of Flow (mm) Trial 1	Distance of Flow (mm) Trial 2
6.35	15	3.81	5.59	13.12
6.35	15	5.08	28.82	24.80
6.35	75	3.81	0.00	0.00
6.35	75	5.08	21.91	28.25
9.53	15	3.81	75.23	72.04
9.53	15	5.08	80.19	76.84
9.53	75	3.81	19.16	21.61
9.53	75	5.08	53.24	51.26

Table 5.7. Parameter Estimates of Taguchi Design of Experiments for Solidification and Flow

Parameter Estimates		
Term	**Estimate (mm)**	**Probability > |t|**
Intercept	*35.89*	*0.0020*
Angle [15 deg.]	*10.62*	*0.1028*
Diameter [3.81 mm]	*-9.90*	*0.1209*
Choke [6.35 mm]	*-19.79*	*0.0171*

As discussed in Section 5.3.2, it was expected that the only significant parameter would be the choke due to its large effect on flow rate. The resulting parameter estimates validated the choke diameter was statistically significant while both angle and channel diameter were not.

Furthermore, the desirability was calculated using the statistical software JMP. The maximum desirability was analyzed in the prediction profiler and is shown in Figure 5.8. Maximizing desirability utilizes the data to determine the best combination of variables for predicting the maximum distance of flow before solidification. It was determined that a smaller angle (15 degrees), a larger channel diameter (5.08 mm), and a larger choke diameter (9.53 mm) provided the best results. It was predicted that both the larger channel diameter and choke diameter would provide maximum flow, but a smaller angle from the horizontal wasn't predicted to maximize desirability. It was expected that the larger angle would have a larger flow distance due to a higher momentum of metal flow from the vertical channel. However, this may have a larger effect when casting metal in strictly horizontal planes. Therefore, it was determined that gravity had a larger effect on the flow of metal than momentum change due to the large differences in pressures (head height - ρgh) in the smaller angle compared to the larger angle from horizontal.

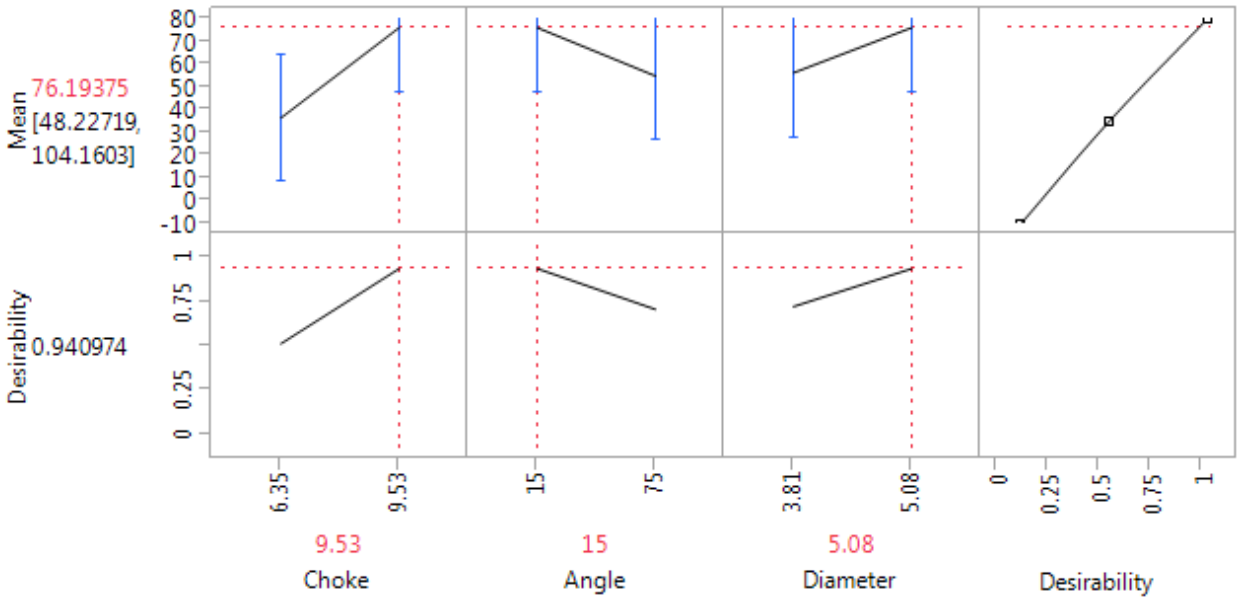

Figure 5.8. Prediction Profiler with Desirability Functions of Solidification and Flow

With this new understanding of the effects of solidification constraints during design of complex geometries, a designer is now better informed to take advantage of the design freedoms offered by AM of sand molds. Specifically, it has been determined that choke diameter has a significant effect in controlling the distance of flow. In addition, it was determined that increased head pressure has a larger affect than momentum (vertical channels). However,

momentum effects should be considered with angle changes in horizontal passages (constant head pressure).

5.4.3. Analytical Solidification and Flow Results

In addition to experimental results of solidification and flow, commercial solidification software (ProCast) was used analyze solidification (freezing of molten metal) in the printed molds. The software was initially used to compare the experimental and analytical results. However, the software fails to take into account variables affecting flow of metals and resulting in error between the software and what happens in experimentation. For example, the software requires a fill time of the entire mold and calculates the velocity. The velocity term assumes the entire cross sectional area of the downsprue is filled creating an "ideal" situation for flow. However, flow in molds experience contraction with a sudden decrease in cross sectional area as in the case with the pour basin to downsprue situation. This contraction decreases the flow rate therefore increasing the time of fill inhibiting the metal from flowing the same distance as the ideal case. Additionally, analytical calculations, like other finite element methods, require a finite number of mesh elements to obtain an accurate model. Utilizing small channel sizes (as those required by the complex geometry) is limited to the amount of elements that can be efficiently calculated by the desktop PC. Only a small element density was able to be run effectively using the computing resources available to the author. Therefore, the analytical software (ProCast) was not used to compare the experimental values as it did not accurately represent the resultant complex casting geometries used in this study.

5.5. Conclusion

The goal of this work was to identify constraints imposed by the Binder Jetting AM process on the resolution of printed sand molds. Specifically, the part resolution was found to be limited first by i) the user's ability to remove unbound powder and ii) the solidification of metal through intricate casting cavities. Depowdering constraints were evaluated to determine the maximum cleaning distance that can be achieved with respect to channel diameter and connectivity (opened/closed). A Taguchi design of experiments was used to evaluate these relationships. It was determined that the channel diameter was statistically significant while the connectivity was not. Additionally, the experimental results revealed a minimum cleaning diameter of 3 mm and

by using curve fitting, an equation relating cleaning distance as a function of channel diameter was established.

Furthermore, metal flow constraints were examined for maximum flow before freezing by varying the choke diameter, flow direction angle, and channel diameter. A Taguchi design of experiments (DOE) was used to evaluate the independent variables. It was determined that the choke diameter was statistically significant while both the channel diameter and angle change were not. Additionally, utilizing a prediction profiler, metal flow before solidification was maximized with a larger choke diameter, larger channel diameter, and smaller angle to the horizontal axis.

Using the resulting relationships of the independent variables for depowdering and solidification, the designer now would have a better understanding of the constraints imposed by the Binder Jetting AM process on intricate castings produced by the ExOne Binder Jetting system.

6. FABRICATION OF METAL-CERAMIC COMPOSITE STRUCTURES THROUGH THE BINDER JETTING AND CASTING PROCESSES

6.1. Introduction

Metal matrix composites are defined as a metal matrix reinforced by a constituent material, usually a ceramic [91], to provide materials with improved properties including low density, high specific strength, high specific modulus, high thermal conductivity, and wear resistance [92]. The matrix of the composite supports and transmits loads distributed to the secondary material used as reinforcement [30]. Metal matrix composites (MMC) can be broken down into two different fabrication processes: 1) solid state processing and 2) liquid state processing. Solid state processing includes using powder metallurgy and diffusion bonding. Liquid-state processing involves infiltrating, dispersion, spraying, and in-situ fabrication [92]. Many of the applications where metal matrix composites could have a significant impact have not been adopted because of the high cost to performance ratio [93] associated with the ceramic insert (e.g., fibers) used to create the reinforcement. For the case of ceramic fibers, the preforms are manufactured by mixing the fibers by press forming or suction forming. The liquid is removed and the preform is dried [94]. Such manufacturing processes are complex and the resulting parts are not reliable and can have unwanted phases. Furthermore, open cell ceramics (ceramic foams) have been used for the formation of MMCs to decrease the cost associated with preforms made with ceramic fibers [93]. But like MMCs fabricated with ceramic fibers, cost and geometric limitations are imposed by the manufacturing process associated with machining the final parts. This work will be focused on infiltration (liquid-state processing), which involves infiltrating molten metal into an ordered macro-porous ceramic printed via Binder Jetting additive manufacturing (AM) technology to produce MMCs.

Utilizing AM to form the ceramic pre-sintered pieces for MMCs, enables the manufacturer the freedom in complexity to create unique composites designed for specific applications. Traditional forming of ceramics, include pressing, casting, or plastically forming the ceramics into a green part. The green parts are then sintered by a pressure-less or pressure-assisted cycle to create the final ceramic artifact [95]. These ceramic forming methods are unable to manufacture complex geometries such as ordered cellular geometries (repeating unit cells

featuring voids ordered throughout the structure) and rely on extensive post processing means to attain the desired ceramic shape. The goal of this work was to print, via Binder Jetting, a ceramic in structurally ordered cellular preforms for the manufacture of ceramic-zinc MMCs. The author studied the forming, characterization, and sintering of Additively Manufactured ceramics to fabricate metal-ceramic composites or metal-matrix composites (MMC). Manufacturing MMCs with ordered cellular preforms would provide multiple functionality to the resultant part including decreased mass (and therefore weight) while increasing strength and stiffness and would allow the engineer to produce intricate geometries for specific design purposes as opposed to stochastic ceramic fiber and open cell preforms.

6.1.1. Binder Jetting Process and Capabilities

Binder Jetting is an AM technology that creates artifacts through the deposition of binder into a powder bed of raw material. Once a layer has been printed, the powder feed piston raises, the build piston lowers, and a counter-rotating roller spreads a new layer of powder on top of the previous layer. The subsequent layer is then printed and is adhered to the previous layer by the jetted binder. A schematic of the Binder Jetting AM process can be seen in Figure 6.1.

Binder Jetting is a versatile method of printing powdered materials. Any powder material that can be synthesized, deposited, and bound with a jettable binder may be used [81] including plaster, sand, metal, and other ceramics [8,59,96]. The focus on this work is to create MMCs by printing ordered ceramic preforms. Other AM technologies such as powder bed fusion [97], vat photo polymerization [98], and extrusion [99] have been used to process ceramics, but they are outside the focus of this work. After printing the ceramics in their green state, it has been proved they may be sintered to create parts with a density of up to 99.2% [96]. As with all AM processes, Binder Jetting offers tremendous design freedom for altering geometry. The technology is commercially offered by ExOne's M-Print® and M-Flex® machines [64] and 3D Systems' Professional ProJet® [51].

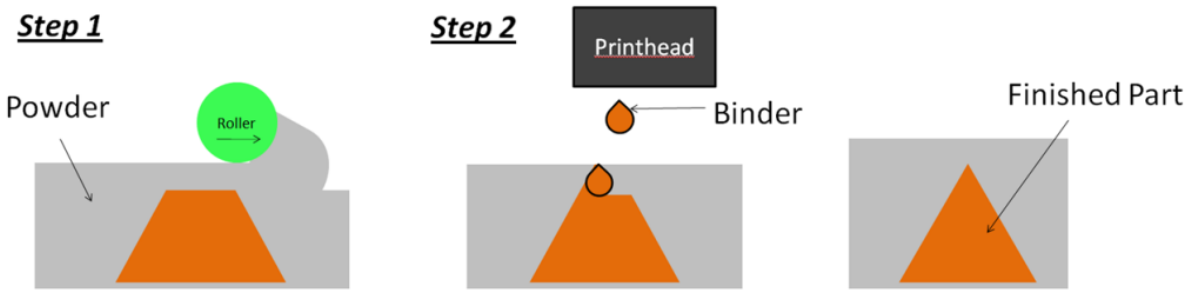

Figure 6.1. Binder Jetting AM Schematic

Ceramics have been successfully printed and sintered for a variety of needs. Yoo and coauthors (1993) printed alumina powders to manufacture structural ceramic components that were 99.2% dense and had a flexural strength of 324 MPa [96]. Additionally, they were able to control the microstructure of zirconia toughened alumina (ZTA) by adding a stabilizer during the jetting process [100]. Seitz and coauthors (2005) used Binder Jetting to print hydroxyapatite (HA) ceramics to produce ceramic scaffolds for bone tissue engineering [101]. They were able to attain internal passage resolutions of 450 µm, wall thicknesses of 330 µm, and 22 MPa in compression. Sachs and coauthors (1990) tested the dimensional accuracy and part strength of printed parts from several ceramic powders including 320 grit (45 µm) aluminum oxide, silica, zirconia, zircon, and silicon carbide. Dimensional control was determined to be approximately ±20 µm along 38 mm dimensions. Part strength was determined to be strong enough to handle and survive during pouring, but not strong enough to overcome the contraction of the metal during cooling. They determined that the geometric freedom offered by Binder Jetting could be used to efficiently prototype materials with specific application considerations and material properties [102].

Furthermore, AM of ceramics has been used to print preforms, but not specifically ordered cellular preforms. Sachs and coauthors (1990) explored the ability of Binder Jetting to create green ceramic preforms for infiltrating molten metal in order to manufacture metal matrix composites [102]. Additionally, they printed macroscopically toughened composites from SiC and Al 224 to eliminate cracks from propagating due to the interface [103]. Moon et al. (2001) printed carbon preforms with a designed mesostructure for reaction-infiltrating creating SiC-Si composites [104]. The print head speed was varied to obtain the desired preform microstructure and was controlled along the length of the complex preforms therefore controlling the carbon

content along the part. This lead to the ability to vary the reaction along the part and produce functionally graded SiC-C composites. The part contained three times the amount of binder saturation from one end to the other, resulting in a Si content of ~8 wt. % at the end with the highest binder saturation compared to ~ 24 wt. % at the end with the least binder.

6.1.2. Overview and Purpose of Work

The goal of this work was to develop a process to effectively manufacture MMCs with printed ceramic (cordierite ordered cellular structure) as the reinforcing material. Cordierite precursor ceramic materials were printed in an ExOne R2® system with a glycol based binder and sintered in an electric furnace. Later, by integrating printed ceramics into bonded sand molds, molten metal was casted into the molds to create the metal matrix composites. As discussed in Section 6.1, this work focused on the forming (printing), sintering, and characterization of ceramic parts to produce cellular geometries for MMCs (Table 6.1). Utilizing cellular geometries could provide sufficient strength in bending and compression modes to cast parts while decreasing the weight of the part [61]. An schematic of the manufacturing process is shown Figure 6.2. The composite was casted with a zinc matrix and tested on a three-point bend fixture and compared to both constituent materials. The objective of this research was guided by a fundamental research question.

Research Question 3
How are mechanical properties (flexural strength and modulus) of MMCs created via Binder Jetting and Metal Casting affected by the manufacturing process parameters (powder preparation, sintering temperatures, and casting process)?

Table 6.1. Overview of experimental methods for the evaluation of Cordierite

Manufacturing Process	Ceramic Process

- Raw Material Preparation (Section 6.2)
  - Ceramic Powder Selection
  - Particle Size Analysis
	- Batching (formulation)
	- Characterization

- Printing Parameters for Green Part Creation (Section 6.2.2)
  - Binder Selection
  - Layer Thickness
  - Heater Temperature
  - Binder Saturation
  - Spread Speed
  - Drying Rate
	- Forming

- Sintering Profile (Section 6.2.3) - Sintering Temperature	- Sintering

- Post-sintered (Section 6.2.4)
  - XRD
  - Density
  - Shrinkage
  - Optical Microscopy of ceramic
	- Characterization

It was expected that the ceramic-zinc MMC would show significant difference on the properties of the final part compared to the individual phases and that it was dependent on the manufacturing process parameters (Table 6.1). Therefore an initial hypothesis was developed:

Hypothesis 3
MMCs produced from printed ceramics with higher density and good bonding (mechanical or chemical) at the metal-ceramic interface will have better mechanical properties (flexural modulus and strength) compared to the matrix material alone (zinc).

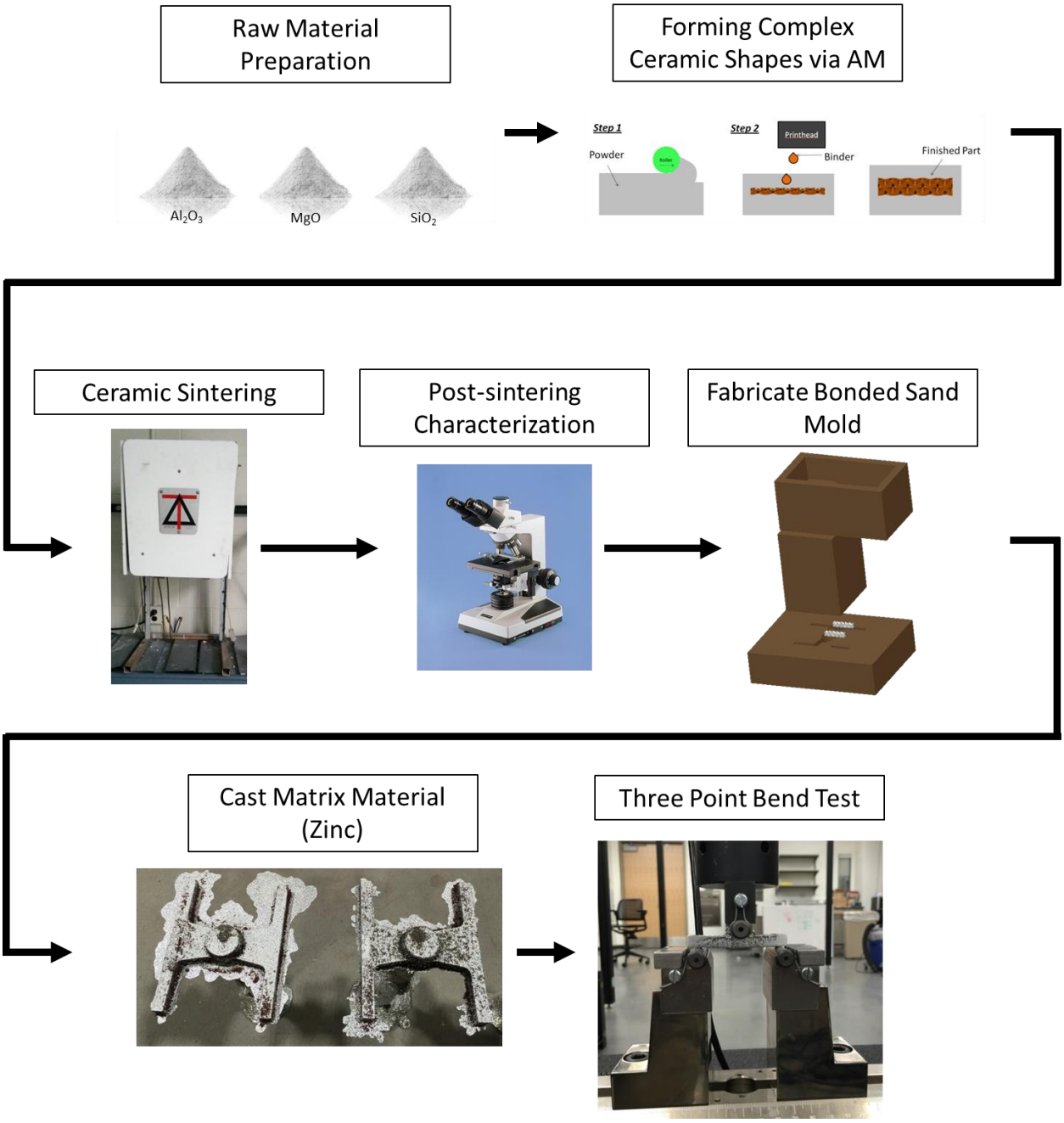

Figure 6.2. Proposed MMC manufacturing process

The ceramic raw material characterization and printing parameters for the green part manufacture, sintering experimentation, and post-sintered characterization were investigated and results are given in Section 6.2. Later, Section 6.3 covers manufacturing of the ceramic-zinc composites and the resulting mechanical properties and interfacial characteristics. Finally, the conclusions are discussed as well as future considerations in Section 6.4.

6.2. Manufacturing Process Parameters

6.2.1. Raw Material Preparation

Before creating the proof of concept MMC, the precursor materials for manufacturing ceramics via AM were selected and characterized. These materials were selected based on the functional requirements of the manufacturing process (printing, sintering, and casting requirements).

6.2.1.1. Powder Selection

Several candidate materials were considered after successfully printing with the ExOne R2® system, yet, these did not meet the functional requirements of the manufacturing process (high thermal shock resistance, high service temperatures, etc.). Due to its poor thermal shock resistance behavior, alumina (Al_2O_3) alone was not considered a useful candidate for higher temperature cast metal matrix. However, when reacted with silica (SiO_2) and magnesia (MgO) cordierite ($2MgO•2Al_2O_3•5SiO_2$) is formed which provides a much improved thermal shock resistance and the presence of a liquid phase during firing. The liquid phase aids in sintering by decreasing the sintering temperature and increasing the rate of diffusion. Additionally, varying combinations of these materials would provide different properties for discrete applications and could be easily adjusted to fit further applications. For example, if increased strength is required and a sintering temperature is not a concern, the composition can be varied based on the properties of the resulting material; thus cordierite was chosen as the candidate ceramic insert material for a MMC part.

6.2.1.2. Particle Size Requirement

The ideal particulate powder size and shape for Binder Jetting is spherical with a mean size of 20 μm. However, off-the-shelf oxide powders for creating sintered ceramics are mostly angular containing smaller mean size distributions. Precursor powders typically are pressed and sintered to increase the final density with less shrinkage of the final part. A smaller mean particle size aids in reactivity, grain size, density requirements, rate of sintering, and temperature [105]. Printing ceramics via Binder Jetting is limited by the ability of the powder to be recoated by the binder evenly across the build tray. Dry powders with small particle sizes (<20 μm) are

difficult to spread due to the cohesive strength of the high surface area of fine particles [85,96]. Additionally, spherical powders are desired for ease of spreading as opposed to angular particle shapes [103]. For this work, off-the-shelf ceramic powders were used as the raw materials for printing in the ExOne R2® system.

6.2.1.3. Precursor Cordierite Materials: Mixture, Binder Compatibility, and Particle Size Analysis

Cordierite was chosen because it has excellent thermal shock properties to withstand molten metal temperatures and also has a sintering temperature in the range of the electric furnace available [106]. Cordierite precursor materials were mixed using the amounts in Table 6.2 derived from the molar composition ($2MgO•2Al_2O_3•5SiO_2$). The raw materials were mixed in a container with Al_2O_3 balls to ensure thorough blending and that agglomerates were broken up.

Table 6.2. Ceramic raw material mixtures

Ceramic	**MgO (wt. %)**	**Al_2O_3 (wt. %)**	**SiO_2 (wt. %)**
Vendor	*Alfa Aesar*	*Catapal*	*N/A*
Cordierite ($2MgO \cdot 2\ Al_2O_3 \cdot 5\ SiO_2$)	*13.78*	*34.86*	*51.36*

The precursor powders were mixed and tested with an ethylene glycol based binder (PM-B-SR2-05) used in the ExOne Binder Jetting AM equipment, to ensure that the material and the binder were compatible. The binder and precursor materials were mixed by hand, pressed into pellets, and sintered to verify that the parts, when printed, would retain their shape after sintering.

The particle size distribution of the precursor materials and the precursor mixture were analyzed using a Horiba LA-950® Laser Scattering Particle Size Distribution Analyzer. By determining the particle sizes, the author was further able to determine if the material was compatible with the printer (Section 6.2.1.2). The mean particle sizes of the precursor mixture and the number fraction and cumulative percent finer distributions of the mixed material are shown in Figure 6.3.

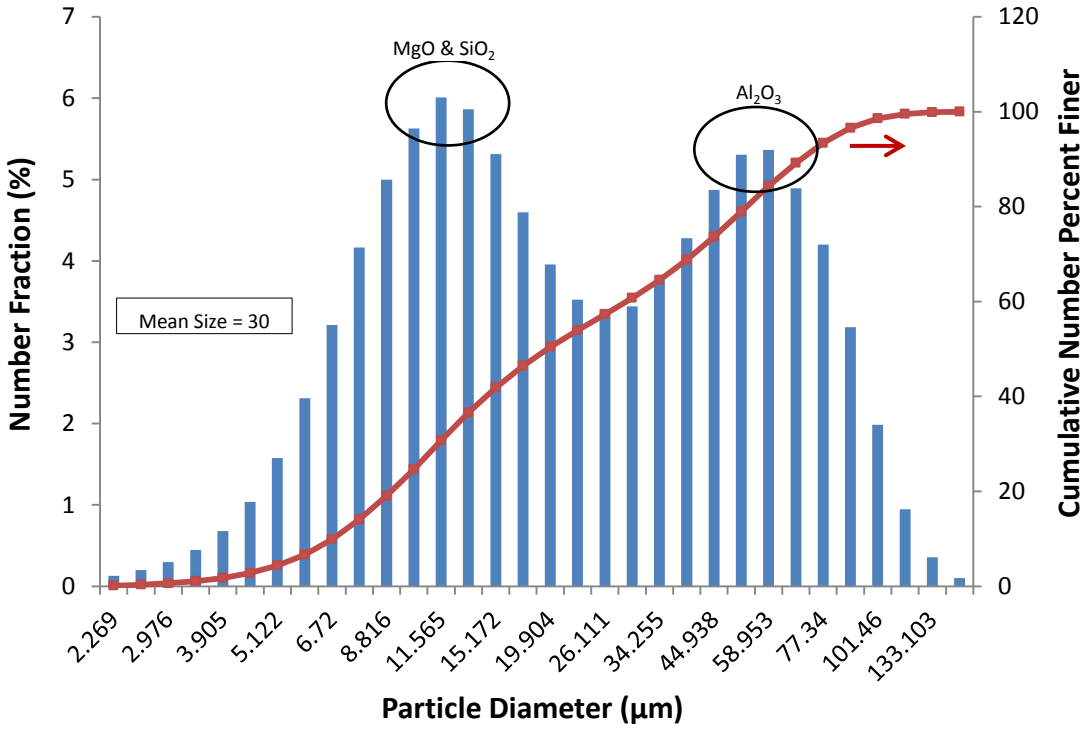

Figure 6.3. Particle size analysis: Number fraction and cumulative number percent finer distributions of cordierite precursor raw materials.

Table 6.3. Mean particle sizes of individual materials and cordierite precursor mixture

Material	Magnesia (MgO)	Alumina (Al_2O_3)	Silica (SiO_2)	Precursor Mixture
Mean Diameter (µm)	11.06	67.89	16.80	30.47

The cordierite precursor powder mixture had a mean particle size (30.5 µm) that was considered satisfactory for spreading in the AM system. However, not all individual materials were above the threshold (Table 6.3) and the trimodal distribution of particles in combination with the angular shape of the raw materials, resulted in a limited homogeneity of the powder mixture spreading step. In order to overcome the spreading restrictions of the available raw material, adjustments were made to the printing parameters in an attempt to maintain a consistent spread by the roller from the feed to the build tray of the AM system, as discussed in Section 6.2.2. Eventually, the powder was able to spread evenly at low spread roller speeds with minor tracks from the previous due to agglomerates forming from the small particles in the wave of powder forming the new layer. The resulting spreads were satisfactory for printing complex shapes for proof of concept MMCs.

6.2.2. Forming via AM: Printing Parameters

The goal of the present forming process was to manufacture geometrically intricate and accurate parts with sufficient green part strength for further handling, e.g., sintering. During the forming process, printing parameters such as binder selection, layer thickness, heater temperature, binder saturation, spread speed, and drying rate were adjusted to achieve these objectives. Small solid rectangular parts were printed to ensure that the green parts had sufficient part strength to cure and be transferred to the furnace for sintering. Additional octet truss unit cells (section A-B in Figure 6.4) were printed to determine the printing parameters of more complex shapes, Figure 6.4. The printing parameters used for successful forming of a green part with sufficient strength are listed in Table 6.4.

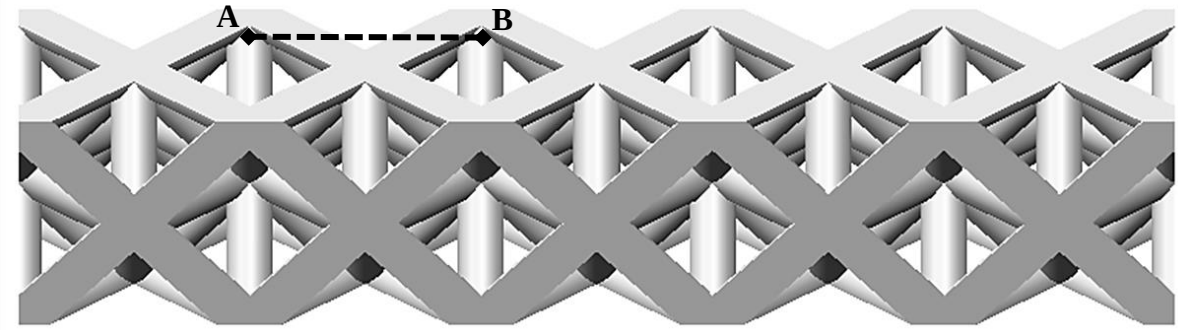

Figure 6.4 CAD Schematic of cellular repeating octet (A-B dotted line) truss pattern.

The printing parameters were adjusted to produce two distinct part types; i) solid parts for characterization purposes and ii) complex cellular parts for the purpose of creating metal-ceramic cellular structures (Section 6.3). It was determined that binder saturation and overhead heater speed values were different for these two types of shapes. Binder saturation was adjusted based on resultant green part strength. Excessive binder would decrease the quality of the final parts due to unwanted binder "bleeding" while green parts with too little binder could have limited strength. Saturation values for complex parts required a higher amount of binder (250%) whereas solid objects required lower values (150-190%). High binder saturation values were not appropriate for solid objects, due to binder bleeding, which would decrease dimensional accuracy by excess bound powder from the surrounding support powder.

Table 6.4. Printing parameters for printing cordierite precursor powders with ExOne R2® system

Parameter	Value	
Binder Selection	PM-B-SR2-05	
Layer Thickness	200 μm	
Heater Temperature	120-170°C	
Spread Speed	1 mm/s	
	Solid	Complex
Binder Saturation	150-190%	250%
Overhead Heater Travel Speed	1 mm/s	20 mm/s

Binder saturation was based on a printer input parameter – packing density. The ExOne R2® system was limited to the amount of additional pressure to create denser "as printed" parts. Typically, spherical powders were used for better spread ability (Section 6.2.1.2) and have similar tap and apparent densities. The tap density could be measured and input into the printer. Additionally, adjusting the particle size distributions (mono-sized particles, bimodal, ternary, quaternary etc.) could be used to increase the initial packing density of the printed material as long as particle segregation effects would not become prominent.

Furthermore, the drying rate produced by the overhead heater on the printer, was dependent on binder saturation values (Table 6.4). The drying rate was the rate that the overhead heater moves across the build tray after each layer was printed. The overhead heater on the AM system was used to dry binder after each layer to avoid excessive bleeding of binder by partially curing the binder. Heating the jetted binder gave the printed part strength during and after printing the part in its green (unfired) state. The larger the saturation values (and consequently more binder) required prolonged heat for curing. Solid parts required slower drying rate for the large volume of material to be dried/cured while complex parts used an accelerated rate to avoid over-drying and delamination of layers during depowdering the green part.

As previously noted, the binder used was a proprietary Ethylene Glycol-based thermosetting liquid that would cure at 190°C. Once printing was completed, the green part was removed from the build bed, depowdered, and placed in an oven at the curing temperature for 2 hours. The cured binder gave strength to the part before placing in a high temperature environment for sintering.

The layer thickness was determined experimentally after printing the materials at different layer thicknesses. Any spreading defects during printing of thinner layers would produce potentially catastrophic results in the previous layer and therefore in the final part. In addition, the larger layer thickness provided much shorter overall build times. Because of the limitations of spreading fine angular powders (Section 6.2.1.3 & 6.2.2), thicker layers were tried and found to yield higher quality parts.

As discussed previously, spreading was satisfactory and was minimally controlled by adjusting spread speed. Setting the spread speed to the slowest value of 1 mm/s provided the best spread of the precursor materials. A slow spread speed minimized agglomerates from being drug across the new layer and instead created a tumble motion from the wave of new powder.

6.2.3. Sintering of printed parts

Small rectangular green parts that were used for testing printing parameters were also used for several firing trials to determine a satisfactory sintering temperature and amount of liquid (glassy) phase presence. Ceramic green specimens were placed in a furnace for firing with a 5 °C/min ramp rate to the binder burnout temperature of 800°C for one hour, a 5 °C/min ramp rate to the final sintering temperature with a dwell of one hour. The fired samples were removed from the furnace, at temperature (1350°C, 1360°C, 1375°C, and 1400°C) and at the end of the dwell period. The ceramic parts acquired a wet (glassy) texture and appeared to be fully melted at 1450°C. This observation determined a rudimentary range of temperatures 1350°C-1400°C for finding the preferred firing cycle. Relative bulk density and shrinkage characterization (Section 6.2.4) was performed on specimens sintered at those specific temperatures and a sintering cycle of 1375°C was deemed sufficient for creating the MMC ceramic inserts.

6.2.4. Post-sintered ceramic characterization

As described in the sections below, in addition to relative bulk density and shrinkage the sintered ceramic parts were submitted to x-ray diffraction (XRD) and Optical Microscopy as the preliminary set of observations to determine the properties of the fired ceramic.

6.2.4.1. Relative bulk density measurements

The relative bulk density, using the Archimedes Principle, for the sintered ceramic parts was evaluated. Because the density determines the ultimate strength of the ceramic, this metric (along with shrinkage and porosity) was used to determine the sintering cycle. The parts were impregnated with oil before testing to seal the surface porosity and eliminate any water from penetrating interconnected porosity of the part (ASTM standard B962). [107] Based on the raw materials utilized in the precursor powder mixture for the AM process, the resulting fired ceramic part was expected to show a cordierite or cordierite like nature. Thus the data shown in Figure 6.5 was based on a theoretical density for cordierite (2.51 g/cc) [108]. As expected the density increased significantly until reaching approximately 92% at 1375°C. At this temperature, the ceramic parts reached the final stage of sintering (~90% density) and any further increase in temperature would generate an excess of the bonding liquid phase (with lower viscosity) and the integrity of the part would be compromised by slumping or by a complete melting of it [95].

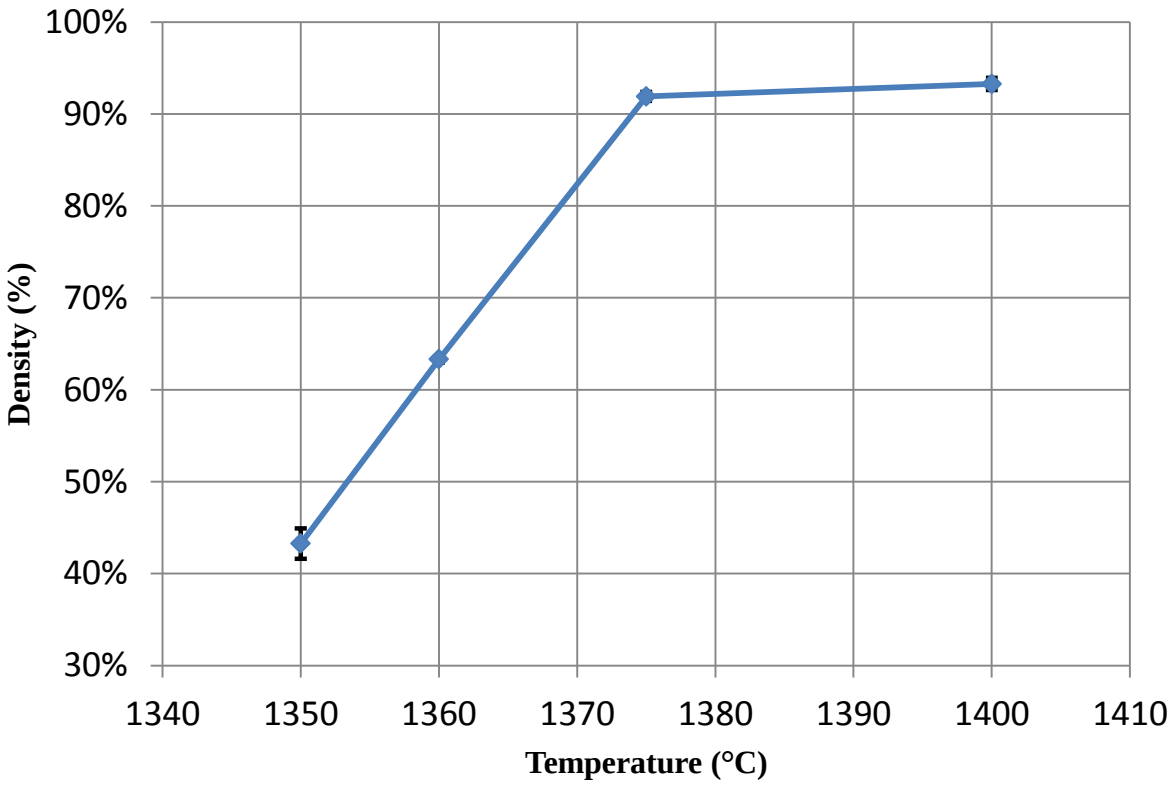

Figure 6.5. Relative bulk densities of fired ceramic parts as a function of the firing temperature

6.2.4.2. Shrinkage measurements

The physical dimensions of the green parts were compared to those from the sintered part to obtain the apparent shrinkage. Additionally, the measurements from the CAD model were compared to those of the green and sintered parts to obtain the correct final part when modeling in CAD. The shrinkage for each dimension as a result of sintering is shown in Figure 6.6. It was expected, given the correlation with the bulk density, that the shrinkage would be significantly greater at higher sintering temperatures. But it was also noted that with large shrinkage values, the ceramic parts experienced significant warping for both solid and complex objects.

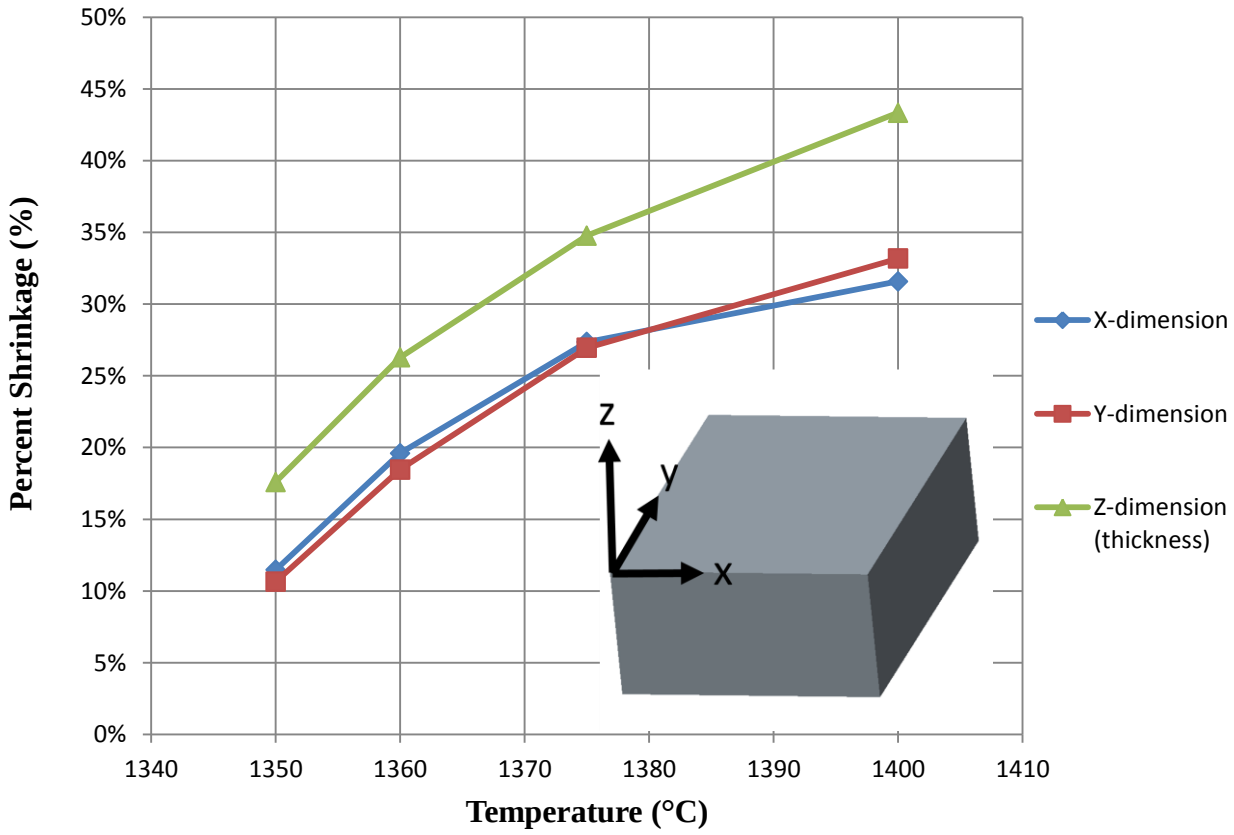

Figure 6.6. Ceramic Shrinkage for ceramic parts at various sintering temperatures

6.2.4.3. Optical microscopy of printed ceramics

Visual inspection was used to confirm the densification of the ceramic structure with each sintering cycle. Each printed ceramic block was mounted in an epoxy media and ground to 600 grit SiC paper, cleaned and examined. Optical micrographs of representative samples are shown in Figure 6.7. There was significant pore reduction in the samples fired from 1350°C to 1400°C

in agreement with their relative bulk densities (Figure 6.5). Although the samples fired at 1400°C had the highest density, they also had the largest shrinkage and warping which was considered not quite beneficial for the stated objectives. In addition, these samples presented a proliferation of micro cracks (~ 400 µm in length) in the bulk of the ceramic body. Thus a firing temperature of 1375°C was selected as appropriate for the ceramic parts.

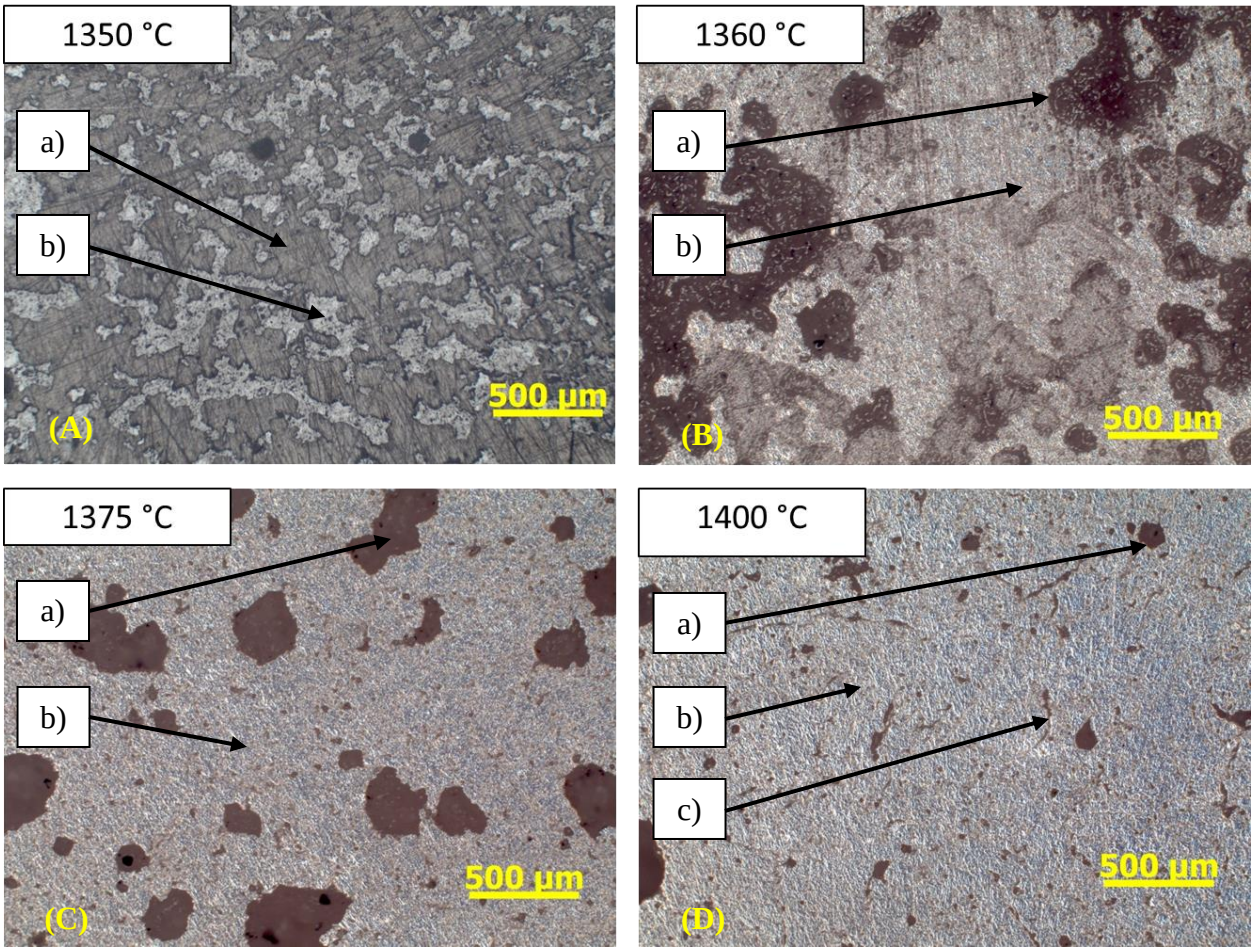

Figure 6.7. Optical microscopy (50x) of sintered ceramics at different sintering cycles: a) porosity with mounting media, b) ceramic material, and c) micro cracks.

6.2.4.4. X-Ray Diffraction (XRD) analysis

The XRD analysis was done to determine how close the sintered ceramic sample's crystallographic structure came to the data found in the literature for a cordierite ceramic material. All samples to be examined were first ground to powder form with a mortar and pestle. Both sets of the collected data are shown in Figure 6.8. The final sintering temperature chosen (1375°C) to fire the ceramic parts for the manufacture of MMCs correlated to a 78% match to

the cordierite crystallographic structure found in the literature and was also the highest resulting match. The mismatch in matching the crystallographic structure of the AM built parts to that of cordierite may have been caused by the somewhat inhomogeneous spreading of the mixed raw materials required to make cordierite. Based on such 78% match, the true values of relative bulk density would differ slightly from those presented in Section 6.2.4.1 due to a change in theoretical density.

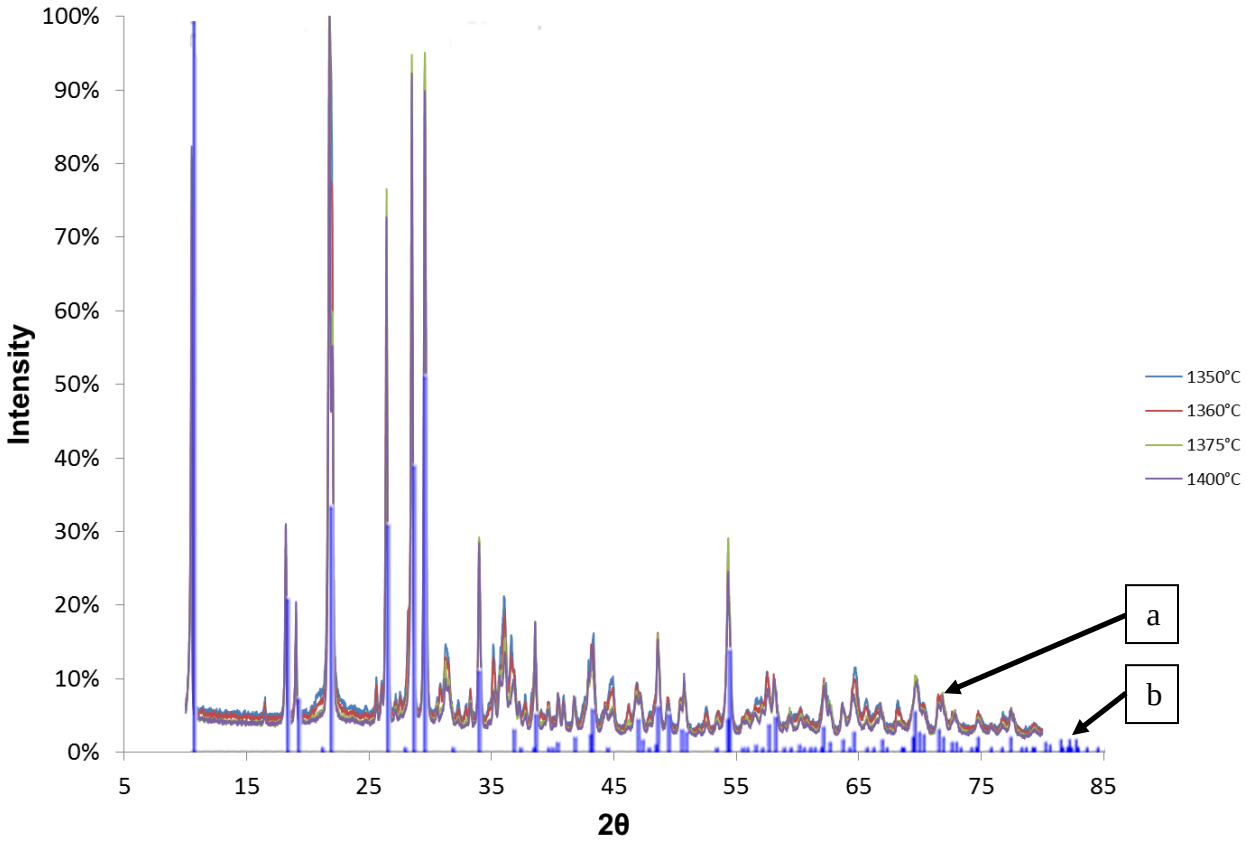

Figure 6.8. a) XRD data from different sintering temperatures of the ceramic samples and b) software values for cordierite

6.3. Manufacturing MMCs with printed ceramic inserts and casted zinc

Printed complex ceramic structures by AM Binder Jetting technology were combined with metal casting to produce metal matrix composites. Three-point bend tests were performed on the MMC samples as well as the pure ceramic and the pure metal samples for comparison. Evaluation of the three materials provided an understanding of the effect of the ceramic insert on the flexural strength and the flexural modulus of the metal matrix. Finally, the metal-ceramic interface was examined by optical microscopy to further characterize the composite.

6.3.1. Printed geometry for cordierite-zinc composite

An ordered octet-truss geometry was chosen as truss panels are known for their strength in bending and compressive loads [61]. The CAD model and final printed part (6.35 mmW x 6.35 mmD x 38.1 mmL) are illustrated in Figure 6.4 and Figure 6.9. The CAD part was digitally scaled before printing to compensate for the shrinkage values determined in Section 6.2.4.2. Given a total shrinkage from CAD to final part of 27% (x-dimension), 26% (y-dimension), and 38% (z-dimension), the final printed part had average dimensions of 8.25 mmW x 8.00 mmD x 88.68 mmL.

6.3.2. Mechanical properties of pure ceramic specimens

Solid ceramic parts were printed for testing their mechanical properties after sintering. Three point bend tests were performed on five solid ceramic bars using an Instron 5984® electro-mechanical testing machine. It was expected that the ceramic properties would have a higher flexural modulus and strength than that of pure zinc metal matrix. Thus incorporating the ceramic in an MMC would enhance the mechanical properties of the part (flexural modulus and strength). The critical parameters of the setup are listed in Table 6.5 and the results of the testing for all specimens in Table 6.6.

The printed solid ceramic bars had significantly lower flexural modulus and strength as compared to those from literature on cordierite ceramics [109]. It was concluded that the ceramic had such low strength and modulus due to the difficulties experienced in spreading the raw material powder mixture during AM part build as discussed in Section 6.2.1.2 as well as due to the highly porous structure developed during firing (Figure 6.7).

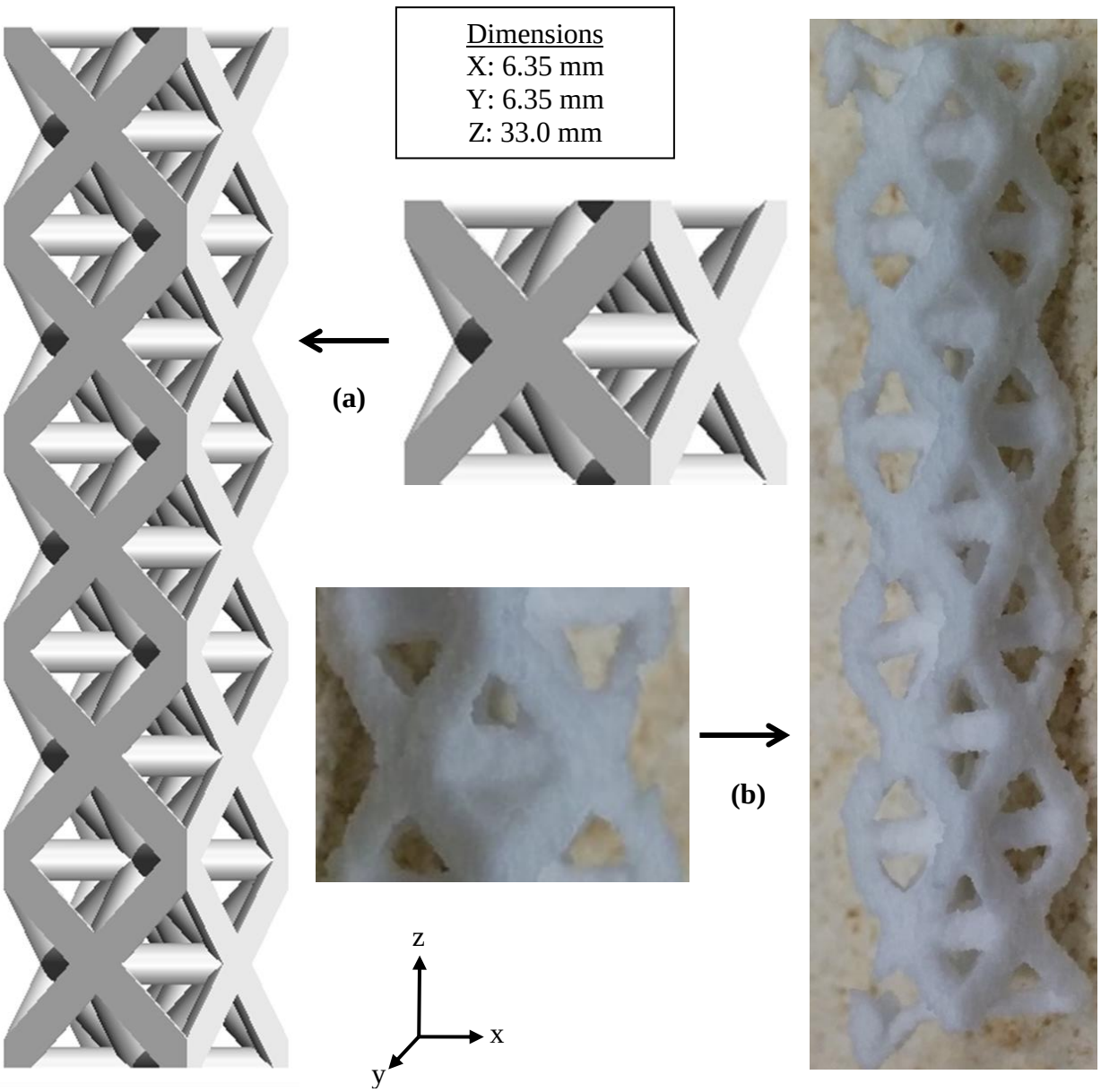

Figure 6.9. Cellular repeating octet truss unit cell: (a) CAD model for unit cell and final part and (b) AM printed and fired cell and final part

Table 6.5. Mechanical testing parameters by three-point bend tests of AM printed ceramic

Critical Testing Parameters	
Parameters	Value
Load Cell	50 kN
Controlled Displacement Rate	0.50 mm/min
Ceramic-Only – Solid Shape	
Approx. Specimen Dimensions	5.00 x 3.00 x 34.25 mm
Span Length	26.00 mm

Table 6.6. Average strength and flexural moduli values of the AM printed ceramic samples

Material Type	Average Maximum Strength (MPa)	Standard Deviation (MPa)	Average Flexural Modulus (GPa)
Printed Ceramic	19.5	3.6	9.3

6.3.3. Matrix material selection

Zinc alloy, Zamak-3®, was chosen as the matrix material for creating MMCs with printed ceramic inserts. Although zinc is significantly heavier than aluminum, it provided similar mechanical properties and has high fluidity for casting. Therefore, zinc was determined to be a valid candidate for the proof of concept of the project. Zinc also has a lower liquidus temperature decreasing the degree of superheating required for casting.

6.3.4. Mold Design

Traditional bonded sand molding was used to create the ceramic-zinc composite. The mold's runner system was modeled in CAD and patterns were printed from Acrylonitrile butadiene styrene (ABS) to produce the bonded sand molds. The composite structure was designed for testing in a three-point bend fixture. The mold's gating system was designed to have one runner meeting at the center of the ceramic and dispersing outward to create the composite flexural bar. The ceramics were placed in the center of the mold before casting (Figure 6.10) and the final casting with gating can be seen in Figure 6.11.

6.3.5. Casting and post-processing

About 3.62 kilograms of zinc was melted in a small silicon carbide crucible at 510℃ then the crucible was removed from the furnace and the temperature of the melt was monitored. Casting was done at a liquid temperature of 482°C to create the test specimens. The castings were removed from the molds; the flashing and gating were also removed to clean the parts. Both composites and pure metal specimens were created in the same molds for comparison testing (Figure 6.12).

6.3.6. Ceramic-metal interface

The resultant composites were sectioned and examined via Dark Field optical microscopy (Figure 6.13). Bonding between the interfaces is an important characteristic to produce effective MMCs and could be developed in two ways: i) mechanical interlocking and ii) chemical reaction [110]. Mechanical interlocking is produced as molten metal particles are wicked into rough surfaces of the ceramic by capillary action and solidifies creating mechanical bonding in ceramic metal composites [93,111]. However, in the present experiments the shrinkage coefficients between the two materials proved to be problematic as the two materials cooled causing delamination. Optical micrographs indicated that there was a degree of mechanical bonding between the two materials. When observations were made using differential image contrast (DIC), small gaps between the ceramic and the metal were revealed (Figure 6.14). The presence of these gaps indicated that there was a limited mechanical bonding and it was thus expected that the resulting composite material would not perform as desired under mechanical testing. Moreover, the resulting optical microscopy observation of the 1375 °C fired ceramic specimens did not show signs of cracking from neither the microstructure formation, thermal shock or hot tearing during metal casting.

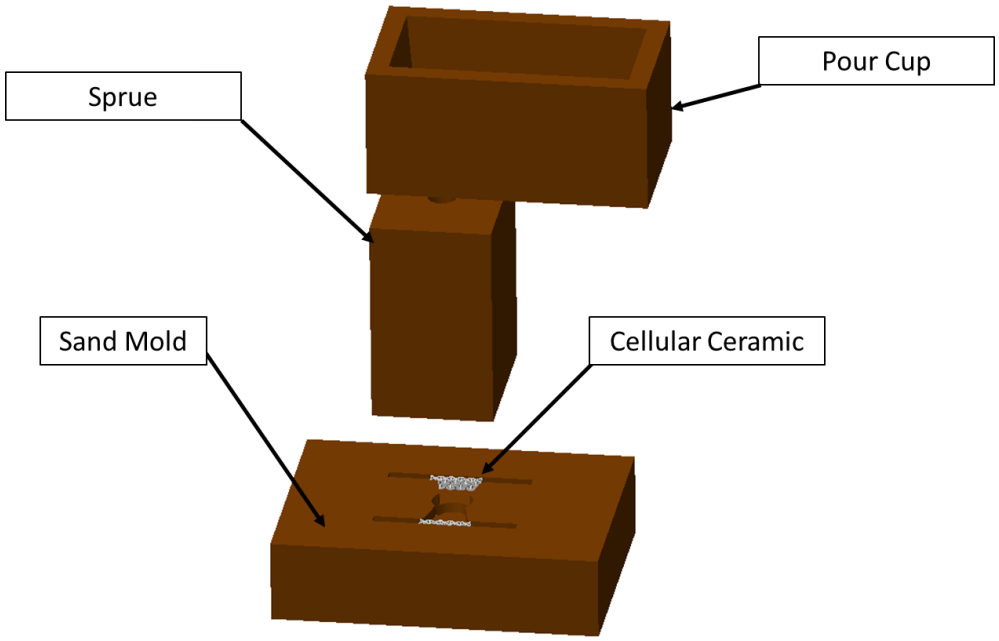

Figure 6.10. Bonded sand mold CAD design for casting MMCs with cellular cordierite

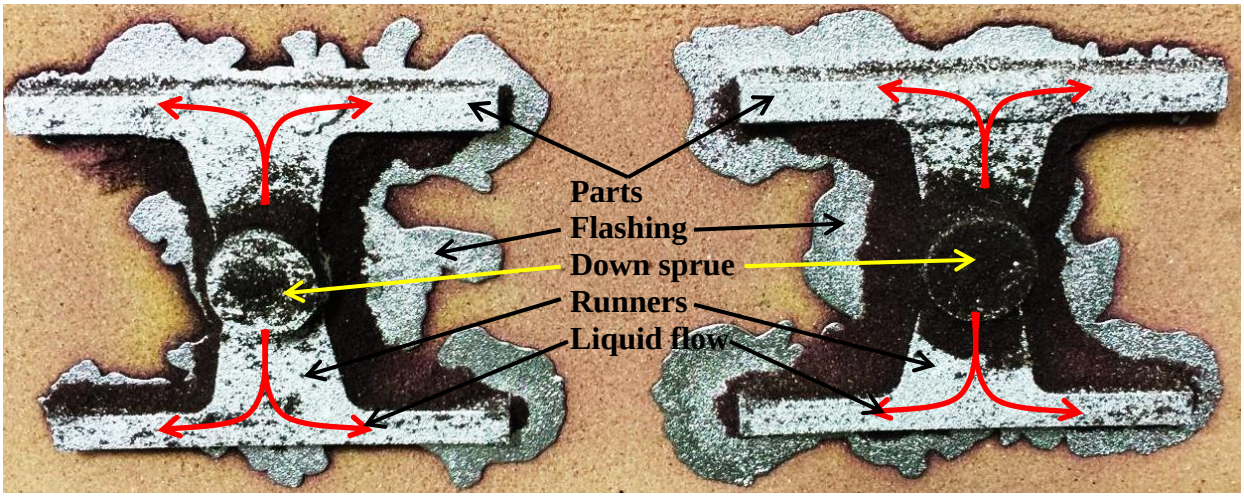

Figure 6.11. As casted final composite castings before a post-processing cleaning

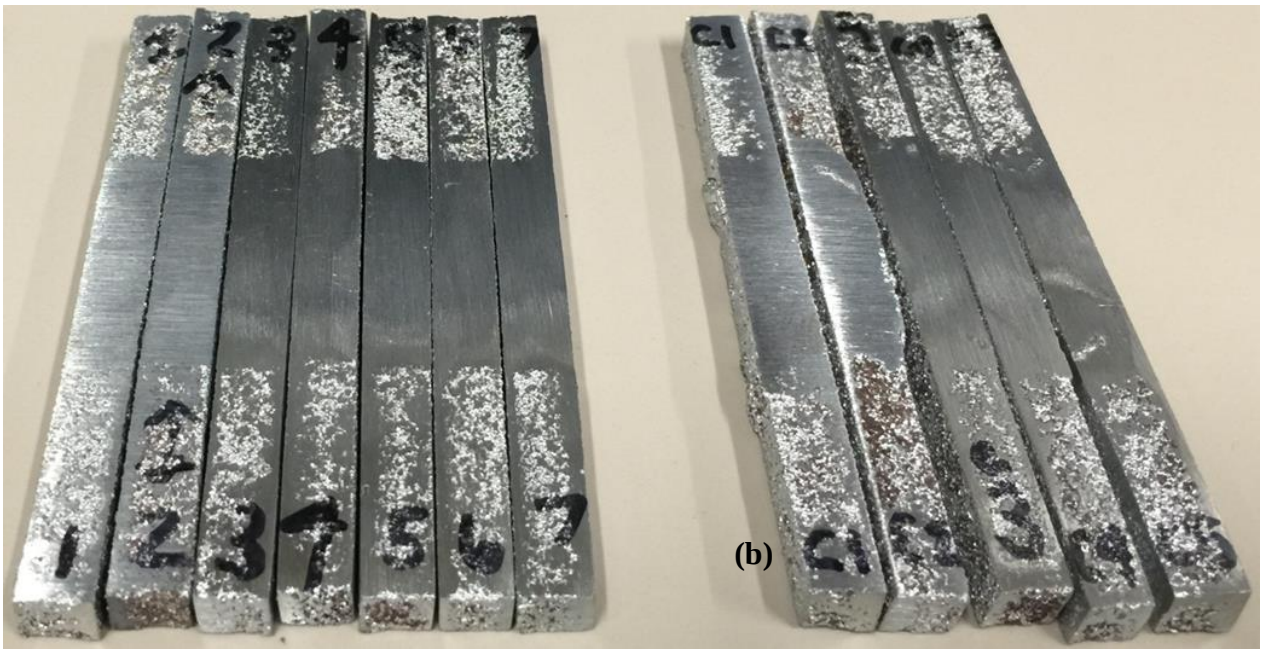

Figure 6.12. Three-point bend specimens: a) metal only and b) ceramic-metal matrix composite)

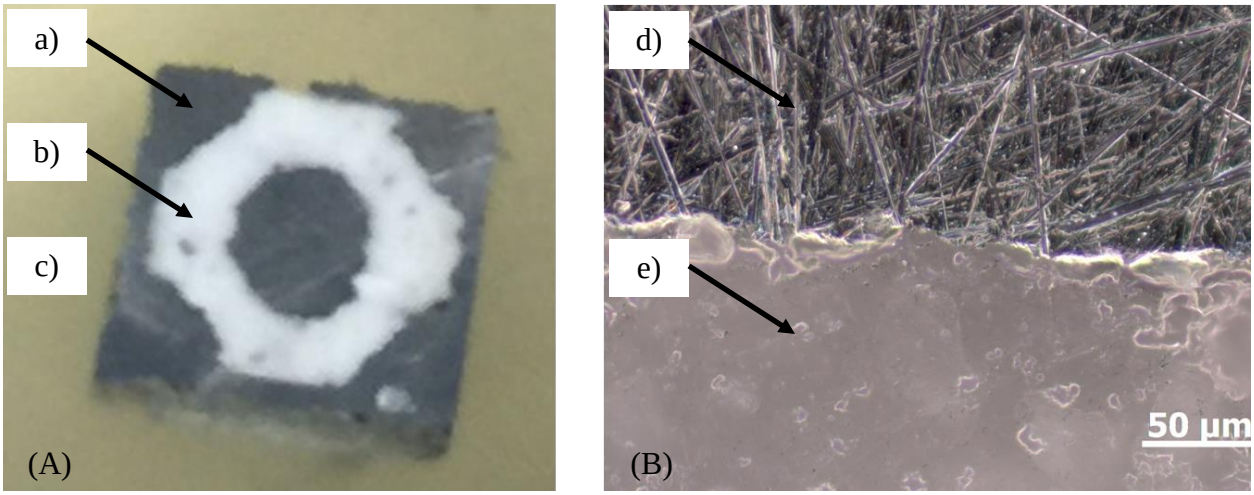

Figure 6.13. Ceramic-zinc composite: (A) sample embedded in a sample mounting media with a) metal matrix, b) ceramic insert and c) mounting media; (B) Ceramic-metal interface with d) metal and e) ceramic fired at 1375°C.

Chemical reactions included reactions between the matrix and insert materials. Although a strong interface was preferred, chemical reactions could have an adverse effect causing degradation of the constituent materials. Due to the stability of oxides and quick metal infiltration (casting), it was expected that no inter diffusion would occur between the two materials and non was apparently observed Figure 6.14 [112].

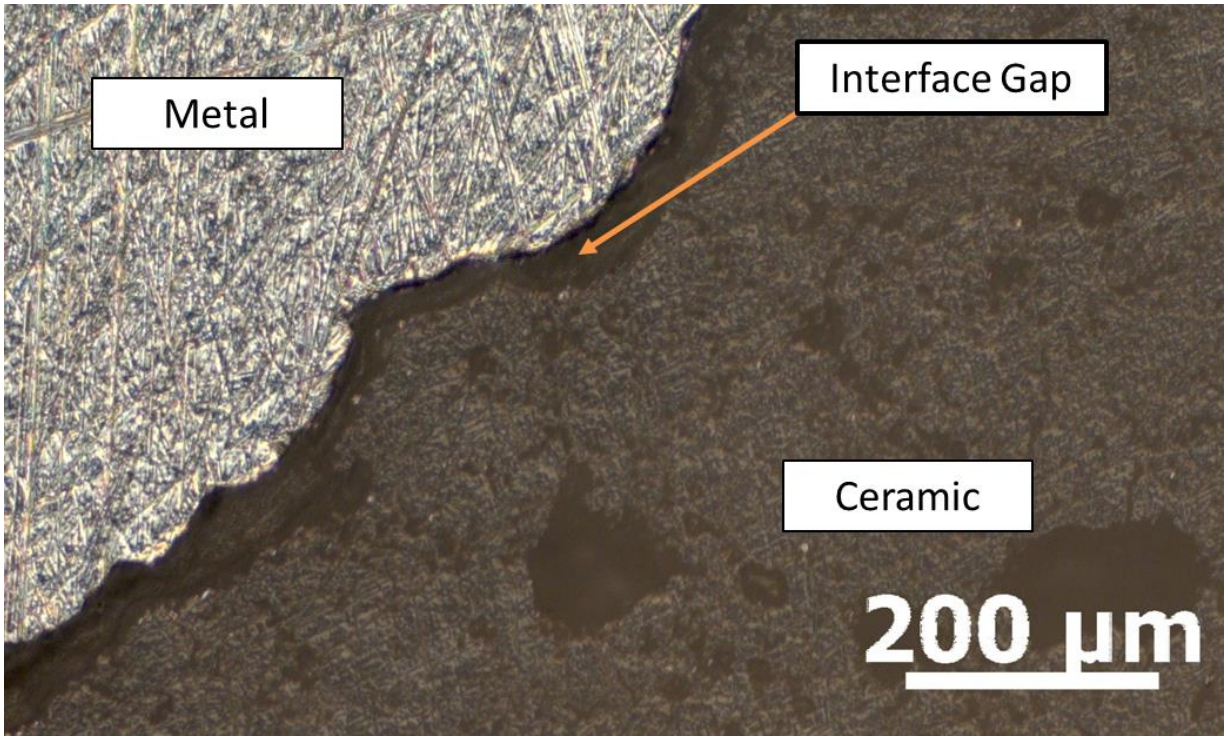

Figure 6.14. Differential image contrast optical micrograph of the ceramic-zinc interface

6.3.7. MMC and pure zinc mechanical testing

Tests were conducted on the proof of concept MMC samples and compared to pure ceramic and pure metal specimens. Three-point bend tests were evaluated on the basis of the flexural modulus and the flexural strength. These metrics were analyzed to determine the effect that the printed ceramic inserts (with cellular geometry) had on the metal as a composite structure. Initially it was expected that the pure ceramic would induce a significant increase in the flexural modulus and the strength in the composite material but instead a decreased toughness as compared to the pure zinc specimen was observed and thought to be due to the brittle nature of the ceramic insert and therefore, the MMC had lower mechanical properties than expected. Additionally, it was also expected that the zinc would provide higher toughness but a significantly lower modulus and strength and that combining the ceramic with zinc (MMC) would enhance the flexural modulus of the zinc while the zinc matrix would provide increased toughness. Five pure zinc specimens, five MMCs, and six ceramic bars were tested on the basis of the flexural modulus and the flexural strength. The critical parameters of the setup are listed in Table 6.7 and the results of the testing for all specimens in Figure 6.15 and Figure 6.16.

Table 6.7. Mechanical testing parameters for three-point bend tests of the metal only and the MMC specimens

Critical Testing Parameters	
Parameters	Value
Load Cell	50 kN
Controlled Displacement Rate	0.50 mm/min
Composite	
Approx. Specimen Dimensions	7.80 x 7.80 x 88.74 mm
Span Length	60.00 mm
Metal-Only	
Approx. Specimen Dimensions	7.80 x 7.80 x 88.74 mm
Span Length	60.00 mm

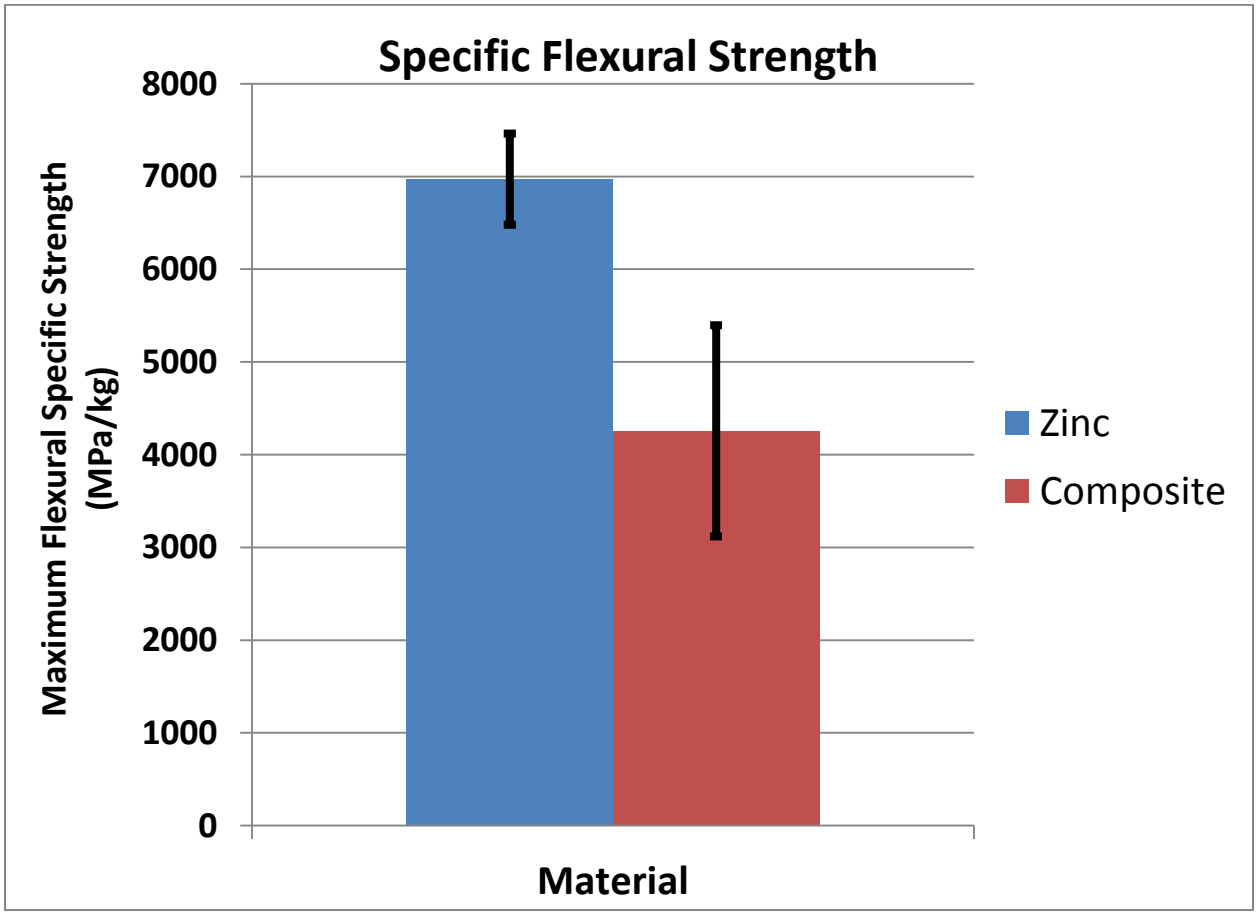

Figure 6.15. Average maximum flexural specific strength of zinc and composite specimens

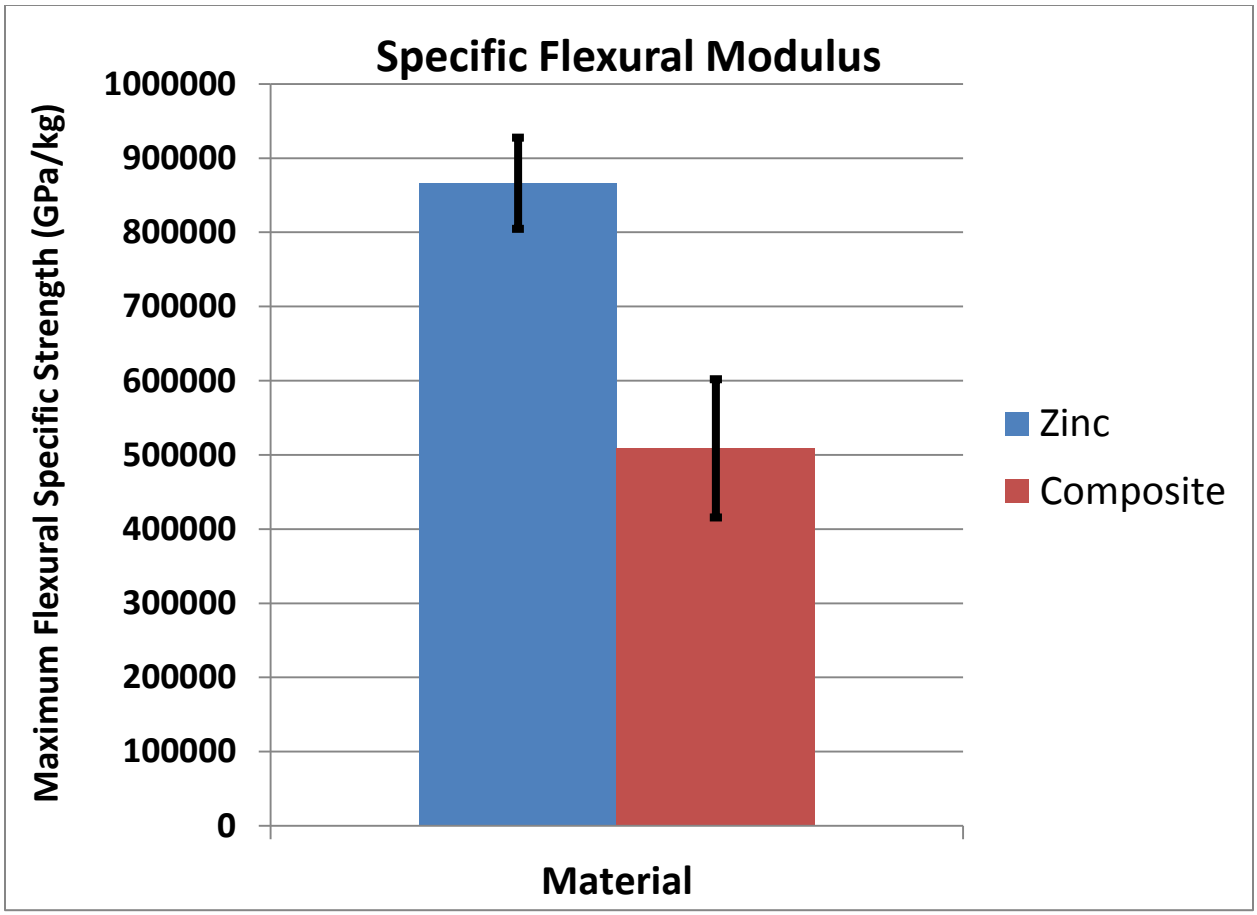

Figure 6.16. Average maximum flexural specific modulus of zinc and composite specimens

The results from the mechanical testing showed that the pure metal specimens had a significantly higher overall strength and flexural modulus than both ceramic only (Section 6.3.2) and composite bars. This was not unusual for gravity cast MMCs. Previous research showed gravity cast MMCs had significantly lower mechanical properties than those used in high pressure die castings [93]. Utilizing pressure to cast MMCs increased the overall flexural strength compared to gravity cast MMCs as well as the flexural modulus of pure matrix (metal) material by 60%. Additionally, typical preforms were manufactured with built-in porosity and utilized pressure to force metal into voids which lead to better mechanical interlocking between materials. Producing higher surface roughness would also increase the mechanical interlocking of the zinc-ceramic interface. The resulting parts yielded higher flexural strength and had higher relative bulk densities [92,93,113]. Furthermore, AM could be used to create intricate geometries with other oxides to be used in pressure-assisted castings including alumina (Al_2O_3,

mullite, enstatite, forsterite, sapphirine spinel, periclase, and corundum) to be used for other applications [114].

However, pressure was not necessary to produce present MMCs and as discussed in Section 6.3.6, matching the correct materials to produce a strong chemical bond between materials in the MMC could aid in increasing mechanical strength. For example utilizing silicon (Si) and carbon (C) to produce silicon carbide (SiC) from which printed preforms were fabricated through gravity casting [104]. Furthermore, refining the process with materials synthesized for AM processes and better spreading techniques would result in better mechanical properties of the resulting printed ceramic and therefore the MMCs.

6.4. Conclusions and Future Work

This work presented a novel process to manufacture metal matrix composites using printed ceramics. The overall research goal was to manufacture, test, and evaluate the interface of proof of concept MMCs specimens using a printed ceramic as the reinforcing material and zinc alloy as the metal matrix. The process included utilizing a ceramic fabricated by Additive Manufacturing from powder precursor materials, printing, sintering, and post sintering characterization.

Traditionally, manufacturers were bound to conventional forming techniques which geometrically limited the design. The use of AM technologies enables the user to manufacture complex ceramic parts that can be tailored for specific applications including MMCs. This work was focused on the use of AM to form the raw materials used for the production of a cordierite like ceramic insert and the manufacturing process to create a ceramic-zinc composite.

Additive manufacturing was used to print the precursor powders, alumina (Al_2O_3), silica (SiO_2), and magnesia (MgO), for the production of a cordierite ($2MgO•2Al_2O_3•5SiO_2$) like material. The correct print parameters (binder selection, layer thickness, heater temperature, binder saturation, spread speed, and drying rate) to successfully print the raw materials were determined experimentally. The materials were characterized pre-and-post sintering to evaluate the properties of the synthetized ceramic. Finally, a proof of concept ceramic-zinc MMC was

fabricated and tested mechanically. The resulting proof of concept MMC did not have sufficient strength as compared to the zinc only specimens due to the control of the initial raw material shape and size and the inability to control packing from the roller of the printer. Controlling the initial particle size (>20 micron mean diameter) and shape (from angular to spherical) would help control the packing minimizing the difference between the in apparent and tap densities observed. Additional particle size distributions can be tested (mono-sized particles, bimodal, ternary, quaternary etc.) to increase the packing density of the printed material.

Upon mechanical testing of the ceramic-zinc MMCs, there was a significant decrease in the flexural modulus and the strength of the composite parts (15.3 GPa and 127.8 MPa) compared to those of pure metal (27.5 GPa and 225.8 MPa). Testing of the ceramic specimens proved them to be significantly weaker than the values reported in the literature for cordierite and greatly influencing the overall strength of the composite. In addition to the effect of the ceramic, the interface between the two materials had a large effect on the strength of the composite. Differential image contrast exhibited a gap between the ceramic insert and the matrix materials possibly due to differences in thermal expansion. A minimal mechanical and no chemical bonding was apparent between the interfaces and was concluded to further decrease the strength of the composite.

Although the results of strength for the MMC were less than the pure matrix material (zinc), the proposed manufacturing process can be used to combine materials that will chemically react when infiltrated by the matrix material by gravity casting. Furthermore, the designer can also use printed materials with intricate geometries including those from other raw oxide materials (Al_2O_3, mullite, enstatite, forsterite, sapphirine spinel, periclase, and corundum) to create MMCs by pressure-assisted casting means. However, the ceramic materials must be able to withstand he drastic thermal shock from the heat and the pressure of the metal matrix being casted.

6.5. Acknowledgements

The author gratefully acknowledge the Department of Mechanical Engineering and the Department of Materials Science and Engineering at Virginia Tech for their resources and support with equipment.

7. CONCLUSIONS AND BROADER IMPACTS

7.1. Summary of Research

The goal of this work was to develop a manufacturing process to create metal matrix composites with complex cellular geometries. The manufacturing method used two distinct additive manufacturing processes: i) fabrication of patternless molds for cellular castings and ii) printing an advanced cellular ceramic for embedding in a metal matrix. This type of manufacturing technique resulted in a proof of concept metal matrix composite with the intent to produce artifacts with lower density, high specific strength, high specific modulus, and wear resistance. However, in order to produce these structures along with the experimental limitations encountered, there was a need to characterize the manufacturing constraints of the manufacturing process. These objectives led to the primary research goal.

Primary Research Goal
To develop and gain an understanding of a manufacturing process to cast complex metal-ceramic composite geometries via Binder Jetting technology.

A new manufacturing process was developed to create cellular structures and evaluated on the basis of analytical impact loading and analytical and experimental quasistatic loading. Novel non-composite aluminum cellular structures were first created and analyzed (Chapter 2) to create a basis for manufacturing and evaluation of MMCs (Chapter 6). Dynamic impact models predicted the structure could better withstand impulse through the mesostructure better than a structure with the same area density provide by the reaction forces of the rigid sandwich plate and trusses of the cellular structure. Experimental quasistatic tests results showed the cellular structure could withstand a maximum force of 133.45 kN before overloading the load frame on the Instron electromechanical machine. Experimental and Analytical results differed by 16.4 % which were taken to be within an acceptable range.

7.2. Guiding Research Questions

The format of this dissertation includes publications and planned publications listed as chapters. Chapters 3-6 seeks to answer guiding research questions developed to meet the primary research goal. The chapters are listed in the publication section of this document (Section 7.3).

7.2.1. Research Question 1

Research question 1 (Chapter 4) was developed based on experimental limitations experienced during pouring of molten metal in printed molds. The goal of this work was to utilize the geometric freedom offered by AM combined with the lightweight-strong nature of organic cellular materials. Upon making these cellular castings, incomplete fill produced degraded part quality which prompted work to mitigate gas defects.

It was predicted that based on the initial printing technology used for this work (Binder Jetting with single part binder) produced gas defects due to the large amount of binder needed to form the patternless molds. From the results of the conducted on ZCast castings, it was concluded there was initially >8% binder compared to approximately 1.5% in traditional no-bake molds. A curing cycle of 304 °C was used to mitigate these effects however the molds still maintained >3% binder. From this preliminary evaluation, the first hypothesis was developed.

Furthermore, this prompted another study to determine how different AM Binder Jetting molding techniques affected the quality of the final cast structure prompting the first research question:

Research Question 1
How do castings made from two different 3D Printed sand molding materials compare to those of traditional no-bake molding methods?

After testing the results of binder burnout from the initial study, the author tested molds produced by ExOne. The ExOne material system incorporates a two part binder system into a silica sand molding material similar to traditional no-bake in contrast to the single part ZCast® systems. Therefore it was hypothesized the ExOne printed parts will have similar properties with those made with the traditional approach and prompting the second study on the effects of molds on castings.

Hypothesis 1
Castings from no-bake and ExOne molds will produce similar results, as compared to those produced via ZCast®.

Two different AM patternless sand casting molding techniques were used to create castings and compared to traditional sand as a basis for comparison. It was further hypothesized molds produced by the ExOne system was similar to molds produced by traditional means because both used a two part binder system compared to the one part ZCast system. ExOne was statistically significant in only 4 out of the 7 tests performed including microstructure (Table 6.5), porosity (Table 6.6), surface roughness (Table 6.9), and tensile strength (Table 6.10). They differed in sand tensile strength (Table 6.4), hardness (Table 6.7), and density (Table 6.8). These differences are attributed to better control of sand distribution in ExOne sand molds, sub-surface pores affecting low hardness values in no-bake castings, and error associated in small relative mean differences for density. Castings produced in ExOne molds outperformed the other materials as they had better quantitative mean values in all seven tests. Furthermore, ZCast® molds produced poorer quality castings in comparison with no-bake and ExOne molds. Conversely, the large amounts of binder from ZCast molds adversely affected the results (porosity and surface roughness) of the final castings. Different molding materials did indeed affect the final castings verifying Hypothesis 1; however, all molding techniques produced values that were acceptable by industry standards.

7.2.2. Research Question 2

In addition to evaluating experimental limitations, it was necessary to evaluate manufacturing constraints to create "rules" of casting using AM patternless molds (Chapter 5). The goal of this work was to evaluate the limiting resolution constraints of the Binder Jetting process on sand molds. The critical constraints limiting the user's ability to cast small features is dependent the ability to (i) efficiently clean unbound powder from the printed mold and (ii) effectively cast metal through small intricate geometries. It is important to understand the proposed constraints to accurately take advantage of the design freedom in designing molds for metal casting with AM. This work was guided by a fundamental research question that was divided into two sub-research questions:

Research Question 2	
What are the resolution constraints of the Binder Jetting printing process and how is it limited by metal solidification and depowdering?	
Sub Question 2.1	**Sub Question 2.2**
How are the resolution constraints limited by depowdering complex geometries?	*How are the resolutions constraints limited by metal solidification through complex geometries?*

In order to determine the constraints imposed on complex geometries by the Binder Jetting AM processes, initial hypotheses were forumulated. Hypotheses for both sub-questions are derived from resulting literature and fundamental knowledge of metallurgy.

Hypothesis 2.1
The cleaning length of circular channels printed via Binder Jetting is dependent on the smallest cleanable diameter, cleaning diameter, and connectivity.
Hypothesis 2.2
Complex geometry will promote freezing due to an increase in path length and change in direction.

The experimental approach consisted of two separate foci: determining the constraints imposed by depowdering (Section 5.4.1) and determining the constraints imposed by metal solidification (Section 5.4.2). Depowdering constraints were evaluated to determine the maximum cleaning distance that can be achieved with respect to i) channel diameter and ii) connectivity (opened/closed). Metal flow constraints were examined for maximum flow before freezing while varying i) choke diameter, ii) flow direction angle, and iii) channel diameter. For both depowdering and solidification, a Taguchi design of experiments (DOE) was used to evaluate the independent variables, each with two factors.

To identify the smallest cleanable channel and the variables that affect cleaning length, depowdering experiments were conducted on mold channels of various diameters and connectivity conditions. Specifically, eight total individual diameters (1/2, 1, 2, 3, 4, 5, 6, 7 mm) were designed and printed using ExOne's rounded silica sand material. The results of the tests were input into the design of experiments to analyze the statistical significance of the independent variables (channel diameter and connectivity). It was determined that channel diameter was statistically significant while connectivity was not. Additionally, experimental

results revealed a minimum cleaning diameter of 3 mm and using curve fitting, an equation relating cleaning distance as a function of channel diameter was established.

Furthermore, metal flow constraints were examined for maximum flow before freezing by varying choke diameter, flow direction angle, and channel diameter. A Taguchi design of experiments (DOE) was used to evaluate the independent variables. It was determined that choke diameter was statistically significant while both channel diameter and angle change was not. Additionally, utilizing a prediction profiler, metal flow before solidification is maximized with a larger choke diameter, larger channel diameter, and smaller angle to the horizontal axis.

7.2.3. Research Question 3

To complete the final step toward the goal of manufacturing MMCs from two distinct AM processes, Research Question 3 was developed. Guided by RQ3, a process to effectively manufacture MMCs with printed cordierite (ordered cellular structure) as the reinforcing material was developed.

Research Question 3
How are mechanical properties (flexural strength and modulus) of MMCs created via Binder Jetting and Metal Casting affected by the manufacturing process parameters (powder preparation, sintering temperatures, and casting process)?

It was expected that the cordierite-zinc MMC fabricated by printed ceramic precursor materials will have significant effect on the properties of the final part and is dependent on the manufacturing process parameters. Therefore an initial hypothesis is developed:

Hypothesis 3
MMCs produced from printed ceramics with higher density and good bonding (mechanical or chemical) at the metal-ceramic interface will have better mechanical properties (flexural modulus and strength) compared to the matrix material alone (zinc).

After selecting the materials for creating the proof of concept MMC, the overall ceramic printing process was characterized. This includes pre-sintering characterization (ceramic powder selection and particle size analysis: Section 6.2.1), forming parameters (binder selection, layer thickness, heater temperature, binder saturation, spread speed, and drying rate: Section 6.2.2),

sintering (sintering temperature profile: Section 6.2.3), and post-sintered characterization (XRD, relative bulk density, shrinkage, and optical microscopy: Chapter 6.2.4). Printing parameters were obtained experimentally, and listed in Table 6.4. Parameters differed from solid printed objects as compared to complex objects due to the saturation, spread speed, and drying rate of the varying volume of powder being printed.

Additive manufacturing was used to print precursor powders alumina (Al_2O_3), silica (SiO_2), and magnesia (MgO) for the production of cordierite. The correct print parameters (Binder Selection, Layer Thickness, Heater Temperature, Binder Saturation, Spread Speed, and Drying Rate) to successfully print the raw materials were determined experimentally. The materials were characterized pre-and-post sintering (***pre:*** raw material preparation and ***post:*** XRD, Density, Shrinkage, and Optical Microscopy) to evaluate the properties of the ceramic (Chapter6 – Section 2). Finally, a proof of concept cordierite-zinc MMC was fabricated and tested mechanically (Section 6.3.7). The resulting proof of concept MMC did not have sufficient strength as compared to the zinc only specimens due to the control of the initial raw material shape and size and the inability to control packing from the roller of the printer. Controlling the initial particle size (>20 micron mean diameter) and shape (from angular to spherical) will help control the packing making the difference in apparent and tap densities less. Additional particle size distributions can be tested (mono-sized particles, bimodal, ternary, quaternary etc.) to increase the packing density of the printed material.

Upon mechanical testing of cordierite-zinc MMCs, there was a significant decrease in flexural modulus and strength of the composite parts (15.3 GPa and 127.8 MPa) compared to those of pure metal (27.5 GPa and 225.8 MPa). From the results of the ceramic testing, cordierite was significantly weaker than the values reported in literature greatly influencing the overall strength of the composite. In addition to the effect of the ceramic, the interface between the two materials had a large effect on the strength of the composite. Differential image contrast exhibited a small gap between the constituent and matrix materials from differences in thermal expansion. Minimal mechanical and no chemical bonding occurred between the interface further decreasing the strength of the composite.

7.3. Limitations and Future Work

While developing a manufacturing process to produce proof of concept MMCs, the author encountered limitations and areas of future work. The limitations and areas for improvement are divided by chapter/publication in the following Sections, along with additional research questions for continued development.

7.3.1. Chapter 2: Lightweight Metal Cellular Structures Fabricated via 3D Printing of Sand Cast Molds

Slight geometrical limitations existed in the manufacturing process of the cast cellular structure when comparing to the analytical model. Because the core was printed and surrounded with traditional sand, the homogeneous plates contained flashing and overhangs. Additionally, the original cellular structures were cast to dimensions 101.6 x 50.8 x 63.5 mm and sectioned with a band saw to 50.8 x 50.8 x 63.5 for compression testing. The band saw limited the resolution of the cut giving further error in the results.

For future work, the entire mold and outer molds should be printed to dimensions for testing to control dimensional accuracy. This will help eliminate errors in experimental results and more accurately match the model. Further research should be focused on combining topology optimization with the proposed Binder Jetting process during the initial digital mold creation phase to allow for structures that are tailored to perform optimally under certain loading conditions eliminating the proof of concept cellular geometry principle in this work.

New Research Question 1
How does a better controlled geometry affect the analytical quasistatic model?

Additional metals can be used to create castings and tested to determine properties. Shear testing on proof of concept cellular structures can be performed dependent on the necessary application. Further dynamic modeling can be used to determine if other materials have higher resistance and energy absorption. Experimental blast tests were not performed due to limited testing resources, but would help to verify the models used for impact modeling.

New Research Question 2
How does experimental blast tests compare to dynamic simulations of the proof of concept cellular structures with different materials?

7.3.2. Chapter 3: Mitigating Gas Defects in Castings Produced from 3D Printed Molds (RQ1)

Further testing should be done to verify these methods provide consistent results. Only single sand characterization, binder burnout, curing cycle, and casting trials were performed and reported. Performing more tests with mean and standard deviations values will make this study more robust. Additionally, an optimized curing cycle (longer dwell time, different temperatures, etc.) can be used to test the gas generation effects on castings through repeated casting trials enabling a more usable printed material for single part binder systems.

New Research Question 3
How does printed sand, manufactured via Binder Jetting affect the metal properties being cast?

7.3.3. Chapter 4: The Effects of 3D Printed Molds on Metal Castings (RQ1)

Although two commercially available, Binder Jetted, AM materials were compared against traditional no-bake sand, other molding materials are available that will potentially affect the quality of the final castings. For example, multiple traditional binders and molding materials can be used for comparison and leads to new research question 4:

- **Printed**
  - ***Binders***
    - ExOne R2 Binder (single-part binder)
  - ***Materials***
    - Synthetic Materials
    - Angular Silica Sand
    - Varying Sand Distibutions
    - Olivine
- **Traditional**
  - ***Binders***
    - Furan/Acid Catalyst
    - Sodium Silicate/Glycerin Catalyst

- Alkyd Resin/Catalyst

- ***Materials***
  - Synthetic Materials
  - Green Sand

New Research Question 4
How do multiple printed materials, manufactured via Binder Jetting affect the metal properties being cast and how do these compare to the same materials molded by traditional methods?

7.3.4. Chapter 5: Effects of Complex Geometries on Depowdering and Solidification in Sand Molds Fabricated via Binder Jetting (RQ2)

Testing depowdering and solidification through complex geometries was limited by the ability to print and ship large molds for castings. Although the experimentation was sufficient for testing depowdering and solidification, additional repetitions of each test will provide more robust data. Also, the addition of analytical solidification modeling will provide a comparison to the experimental results through complex geometries giving the user an understanding of the process during the design process.

New Research Question 5
How does the experimental results of solidification in complex molds geometries compare to the analytical results of commercial solidification modeling software?

7.3.5. Chapter 6: Binder Jetting Advanced Ceramics for Metal-Ceramic Composite Structures (RQ3)

In an effort to create MMCS, cordierite was formed using AM and characterized pre-and-post sintering to determine the necessary properties of the materials. Issues were discovered in the overall process, most of which stemmed from the initial synthesized powder used for printing. For example, utilizing off-the-shelf powders (angular) typically used in applications where pressure is applied during forming is not ideal for used in printing process where spreading is required. Smaller (<20 μm) powder sizes agglomerate and form tracks over the previous layer when spread causing defects. Using approximately equivalent particle spherical sizes (mean diameter >20 μm) would enhance spreading by minimizing the difference in apparent and tap packing densities. A more uniform tap/apparent packing density will enable

better control over the sintering process. As additive manufacturing grows in popularity, special batches of powders should be synthesized specifically for printing. Additionally, trying various size distributions (keeping mean around 20 μm) could benefit the final part as well.

New Research Question 6
What are the printing parameters affected by change in ceramic powder sizes and distributions?

After refining the printing process with more uniform materials, further characterization including mercury porosimetry will give provide more insight into whether open porosity still exists and a more accurate measurement of porosity. Although not reported, BET data was taken but only provided microporosity of particles where macroporosity between powder particles was needed for this work.

Additionally, manufacturing the composite structure has opportunity for further testing. Zinc was used as the matrix material for its high fluidity, low melting point, and good mechanical properties however it was used only by gravity casting. Introducing other casting process such as die casting, vacuum casting, or investment casting will produce more uniform results as long as the ceramic can withstand the pressures required for its respective application. These ideas are discussed in the Broader Impacts Section 7.6. Four point bending will give better "pure tension" results than three point bend tests. Tension testing may be done on the structure by redesigning the test specimen as well as compression testing depending on the application. Upon testing a Weibull Modulus can be established for the printed material to for probability of failure predictions.

New Research Question 7
How do the refined raw ceramic materials affect the mechanical properties (including Weibull Modulus) of the final printed ceramic?

7.4. Publications

As discussed in Secion 7.2, publications and planned publications are listed as chapters in this dissertation. They are listed with their corresponding guiding research questions. Additional conference articles are also listed.

- Lightweight Metal Cellular Structures Fabricated via 3D Printing of Sand Cast Molds (Chapter 2)
- Mitigating Gas Defects in Castings Produced from 3D Printed Molds (Chapter 3) – RQ1
- The Effects of 3D Printed Molds on Metal Castings (Chapter 4) – RQ1
- Effects of Complex Geometries on Depowdering and Solidification in Sand Molds Fabricated via Binder Jetting (Chapter 5) – RQ2
- Binder Jetting Advanced Ceramics for Metal-Ceramic Composite Structures (Chapter 6) – RQ3
- Mitigating Gas Defects in Castings Produced from 3D Printed Molds – (AFS 117th Metal Casting Congress – April 6-9, 2013 in St. Louis, MO.)
- The Effects of 3D Printed Molds on Metal Castings – (2013 International Solid Freeform Fabrication Symposium – August 12-14, 2013 in Austin, TX.)
- A Comparison of Binder Burnout and Mechanical Characteristics of Printed and Chemically Bonded Sand Molds - (2014 International Solid Freeform Fabrication Symposium – August 4-6, 2014 in Austin, TX.)

7.5. Research Contributions

In accomplishing this work, a new manufacturing method was established for the creation of metal-ceramic cellular materials with designed mesostructure. Introducing ceramics in combination with cellular materials through AM and casting processes, parts can be produced with excellent properties including lower density, high specific strength, high specific modulus, and wear resistance. If successful, the following contributions will be made:

- A scalable manufacturing process to create complex structures including the ability to embed ceramics
- A basis for future research in the area of Binder Jetting patternless molds
- An understanding of the effects of molds from commercially available powders produced by Binder Jetting on cast properties
- An understanding of the manufacturing constraints of the Binder Jetting process including i) depowdering and ii) flow through complex structures

- An understanding of how metal-ceramic parts produced via Binder Jetting is manufactured
- An process to form, characterize and sinter advanced ceramics via Binder
- A manufacturing process to embed ceramics in the sand casting process creating proof of concept MMCs

7.6. Broader Impacts

In addition to the contributions provided by this work, a significant amount of work may be done to enhance this basis of knowledge. For example:

- Topology optimization may be implemented to taking advantage of the geometrical complexity when designing metal-ceramic composites. Using topology optimization during the initial digital mold creation phase will allow for structures that are tailored to perform optimally under certain loading conditions. Modeling of deformations under quasi-static and impact loads will be used to optimize the design of cellular structures for minimizing the momentum and the peak pressure transferred to the substrate being protected by the cellular structure.

- From a metallurgical perspective, varying alloys may be conducted to enhance or impede wetting to ceramics to create a strong mechanical bond. Additionally, finding alloys that could be reactive with the ceramics like Si – C discussed in the literature of Chapter 6 can be useful for certain applications. Also, varying alloys will allow the user to change properties based on application.

- Improving the sand casting manufacturing process by new binder or materials systems. An ideal process would include a single part binder system that does not require a curing cycle with minimal to no effects on the environment. The single part binder should not generate gas causing defects on the final castings and provide sufficient mold strength for pouring dense metals such as iron based alloys.

- Introducing other casting techniques (briefly discussed in Section 7.3.5) to ensure fully encapsulated ceramics. Techniques such as high-pressure die casting and

vacuum casting will eliminate voids in the metal matrix, however, changing the dynamics of the casting process. It is important to note that these techniques can require complicating tooling and is only viable for lower melting point alloys (zinc, aluminum, copper, etc.).

Utilizing this manufacturing process and knowledge of constraints will enable designers to manufacture parts with desirable properties regardless of the application. Although no specific purpose is proposed, utilizing the flexibility of Binder Jetting and casting, parts may be designed with specific applications in mind. Some applications include:

- *Armor:* The combination of impact modeling results with ceramics can mitigate blast and provide ballistics protection simultaneously. Utilizing AM both metal matrix and ceramic can be selectively placed to attenuate the threat.
- Heat transfer components: Like topology optimization, the cellular geometry can be optimized to increase surface area for heat transfer applications. For example, because the structure is a homogeneous sandwich panel, water can transferred between the panels to transfer heat to or from the medium. Additionally, tiles can have a significant effect (either insulators or conductors) as the composite material.
- Nuclear components: Furthermore, advanced ceramics such as boron carbide (B_4C) can be used as a neutron absorber for nuclear applications in combination with heat transfer within reactor components.
- Automotive parts: The proposed composite structures can be used as brake rotors for increased wear resistance while also transferring heat from the friction of the brake pads. Additionally, stiff lightweight components of cars can be used to save energy.
- Infrastructure: Because of the scalablitiy (Section 2.2.4) of the proposed manufacturing process, large lightweight load-bearing components can be fabricated to decrease weight and therefore save energy.
    - General applications for decreased energy consumption: Because the cellular structures have decreased volume of material while still maintaining mechanical properties, there is a decrease in the amount of energy required to create work. There are abundant applications where this is applicable and can be adapted with the use of the proposed manufacturing process.

REFERENCES

[1] Gibson, J. W., and Ashby, M. F., 1997, Cellular Solids: Structures and Properties, Cambridge University Press, Cambridge, UK.

[2] Banhart, J., 2000, "Manufacturing Routes for Metallic Foams," Memb. J. Miner. Met. Mater. Soc., **52**(12), pp. 22–27.

[3] Degischer, H.-P., and Kriszt, B., 2002, Handbook of Cellular Metals: Production, Processing, Applications.

[4] Thompson, S. C., Muchnick, H., Choi, H., and Mcdowell, D., 2006, "Robust Materials Design of Blast Resistant Panels," Multidisciplinary Analysis and Optimization Conference, pp. 1–15.

[5] Ashby, M. F., Evans, A. G., Fleck, N. A., Gibson, J. W., Hutchinson, J. W., and Wadley, H. N. G., 2000, Metal Foams: A Design Guide, Butterworth-Heinemann, Woburn, MA.

[6] Nguyen, J., Park, S., and Rosen, D. W., 2012, "Cellular structure design for lightweight components," Innov. Dev. Virtual Phys. Prototyp., pp. 203–210.

[7] Williams, C. B., Mistree, F., and Rosen, D. W., 2005, "Investigation of Solid Freeform Fabrication Processes for the Manufacture of Parts with Designed Mesostructure," ASME IDETC Design for Manufacturing and the Life Cycle Conference, Long Beach, CA, pp. 1–13.

[8] Gibson, I., Rosen, D. W., and Stucker, B., 2010, Additive Manufacturing Technologies.

[9] Seals, M. E., Mckinney, S. R., Stockhausen, P. J., Bottoms, S. R., Druschitz, A. P., and Tech, V., "Evaluation of 3D Printed Polymers for Investment Casting Expendable Patterns," American Foundry Society.

[10] Pham, D. T., Dimov, C. J., and Gault, R. S., 2003, "Layer Manufacturing Processes: Technology Advances and Research Challenges," 1st International Conference on Advanced Research in Virtual and Rapid Prototyping, Leiria, Portugal, pp. 107–113.

[11] Brooks, W., Sutcliffe, C., Cantwell, W., Fox, P., Todd, J., and Mines, R., 2005, "Rapid Design and Manufacture of Ultralight Cellular Materials," International Solid Freeform Fabrication Symposium, Austin, TX, pp. 231–241.

[12] Cansizoglu, O., Cormier, D., Harrysson, O., West, H., and Mahale, T., 2006, "An Evaluation of Non-Stochastic Lattice Structures Fabricated Via Electron Beam Melting.," International Solid Freeform Fabrication Symposium, Austin, TX, pp. 209–219.

[13] Yang, L., Harrysson, O., West II, H., and Cormier, D., 2011, "Design and characterization of orthotropic re-entrant auxetic structures made via EBM using Ti6Al4v and pure copper," International Solid Freeform Fabrication Symposium, Austin, TX, pp. 464–474.

[14] Agarwala, M., Bourell, D., Beaman, J., Marcus, H., and Barlow, J., 1995, "Direct selective laser sintering of metals," Rapid Prototyp. J., **1**(1), pp. 26–36.

[15] EOS GmbH, 2014, "EOS M 400" [Online]. Available: http://www.eos.info/systems_solutions/metal/systems_equipment/eos_m_400.

[16] Bassoli, E., and Atzeni, E., 2009, "Direct metal rapid casting: mechanical optimization and tolerance calculation," Rapid Prototyp. J., **15**(4), pp. 238–243.

[17] Mckenna, N., Singamneni, S., Diegel, O., Singh, D., Neitzert, T., George, J. S., Choudhury, A. R., and Yarlagadda, P., 2008, "Direct Metal casting through 3D printing : A critical analysis of the mould characteristics," 9th Global Congress on Manufacturing and Management, Surfers Paradise, Australia, pp. 12–14.

[18] Gill, S. S., and Kaplas, M., 2010, "Efficacy of powder-based three-dimensional printing (3DP) technologies for rapid casting of light alloys," Int. J. Adv. Manuf. Technol., **52**(1-4), pp. 53–64.

[19] Gill, S. S., and Kaplas, M., 2009, "Comparative Study of 3D Printing Technologies for Rapid Casting of Aluminium Alloy," Mater. Manuf. Process., **24**(12), pp. 1405–1411.

[20] Chhabra, M., and Singh, R., 2012, "Obtaining desired surface roughness of castings produced using ZCast direct metal casting process through Taguchi's experimental approach," Rapid Prototyp. J., **18**(6), pp. 458–471.

[21] Bassoli, E., Gatto, A., Iuliano, L., and Violante, M. G., 2007, "3D printing technique applied to rapid casting," Rapid Prototyp. J., **13**(3), pp. 148–155.

[22] Beely, P. R., 2001, Foundry Technology, Butterworth-Heinemann.

[23] King, D., and Tansey, T., 2002, "Alternative materials for rapid tooling," **121**(September 2001), pp. 313–317.

[24] Bernard, A., Delplace, J.-C., Perry, N., and Gabriel, S., 2003, "Integration of CAD and rapid manufacturing for sand casting optimisation," Rapid Prototyp. J., **9**(5), pp. 327–333.

[25] Meisel, N. A., Williams, C. B., and Druschitz, A., 2012, "Lightweight Metal Cellular Structures via Indirect 3D Printing and Casting," International Solid Freeform Fabrication Symposium.

[26] Budzik, G., 2007, "Possibilities of utilizing 3DP technology for foundry mould making," Arch. Foundry Eng., **7**(2), pp. 65–68.

[27] Kawola, J., 2003, "ZCast Direct Metal Casting: From Data to Cast Aluminum in 12 hours" [Online]. Available: http://www.3dprint.no/images/Nyheter_info/ZCast info.pdf.

[28] Mattern, a., Huchler, B., Staudenecker, D., Oberacker, R., Nagel, a., and Hoffmann, M. J., 2004, "Preparation of interpenetrating ceramic–metal composites," J. Eur. Ceram. Soc., **24**(12), pp. 3399–3408.

[29] Snelling, D. A., Kay, R., Druschitz, A. P., and Williams, C. B., 2014, "Mitigating Gas Defects in Casting Produced from 3D Printed Molds," Int. Foundry Res., **66**(2), pp. 30–36.

[30] Schleg, F. P., 2003, Technology of Metalcasting, American Foundry Society, Schaumburg, IL.

[31] Vayre, B., Vignat, F., and Villeneuve, F., 2013, "Identification on Some Design Key Parameters for Additive Manufacturing: Application on Electron Beam Melting," Procedia CIRP, **7**, pp. 264–269.

[32] Banhart, J., and Weaire, D., 2002, "On the Road Again: Metal Foams Find Favor," Phys. Today, **55**(7), p. 37.

[33] Evans, A. G., Hutchinson, J. W., and Ashby, M. F., 1999, "Multifunctionality of cellular metal systems," Prog. Mater. Sci., **43**, pp. 171–121.

[34] Evans, A. G., Hutchinson, J. W., Fleck, N. A., Ashby, M. F., and Wadley, H. N. G., 2001, "The topological design of multifunctional cellular metals," Prog. Mater. Sci., **46**(3-4), pp. 309–327.

[35] Seepersad, C. C., Kumar, R. S., Allen, J. K., Mistree, F., and Mcdowell, D. L., 2004, "Multifunctional Design of Prismatic Cellular Materials," J. Comput. Mater. Des., **11**(2), pp. 163–181.

[36] Seepersad, C. C., Allen, J. K., McDowell, D. L., and Mistree, F., 2006, "Robust Design of Cellular Materials With Topological and Dimensional Imperfections," J. Mech. Des., **128**(6), p. 1285.

[37] Wadley, H., 2003, "Fabrication and structural performance of periodic cellular metal sandwich structures," Compos. Sci. Technol., **63**(16), pp. 2331–2343.

[38] Mori, L., Lee, S., Xue, Z., Vaziri, A., Queheillalt, D., Dharmasena, K., Wadley, H., Hutchinson, J., and Espinosa, H., 2007, "Deformation and fracture modes of sandwich structures subjected to underwater impulsive loads," J. Mech. Mater. Struct., **2**(10), pp. 1981–2006.

[39] Queheillalt, D. T., Murty, Y., and Wadley, H. N. G., 2008, "Mechanical properties of an extruded pyramidal lattice truss sandwich structure," Scr. Mater., **58**(1), pp. 76–79.

[40] Queheillalt, D., Deshpande, V., and Wadley, H., 2007, "Truss waviness effects in cellular lattice structures," J. Mech. Mater. Struct., **2**(9), pp. 1657–1675.

[41] Moongkhamklang, P., and Wadley, H. N. G., 2010, "Titanium Alloy Lattice Structures with Millimeter Scale Cell Sizes," Adv. Eng. Mater., **12**(11), pp. 1111–1116.

[42] Jamcorp Inc., 2004, "Jonathon Aerospace Materials Website" [Online]. Available: www.jamcorp.com.

[43] Nathal, M. V., Wittenberger, J. D., Hebsur, M. G., Kantzos, P. T., and Krause, D. L., 2004, "Superalloy Lattice Block Structures," 10th International Symposium on Superalloys, Champion, PA.

[44] Sypeck, B. D. J., and Wadley, H. N. G., 2002, "Cellular Metal Truss Core Sandwich Structures," Adv. Eng. Mater., **1028**(10), pp. 759–764.

[45] Hattiangadi, A., and Bandyopadhyay, A., 1999, "Processing , Characterization and Modeling of Non-Random Porous Ceramic Structures," International Solid Freeform Fabrication Symposium, pp. 319–326.

[46] Chiras, S., Mumm, D. R., Evans, A. G., Wicks, N., Hutchinson, J. W., Dharmasena, K., Wadley, H. N. G., and Fichter, S., 2002, "The structural performance of near-optimized truss core panels," Int. J. Solids Struct., **39**(15), pp. 4093–4115.

[47] Lyons, A., Krishnan, S., Mullins, J., Hodes, M., and Hernon, D., 2009, "Advanced Heat Sinks Enabled by Three-Dimensional Printing," International Solid Freeform Fabrication Symposium, Austin, TX, pp. 749–760.

[48] Zaeh, M. F., and Branner, G., 2009, "Investigations on residual stresses and deformations in selective laser melting," Prod. Eng., **4**(1), pp. 35–45.

[49] Shiomil, M., Osakada, K., Nakamura, K., Yamashita, F., and Abe, F., 2004, "Residual Stress within Metallic Model Made by Selective Laser Melting Process," CIRP Ann. - Manuf. Technol., **53**(1), pp. 195–198.

[50] Mumtaz, K., Vora, P., and Hopkinson, N., 2011, "A Method to Eliminate Anchors/Supports from Directly Laser Melted Metal Powder Bed Processes," International Solid Freeform Fabrication Symposium, Austin, TX, pp. 55–64.

[51] 3D Systems, "Solutions: Metal Casting" [Online]. Available: http://www.zcorp.com/en/Solutions/Castings-Patterns-Molds/spage.aspx.

[52] ExOne, 2012, "S-Print: Improved Productivity in a Compact Design" [Online]. Available: http://www.exone.com/en/materialization/systems.

[53] Voxeljet, 2012, “Large-format sand moulds for metal casting” [Online]. Available: http://www.voxeljet.de/fileadmin/Voxeljet/Services/Sand_casting_2012.pdf.

[54] Chhabra, M., and Singh, R., 2011, “Rapid casting solutions: a review,” Rapid Prototyp. J., **17**(5), pp. 328–350.

[55] Stankiewicz, M., Budzik, G., Patrza, M., Wieczorowski, M., Grzelka, M., Matysiak, H., and Slota, J., 2010, “The scope of application of incremental rapid prototyping methods in foundry engineering,” Arch. Foundry Eng., **10**(1), pp. 405–410.

[56] Campbell, J., 2004, Castings Practice: The Ten Rules of Castings, Butterworth-Heinemann, Oxford, UK.

[57] Williams, C. B., Mistree, F., and Rosen, D. W., 2005, “Towards the Design of a Layer-Based Additive Manufacturing Process for the Realization of Metal Parts of Designed Mesostructures,” International Solid Freeform Fabrication Symposium, Austin, TX, pp. 1–16.

[58] NetFabb, 2011, “Selective Space Structures (3S) - your tool for creation of complex structures.”

[59] Snelling, D. A., Kay, R., Druschitz, A., and Williams, C. B., 2012, “Mitigating Gas Defects in Castings Produced from 3D Printed Molds,” 117th Metalcasting Congress.

[60] Dassault Systèmes, 2011, “Abaqus Version 6.11 Documentation.”

[61] Deshpande, V. S., Fleck, N. A., and Ashby, M. F., 2001, “Effective properties of the octet-truss lattice material,” J. Mech. Phys. Solids, **49**, pp. 1747–1769.

[62] American Foundry Society, 2004, Mold and Core Test Handbook, American Foundry Society, Des Plaines.

[63] Z_Corporation, 2006, “ZCast^{TM} 501 powder MSDS.”

[64] ExOne, “ExOne: Digital Part Materialization” [Online]. Available: http://www.exone.com/materialization/what-is-digital-part-materialization/sand.

[65] Viridis3D, “Metal Casting” [Online]. Available: http://www.viridis3d.com/metalcasting.htm.

[66] Voxeljet, “Rapid and Efficient Sand Casting of Molds” [Online]. Available: http://www.voxeljet.de/en/services/sand/.

[67] Campbell, J., 2003, Castings, Butterworth-Heinemann, Oxford, UK.

[68] Drokina, V. V., and Belov, V. D., 2013, "Study of casting and mechanical properties of the AK8L alloy in castings fabricated using printed molds made of the ZCAST mixture," Russ. J. Non-Ferrous Met., **54**(1), pp. 48–50.

[69] ASM International, 1990, Metals Handbook: Properties and Selection: Nonferrous Alloys and Pure Metals, ASM International.

[70] Snelling, D., Williams, C. B., and Druschitz, A. P., 2014, "A Comparison of Binder Burnout and Mechanical Characteristics of Printed and Chemically Bonded Sand Molds," SFF Symposium, Austin, TX.

[71] ASTM Standard E8-13a, 2013, "Standard Test Methods for Tension Testing of Metallic Materials."

[72] National Institutes of Health, "ImageJ: Image Processing and Analysis in Java" [Online]. Available: http://rsb.info.nih.gov/ij.

[73] Incropera, F. P., DeWitt, D. P., Bergman, T. L., and Lavine, A. S., 2007, Fundamentals of Heat and Mass Transfer, John Wiley & Sons, New York.

[74] Granta Design Limited, 2013, "CES EduPack."

[75] Hatch, J. E., 1984, Aluminum: Properties and Physical Metallurgy, ASM International.

[76] L. J. Star Inc., "Surface Finish Charts" [Online]. Available: http://www.ljstar.com/design/surface_charts.aspx.

[77] Kaufman, J. G., and Rooy, E. L., 2004, Aluminum Alloy Castings: Properties, Processes, and Application, ASM International.

[78] MatWeb, "MatWeb: Material Property Data" [Online]. Available: http://www.matweb.com.

[79] Davies, J. R., 1993, Aluminum and Aluminum Alloys, ASM International.

[80] Frank, M. C., Peters, F. E., Luo, X., Meng, F., and Petrzelka, J., 1999, "A Hybrid Rapid Pattern Manufacturing System for Sand Castings," SFF Symposium, pp. 35–46.

[81] Utela, B., Storti, D., Anderson, R., and Ganter, M., 2008, "A review of process development steps for new material systems in three dimensional printing (3DP)," J. Manuf. Process., **10**(2), pp. 96–104.

[82] Snelling, D., Li, Q., Meisel, N. A., Williams, C. B., Batra, R., and Druschitz, A. P., 2015, "Lightweight Metal Cellular Structures via 3D Printing of Sand Cast Molds," Adv. Eng. Mater., **Submitted**.

[83] Jacobs, P., 1995, “World Class Design to Manufacture,” Rapid Prototyp. J., **5**(4), pp. 164–169.

[84] Tang, Y., Fuh, J. Y. H., Loh, H. T., Wong, Y. S., and Lu, L., 2003, “Direct laser sintering of a silica sand,” Mater. Des., **24**(8), pp. 623–629.

[85] Cima, M. J., Haggerty, J. S., Sachs, E. M., and Williams, P. A., 1993, “Three-dimensional printing techniques.”

[86] Hague, R., D’Costa, G., and Dickens, P. M., 2001, “Structural design and resin drainage characteristics of QuickCast 2.0,” Rapid Prototyp. J., **7**(2), pp. 66–73.

[87] Sachs, E., Newton, S. P., Carlisle, M., and Allen, S. M., 1998, “Enhancement of Thermal Properties of Tooling Made by Solid Free Form Fabrication Techniques.”

[88] Cima, M. J., James, F., Khanuja, S., and Silbaugh, P. E. H., 1996, “Process for Removing Loose Powder Particles from Interior Passages of a Body.”

[89] Monkhouse, D. C., Kumar, S., Rowe, C. W., and Yoo, J., 2003, “Rapid Prototyping and Manufacturing Process,” **1**(12).

[90] Munson, B. R., Young, D. F., and Okiishi, T. H., 1998, Fundamentals of fluid mechanics, John Wiley & Sons, New York.

[91] Clyne, T. W., and Withers, P. J., 1993, An Introduction to Metal Matrix Composites, Cambridge University Press.

[92] Suresh, S., Mortensen, A., and Needleman, A., 1993, Fundamentals of Metal-Matrix Composites, Butterworth-Heinemann, Boston.

[93] Standke, G., Müller, T., Neubrand, A., Weise, J., and Göpfert, M., 2010, “Cost-Efficient Metal-Ceramic Composites-Novel Foam-Preforms, Casting Processes and Characterisation,” Adv. Eng. Mater., **12**(3), pp. 189–196.

[94] Chawla, N., and Chawla, K. K., 2005, Metal Matrix Composites, Springer Science+Business Media.

[95] Rahaman, M. N., 2003, Ceramic Processing and Sintering, Marcel Dekker, Inc.

[96] Yoo, J., Cima, M. J., Khanuja, S., and Sachs, E. M., 1993, “Structural Ceramic Components by 3D Printing,” International Solid Freeform Fabrication Symposium, Austin, TX, pp. 40–50.

[97] Lakshminarayan, U., Ogrydiziak, S., and Marcus, H. L., 1990, “Selective Laser Sintering of Ceramic Materials,” International Solid Freeform Fabrication Symposium, Austin, TX, pp. 16–26.

[98] Griffith, M. L., and Halloran, J. W., 1996, "Freeform Fabrication of Ceramics via Stereolithography," J. Am. Ceram. Soc., **79**(10), pp. 2601–2608.

[99] Agarwala, M. K., Weeren, R. Van, Vaidyanathan, R., Langrana, N., Safari, A., Garofalini, S. H., and Danforth, S. C., 1990, "Structural Ceramics by Fused Deposition of Ceramics," International Solid Freeform Fabrication Symposium, Austin, TX.

[100] Yoo, J., Cima, M. J., and Suresh, S., 1995, "Fabrication and Microstructural Control of Advanced Ceramic Components by Three Dimensional Printing," Ceram. Eng. Sci. Proc., **16**(5), pp. 755–762.

[101] Seitz, H., Rieder, W., Irsen, S., Leukers, B., and Tille, C., 2005, "Three-dimensional printing of porous ceramic scaffolds for bone tissue engineering.," J. Biomed. Mater. Res. B. Appl. Biomater., **74**(2), pp. 782–8.

[102] Sachs, E., Cima, M., Cornie, J., Brancazio, D., Bredt, J., Curodeau, A., Esterman, M., Fan, T., Harris, C., Kremmin, K., Lee, S. J., Pruitt, B., and Williams, P., 1990, "Dimensional Printing : Rapid Tooling and Prototypes Directly from CAD Representation," International Solid Freeform Fabrication Symposium, Austin, TX, pp. 27–47.

[103] Sachs, E., Cima, M., Cornie, J., Brancazio, D., Bredt, J., Curodeau, A., Fan, T., Khanuja, S., Lauder, A., Lee, J., and Michaels, S., 1993, "Three-Dimensional Printing: The Physics and Implications of Additive Manufacturing," CIRP Ann. - Manuf. Technol., **42**(1), pp. 257–260.

[104] Moon, J., Caballero, A. C., Hozer, L., Chiang, Y.-M., and Cima, M. J., 2001, "Fabrication of functionally graded reaction infiltrated SiC–Si composite by three-dimensional printing (3DP^{TM}) process," Mater. Sci. Eng. A, **298**(1-2), pp. 110–119.

[105] Sōmiya, S., Aldinger, F., Claussen, N., Spriggs, R. M., Uchino, K., Koumoto, K., and Kaneno, M., 2003, Handbook of Advanced Ceramics, Elsevier Inc.

[106] Boudchicha, M. R., Achour, S., and Harabi, A., 2001, "Crystallization and sintering of cordierite and anorthite based," J. Mater. Sci. Lett., **20**, pp. 215–217.

[107] ASTM Standard B962-14, 2014, "Standard Test Methods for Density of Compacted or Sintered Powder Metallurgy (PM) Products Using Archimedes' Principle."

[108] Bedard, R. L., and Flanigen, E. M., 1990, "High Density Cordierite Ceramics from Zeolite."

[109] Ogiwara, T., Noda, Y., Shoji, K., and Kimura, O., 2010, "Solid state synthesis and its characterization of high density cordierite ceramics using fine oxide powders," J. Ceram. Soc. Japan, **118**(1375), pp. 246–249.

[110] Vaucher, S., and Empa, O. B., 2001, “Bonding and interface formation in Metal Matrix Composites MMC - Assess Thematic Network.”

[111] Kainer, K. U., 2006, Metal Matrix Composites: Custom-made Materials for Automotive and Aerospace Engineering, John Wiley & Sons.

[112] Ellingham, H. J. T., 1944, “Reducibility of Oxides and Sulphides in Metallurgical Processes,” J. Soc. Chem. Ind., **63**(10), pp. 289–320.

[113] Naplocha, K., Janus, a, Kaczmar, J. ., and Samsonowicz, Z., 2000, “Technology and mechanical properties of ceramic preforms for composite materials,” J. Mater. Process. Technol., **106**(1-3), pp. 119–122.

[114] Günay, E., 2011, “Sintering behavior and properties of sepiolite-based cordierite,” **35**, pp. 83–92.